

**UCLA**

**UCLA Electronic Theses and Dissertations**

**Title**

Innovations in Optical Microscopy Methods for Studying Neural Circuit Function In-Vivo

**Permalink**

<https://escholarship.org/uc/item/65k3h6dq>

**Author**

Madruga, Blake Alexander

**Publication Date**

2024

**Supplemental Material**

<https://escholarship.org/uc/item/65k3h6dq#supplemental>

Peer reviewed|Thesis/dissertation

UNIVERSITY OF CALIFORNIA  
Los Angeles

Innovations in Optical Microscopy Methods for Studying Neural Circuit Function *In-Vivo*

A dissertation submitted in partial satisfaction  
of the requirements for the degree  
Doctor of Philosophy in Neuroscience

by

Blake Alexander Madruga

2024

© Copyright by  
Blake Alexander Madruga  
2024

## ABSTRACT OF THE DISSERTATION

Innovations in Optical Microscopy Methods for Studying Neural Circuit Function *In-Vivo*

by

Blake Alexander Madruga

Doctor of Philosophy in Neuroscience

University of California, Los Angeles, 2024

Professor Peyman Golshani, Chair

This dissertation is focused on the design, development, and implementation of two high performance optical microscopy systems that enable study of neuronal circuit function in new and innovative ways.

Firstly, an easily adopted, open-source miniature 2-photon microscope (UCLA 2P Miniscope) capable of recording calcium dynamics from neurons located in deep structures and in dendrites over a (445 $\mu\text{m}$  x 380 $\mu\text{m}$ ) field of view (FOV) during free behavior is described. The system weighs approximately 4g and utilizes two on-board silicon-based photon detectors for highly sensitive measurements. All hardware is designed for high performance and ease of assembly, while minimizing cost. To test the 2P miniature microscope, recordings in three experimental conditions were conducted to highlight system capabilities during free behavior in mice. First, calcium dynamics from place cells in hippocampal area CA1 were recorded. Next, calcium transients from dendrites in retrosplenial cortex were resolved during 30 minutes of free behavior. Lastly, dentate granule cell activity was recorded at a depth of over 620 $\mu\text{m}$ , through an intact hippocampal formation during an open field behavior. The dentate granule cell recordings, to our knowledge, are the first optical recordings from these neurons ever performed in the intact hippocampus during free behavior. The miniature microscope itself and all supporting equipment are open-source and all files needed for building the scope can be accessed through the UCLA Golshani

Lab [GitHub repository](#).

Secondly, a high-speed, open-source voltage imaging microscope is presented, capable of resolving (920 $\mu\text{m}$  x 460 $\mu\text{m}$ ) fields of view at 500 frames per second. This microscope enables the study of fast-spiking neural populations such as interneurons with single action potential sensitivity over periods greater than 10 minutes. The system is also able to resolve activity from populations of many neurons simultaneously, with some recordings exceeding 30 active neurons in a single FOV. Additionally, this microscope system is able to quantify sub-threshold membrane potentials, making the recording of oscillatory dynamics and excitatory post synaptic potentials possible in large neural circuits *in-vivo*. Altogether, this high-speed, large FOV system enables new studies into the critical mechanisms key subpopulations of neurons employ to support computation and learning over time.

Both of the microscope systems described here enable new insights into the function of the central nervous system. The first (Part I) is a miniature multiphoton microscope capable of studying fine structures deep in the brain during free and naturalistic behavior. The second (Part II) is a high-speed system able to record rapidly changing electrical dynamics across large neural populations. Together they will lead to new understandings of how the brain functions both in disease and health.

The dissertation of Blake Alexander Madruga is approved.

Hugh T. Blair

Matthew Shtrahman

Daniel Benjamin Aharoni

Peyman Golshani, Committee Chair

University of California, Los Angeles

2024

To my Mother **Sarah**, whose unconditional love enabled me to follow my dreams;  
to my Father **Rick**, who is my moral compass and biggest role model;  
to my Brother, **Ben**, whose support keeps me steadfast in my passions;  
to my Grandfather, **Frank**, for instilling a love of physics that is an integral part of me;  
to my Grandmother, **Mary**, for showing me how to be patient and empathetic;  
to my Abuela, **Mary**, for demonstrating what it means to be strong and selfless;  
to my Grandfather, **Robert**, and his Father, **Edward**, for inspiring me to always go  
further than where I've been before, and to make life what I want it to be;  
and to **myself**.

*Non enim tranquillis maribus naucleri periti fiunt*

## TABLE OF CONTENTS

<b>1</b>	<b>Introduction to Fluorescent Imaging and Microscopy in Neuroscience</b>	<b>1</b>
1.1	A Brief History of Using Light to Study Nature . . . . .	1
1.2	Fluorescence as a Physical Process . . . . .	2
1.3	Advantages of Fluorescent Imaging in Combination with Viral Labeling Strategies . . . . .	3
1.4	Genetically Encoded Activity Indicators: Why $\text{Ca}^{2+}$ ? . . . . .	5
1.5	Interim Summary . . . . .	8
<b>2</b>	<b>1P Excitation Imaging in Neuroscience</b> . . . . .	<b>9</b>
2.1	Core 1P Microscopy Ideology . . . . .	9
2.1.1	Example 1P Microscope Setup and Operational Principles . . . . .	9
2.2	Advantages and Disadvantages of 1P Microscopy . . . . .	11
2.3	Interim Summary . . . . .	13
<b>3</b>	<b>2P Excitation Microscopy in Neuroscience</b> . . . . .	<b>15</b>
3.1	Core 2P Microscopy Ideology . . . . .	15
3.1.1	Example 2P Microscope Setup and Operational Principles . . . . .	20
3.2	Advantages and Disadvantages of 2P Microscopy . . . . .	21
3.3	Interim Summary . . . . .	22
<b>4</b>	<b>Miniature Microscopy: The Logic in Making Large Systems Small</b> . . . . .	<b>23</b>
4.1	1P Miniature Microscopes and the UCLA Miniscope Project . . . . .	24
4.2	Miniature Microscopes Using More than One Photon, a (not so) Brief History . . . . .	25
4.2.1	Foundational 2P Miniature Microscopes in the literature . . . . .	25



4.2.2	3P Miniature Microscopes . . . . .	28
4.2.3	Current State-Of-The-Art . . . . .	29
4.2.4	Addressing a clear gap in the field . . . . .	30
<b>5</b>	<b>Part I: UCLA 2P Miniscope System Development . . . . .</b>	<b>32</b>
5.1	Initial Versions and Design Trajectory . . . . .	32
5.1.1	Learning from the Literature . . . . .	32
5.1.2	Innovation by Iteration . . . . .	33
5.1.3	The Iterative Optimizer . . . . .	36
5.2	Optical System Design . . . . .	39
5.2.1	Excitation Path . . . . .	39
5.2.2	Emission Path . . . . .	40
5.2.3	Complete System Path . . . . .	41
5.2.4	Silicon Photon Counters . . . . .	42
5.3	Mechanical System . . . . .	44
5.3.1	Optomechanical System Design . . . . .	44
5.3.2	Fabrication . . . . .	44
5.3.3	Assembly . . . . .	47
5.4	Electronic System . . . . .	47
5.4.1	General Overview . . . . .	47
5.4.2	Flex-PCB Design . . . . .	48
5.4.3	Signal Interface PCB Design . . . . .	50
5.4.4	Complete System and Wiring Diagram . . . . .	52
5.5	Software System . . . . .	52

<b>6</b>	<b>UCLA 2P Miniscope: Optical Performance Assessments . . . . .</b>	<b>55</b>
6.1	Field of View Measurements . . . . .	55
6.2	Electronic Focus Range Measurements . . . . .	55
6.3	Point-Spread-Function Measurements . . . . .	57
6.4	Comparison Between Zemax Optical Simulation and Measurements . . . . .	58
6.5	Resolving Biological Tissue . . . . .	59
<b>7</b>	<b>UCLA 2P Miniscope: <i>In-vivo</i> free behavior recordings . . . . .</b>	<b>63</b>
7.1	Animal Protocols and Well-Being . . . . .	63
7.2	CA1 - Resolving Dense Neuronal Populations During Free Behavior . . . . .	65
7.3	Retrosplenial Cortex (RSC) - 2-Color Dendritic Calcium Signals During Free Behavior . . . . .	66
7.4	DG - Imaging Neurons Hundreds of Microns Deep . . . . .	69
7.5	Analysis Methods . . . . .	70
<b>8</b>	<b>UCLA 2P Miniscope: Design Philosophy and Filling a Gap in the Field</b>	<b>74</b>
8.1	A cost-effective 2P Miniature Microscope . . . . .	74
8.2	Prioritization Given Towards Ease of Assembly . . . . .	74
8.3	Designed to Be Sensitive to Dim Signals . . . . .	75
8.4	Designed to Be Shared . . . . .	76
8.5	Designed to Be Experimentally Robust . . . . .	77
<b>9</b>	<b>UCLA 2P Miniscope: Dissemination Efforts and Future Directions . . . . .</b>	<b>78</b>
9.1	GitHub Repository . . . . .	78
9.2	Workshops . . . . .	78
9.3	Future Directions . . . . .	80

9.3.1	Extending Current Technology . . . . .	80
9.3.2	Learning From Large Systems . . . . .	82
9.4	Conclusions . . . . .	87
<b>10</b>	<b>Part II: Spatially-Confined 1P Excitation Voltage Imaging Microscope</b>	<b>89</b>
10.1	Introduction to Voltage Imaging . . . . .	89
10.1.1	Constraints on Parameter Space . . . . .	90
10.1.2	Existing Methodologies . . . . .	91
10.1.3	Need For Simple Solutions . . . . .	92
10.2	Spatially Confined 1P Excitation Voltage Imaging Microscope . . . . .	92
10.2.1	Need For High Irradiance . . . . .	93
10.2.2	Necessity of Restricting Excitation Light . . . . .	94
10.2.3	Consideration of qCMOS Architecture . . . . .	94
10.3	Optomechanical System . . . . .	95
10.3.1	Strip Excitation Module . . . . .	95
10.3.2	High Efficiency Collection and De-Magnification . . . . .	98
10.3.3	Complete Voltage Imaging System . . . . .	98
10.4	Results . . . . .	101
10.4.1	Resolving Fast-Spiking Interneuron Dynamics Over 10 Minutes . . .	101
10.4.2	Capturing Membrane Potential From Many Neurons At Once . . .	101
10.5	Future Directions . . . . .	104
10.5.1	Extending the Technology . . . . .	104
10.5.2	Voltage Imaging Miniature Microscopes . . . . .	105
	<b>References . . . . .</b>	<b>107</b>

## LIST OF FIGURES

1.1	<b>Approximate Single Photon Spectral Properties of GFP</b> . . . . .	2
1.2	<b>Jablonski Energy Diagram</b> . . . . .	4
1.3	<b>Equilibrium Potentials and I-V</b> . . . . .	6
2.1	<b>General Properties of Numerical Aperture, Working Distance, and Resolution Interdependencies</b> . . . . .	12
2.2	<b>Imaging Simulation at 0.15 NA</b> . . . . .	13
2.3	<b>Imaging Simulation at 0.8 NA</b> . . . . .	14
3.1	<b>Simulated 2P Optical Pulse Generation</b> . . . . .	16
5.1	<b>ZEMAX Model for Excitation Laser Scanning and Electronic Focusing Subsystem</b> . . . . .	40
5.2	<b>ZEMAX Model of Green SiPM Detector Channel</b> . . . . .	41
5.3	<b>ZEMAX Model of Red SiPM Detector Channel</b> . . . . .	42
5.4	<b>UCLA 2P Miniscope Full Optical System Design</b> . . . . .	43
5.5	<b>UCLA 2P Miniscope Optomechanical Drawing</b> . . . . .	45
5.6	<b>UCLA 2P Miniscope Exploded View</b> . . . . .	46
5.7	<b>UCLA 2P Miniscope Flex-PCB Schematic</b> . . . . .	49
5.8	<b>UCLA 2P Miniscope Flex PCB design</b> . . . . .	49
5.9	<b>UCLA 2P Miniscope Signal interface Schematic</b> . . . . .	50
5.10	<b>UCLA 2P Miniscope Signal interface PCB</b> . . . . .	51
5.11	<b>UCLA 2P Miniscope Signal interface PCB 3D Rendering</b> . . . . .	51
5.12	<b>UCLA 2P Miniscope Electronic Circuitry</b> . . . . .	53
5.13	<b>MATLAB Control User Interface</b> . . . . .	54

6.1	Resolving 4 $\mu$ m Microspheres for FOV and Z-Range Measurements .	56
6.2	Measured Axial Focus Range Provided by the Electro-Tunable Lens	56
6.3	Measured Lateral and Axial Point-Spread Function (PSF) . . . . .	58
6.4	2D PSF comparisons Between Zemax Simulations and Measurements	59
6.5	Lateral PSF Cross-Sections from Optical Model and Measurements .	60
6.6	FOV Predictions and Results from Measurement . . . . .	61
6.7	GCaMP6f <i>Ex-Vivo</i> Slice Recording . . . . .	62
7.1	Resolving Densely-Labeled CA1 Neurons During Free Behavior . . .	67
7.2	Dendritic 2-Color Imaging in Cortex During Free Behavior . . . . .	68
7.3	Recording Calcium Dynamics from Dentate Granule Cells Through an Intact Hippocampus During Free Behavior . . . . .	71
7.4	Granule Cell Dynamics Between Head-Fixed and Free Behavior . . .	72
9.1	UCLA 2P Miniscope Github Page . . . . .	79
10.1	Comparison Between Voltage and Calcium Kinetics . . . . .	91
10.2	Strip Excitation Module Schematic and Optomechanical Diagram . .	96
10.3	Example Excitation Conditions for a Narrow and Wide Strip . . . . .	96
10.4	Tilttable Objective Module Optomechanical Diagram. . . . .	97
10.5	Spatially Confined Excitation Voltage Imaging Microscope . . . . .	99
10.6	Voltage Imaging Microscope Physical Hardware at UCLA . . . . .	100
10.7	Resolving dynamics from three SST+ OLM cells in CA1 over 10 minutes . . . . .	102
10.8	Population Voltage Imaging from 30 Active, pAce-Expressing Exci- tatory Neurons in CA1 . . . . .	103

## LIST OF TABLES

8.1	<b>Cost breakdown for the UCLA 2P Miniscope microscope headpiece</b>	75
-----	--	----

## ACKNOWLEDGMENTS

**First, I acknowledge and thank my entire PhD committee:** I would especially like to thank my chair, **Peyman Golshani** who believed in me, this project, and provided unwavering support through it all. Without his help and guidance it would be highly unlikely that this project would be even 10% of what it is today. Thank you very much, Peyman, for inspiring me to never keep pushin’.

**I acknowledge and thank Professor Julie Bentley** at the University of Rochester Institute of Optics, for her instrumental work designing the custom tube lens and objective assembly.

**I acknowledge the support of the UCLA community:**

**Conor Dorian:** For massive support with animal surgical preparations, general experimental setup, and data analysis pertaining to the miniature 2P microscope. **Zoë Day:** For constant support with orders, logistical issues, animal surgeries, and general experiments. **Jiannis Taxidis:** For early help with free behavior experiments and constant motivation and support. **Douglas Vormstein-Schneider:** For countless informative discussions and brainstorming. **Samara Miller:** For early help with projection imaging and general help with everything in the lab. **Diego Espino:** For providing the recordings of the fast spiking SST neurons resolved with the voltage imaging microscope. **Liron Sheintuch:** For providing the recordings the large populations of excitatory neurons recorded with the voltage imaging microscope. **Federico Sangiuliano Jimka:** For endless help with electronics and troubleshooting software issues. **Takuya Sasatani:** For electronic design help and discussions regarding SiPM drivers and noise. **João Couto:** For guidance, inspiration and help through each step of the process.

**I acknowledge the contributions of collaborators:**

**Alipasha Vaziri:** For direction and support throughout the project. **Tobias Nöbauer:** For many beneficial optical discussions. **Bruno Pichler:** For discussions around control electronics and thinking to use Digilent devices.

**I acknowledge the funding sources that greatly contributed to my training as a scientist and made this research possible:**

- **NIH T32MH073526**
- **NIH F31MH123111**
- **NIH U01NS128664**



## VITA

- 2010–2015 B.S. in Biology, UCLA
- 2016–2018 M.S. in Electrical and Computer Engineering, UCLA
- 2016–2024 Graduate Student Researcher in Neurology, UCLA

## PUBLICATIONS

**Madruza, B. A.**, Dorian, C. C., Sehgal, M., Silva, A. J., Shtrahman, M., Aharoni, D., & Golshani, P. Open-source, high performance miniature multiphoton microscopy systems for freely behaving animals. *BioRxiv Preprint*, **2024**

Taxidis, J., **Madruza, B.A.**, Melin, M. D., Lin, M. Z., & Golshani, P. Voltage imaging reveals that hippocampal interneurons tune memory-encoding pyramidal sequences. *In Review, Nature Neuroscience*, **2023**

Evans, S. W., Shi, D. Q., Chavarha, M., Plitt, M. H., Taxidis, J., **Madruza, B.A.**, ... & Lin, M. Z. A positively tuned voltage indicator for extended electrical recordings in the brain. *Nature Methods*, **20(7)**, **2023**

**Madruza, B.A.**, Design and Construction of a Rapidly-Reconfigurable SLM-Based Light Sheet Microscope. *Masters Thesis, UCLA*, **2018**

# CHAPTER 1

## Introduction to Fluorescent Imaging and Microscopy in Neuroscience

### 1.1 A Brief History of Using Light to Study Nature

Scientists have used optical systems to study nature for centuries, as these systems extend the capabilities of our native visual capacity as humans. From as early as 1608, scientists designed and used refractive telescopes to better visualize and record the complicated movements of planets and stars, thereby validating the heliocentric model of our solar system proposed by Copernicus (Copernicus, 1543). Cells, the principle units of life, were discovered by Robert Hooke (of spring constant fame) in 1665 in the text *Micrographia*, using a microscope featuring a condenser lenses made of a brine-filled sphere(Hooke, 1665). Nearly two hundred years later, neuroscientists like Camillo Golgi and Santiago Ramón y Cajal used optical means in combination with chemical staining techniques to provide an optical contrast between neural cells and the surrounding tissue background (Golgi, 1873; Ramón y Cajal, 1899). In doing so, these pioneering researchers studied and characterized many foundational structural aspects of the central and peripheral nervous system and used that understanding to make informed predictions as to how the circuitry may function in living systems. Today, researchers rely heavily on fluorescence microscopy systems in combination with genetic molecular tools to provide spectral contrast between neural populations of interest and the surrounding tissue, enabling the study of neurons in high spatial and temporal resolution.

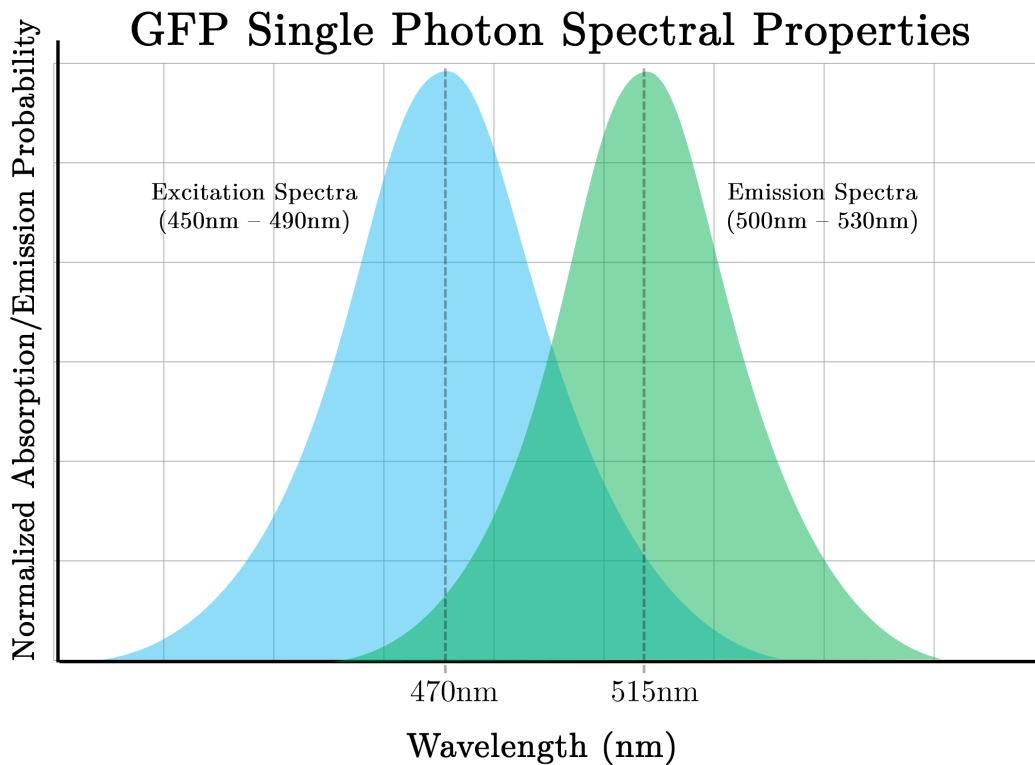


Figure 1.1: **Approximate Single Photon Spectral Properties of GFP**  
 Green fluorescent protein is able to accept photons within the bandwidth shown under the blue curve, with the height denoting the likelihood with which the photon is absorbed. The green curve represents the emission bandwidth and the likelihood of an emitted photon taking a particular energy.

## 1.2 Fluorescence as a Physical Process

Fluorescence is a natural physical process by which select molecules are able to absorb a limited bandwidth of electromagnetic energy and re-emit it with a characteristic frequency shift (Stokes, 1852). In bright sunlight, efficient photoabsorbers (like rhodamine-B) are able to fluoresce via absorption of a single photon roughly once per second (Denk and Svoboda, 1997). Some fluorescent molecules are naturally transcribed as proteins in biological systems, such as green fluorescent protein (GFP) found in *aequorea victoria* (Ormö et al., 1996). GFP is able to accept energy from a range of excitation photons of a specific spectral bandwidth, ranging from approximately 450nm - 490nm in wavelength, in accordance with the molecule's excitation spectrum (the bandwidth over which light is successfully

absorbed and re-emitted as fluorescence). Once a suitable photon within the correct energy range is accepted by the GFP molecule, it transitions to a higher energy state. Following this energy transition, the photoactivated GFP will undergo small vibrational or conformational shifts on the scale of several nanoseconds, thereby releasing a small amount of the input energy it received from photoexcitation. Ultimately, the excited fluorescent molecule will relax back to the ground state, via the emission of a frequency-shifted photon, in the 510nm - 530nm wavelength range(Youvan and Michel-Beyerle, 1996). The energy of a given photon,  $E$ , is proportional to:

$$E = h \cdot c \cdot \lambda^{-1} \tag{1.1}$$

where  $E$  is the energy of the photon,  $h$  is Planck's constant,  $c$  is the speed of light in vacuum, and  $\lambda$  is the wavelength of the photon. Due to the energy expenditure associated with the vibrational and molecular confirmation changes that occur before the fluorescent emission, the energy of the fluorescent photon is reduced, thus taking a longer wavelength  $\lambda$  in a process known as the Stokes shift (Youvan and Michel-Beyerle, 1996). Since there is a spectral difference between the light required to generate a fluorescent event, and the light produced as a result of fluorescence, researchers use optical beam-splitters and filters to only visualize the light generated by cells that express fluorescent molecules such as GFP.

### **1.3 Advantages of Fluorescent Imaging in Combination with Viral Labeling Strategies**

When used in combination with genetic targeting strategies, fluorescence microscopy is a powerful method enabling researchers to study large populations of precise neuronal subtypes over time. Modern viral techniques make the expression of engineered fluorescent molecules only in cells of a known identity possible. One example of this would be to use the

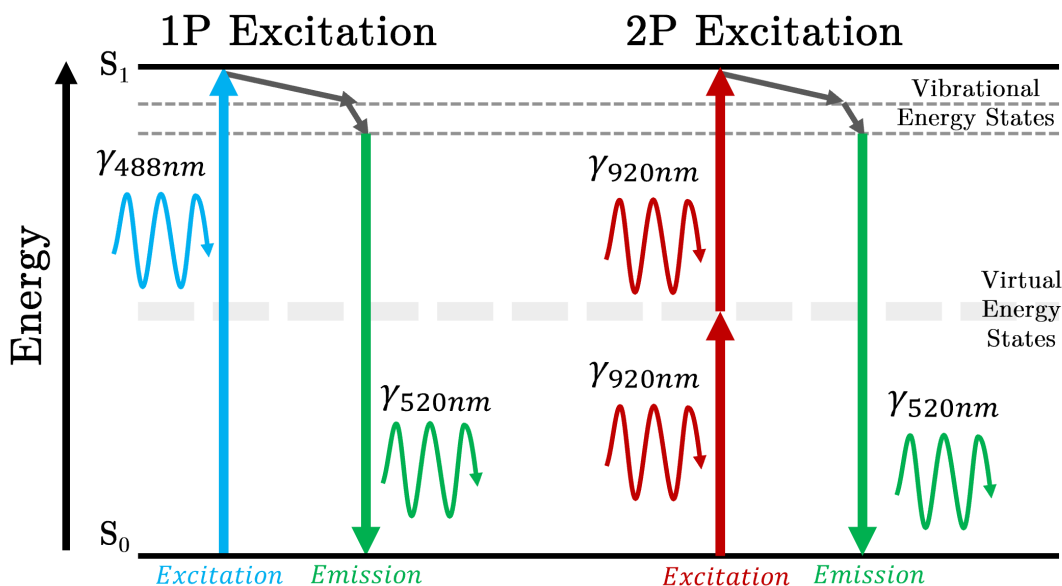


Figure 1.2: **Jablonski Energy Diagram**

1P and 2P fluorescence processes are shown in terms of energy exchange between input excitation photons (either one or two), a fluorescent molecule, and released emission photons. The key insight is the spectral difference between the light used to generate the increase in energy state and the emitted photon. 2P excitation is described in detail in Chapter 3.

Cre-Lox system (Sauer and Henderson, 1988) to target excitatory neurons in hippocampal area CA1 by injecting a combination of two viruses. The first being AAV-CamkII-Cre and the second being AAV-FLEX-GFP. In this approach, only neurons that express CamkII, a popular marker expressed primarily by excitatory neurons (Burgin et al., 1990), will be infected with the AAV-CamkII-Cre virus, thus transcribing Cre recombinase. When the Cre recombinase in excitatory neurons interfaces with Lox sites found in all neurons infected with the FLEX-GFP, it induces Cre-mediated recombination, thus generating a functional GFP molecule. Because this condition only exists in cells that are CamkII positive (thus expressing Cre) we generate fluorescence almost exclusively in excitatory neurons. With this strategy, scientists can target particular neuronal subtypes of interest and resolve their structure and function independently of the rest of the network, a serious advantage on other methods like electrophysiology.

In addition, once neurons are able to express a given fluorescent reporter of interest, the protein is maintained over long periods of time, enabling longitudinal studies of cellular responses to learning, physiological damage, or other perturbations (Miyawaki et al., 1999). It is well known that the potentiation of synapses in response to Hebbian plasticity or learning result in structural changes in dendritic spine morphology (Yuste and Bonhoeffer, 2001; Holtmaat et al., 2009). These measurements are made possible by the ability to return to the same imaging field to identify precisely the same dendritic segments across many hours; carefully characterizing slight changes in spine number and volume. Such time-course measurements would likely not be possible using other methods of studying activity or structure in the brain, such as *in-vivo* electrophysiology or electron microscopy. Fluorescent microscopy therefore is a tool which offers the capability to quantify how neural circuits change on the timescales of days, unlike other methodologies.

Despite a high degree of variability, microscopy methods capable of resolving neurons in brain tissue typically feature fields of view (FOVs) in the range of several hundred micrometers by several hundred micrometers. Depending on cellular density and the specifics of the viral strategy being deployed, such imaging areas can contain hundreds of cells of interest, since neurons are only approximately 15 $\mu\text{m}$  - 30 $\mu\text{m}$  in diameter on average. Because of this difference, optical imaging makes it possible to resolve and quantify dynamics from hundreds of neurons of interest at once, making it a very efficient and high throughput method for studying neural circuit activity in living systems.

## 1.4 Genetically Encoded Activity Indicators: Why $\text{Ca}^{2+}$ ?

Neurons communicate through rapid electrical impulses known as action potentials (Hodgkin and Huxley, 1952). Rapid fluctuations in electrical potential used for transmitting information exist only across the cell membrane, and rapidly propagates from the axon hillock region (typically) down the axon, resulting in presynaptic vesicle release that conveys salient information to postsynaptic neurons. During this elaborate, millisecond

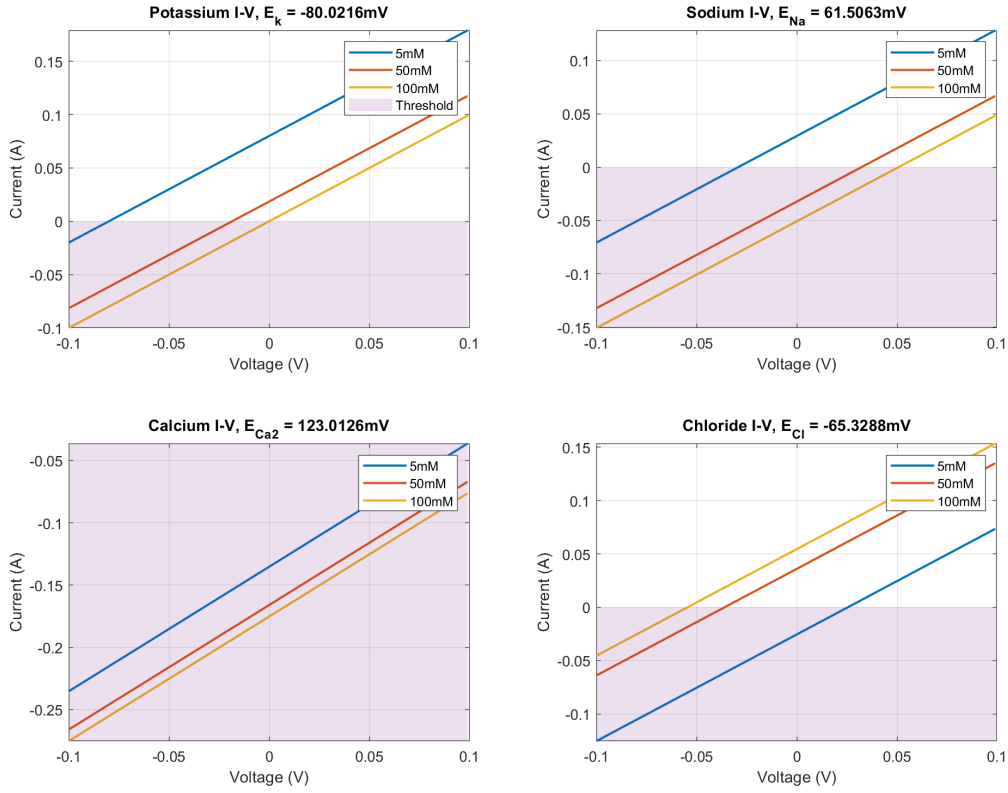


Figure 1.3: **Equilibrium Potentials and I-V**

Current - Voltage relationship for the four main neuronal ions given by the Nernst Equation at various extracellular concentrations.

time scale process, voltage-gated ion channels open, allowing extracellular ions to flow into or out of the cell body, following natural diffusion gradients. The kinetics of these dynamics are dictated not only by the difference in intracellular and extracellular concentrations as described by the Nernst Equation:

$$E_{\text{rev}} = \left( \frac{R \cdot T}{z \cdot F} \right) \cdot \ln \left( \frac{[X]_{\text{extracellular}}}{[X]_{\text{intracellular}}} \right) \quad (1.2)$$

but also by the equivalent resistance and capacitance properties of the neuron (Hodgkin and Huxley, 1952).  $E_{\text{rev}}$  = Reversal potential,  $R$  = Universal gas constant,  $T$  = Temperature (in degrees Kelvin),  $z$  = ion charge,  $F$  = Faraday's constant,  $[X]_{\text{extracellular}}$  = Extra-cellular concentration of ion X, and  $[X]_{\text{intracellular}}$  = Intra-cellular concentration of

ion X. Equilibrium potentials can be calculated for a variety of voltage and extracellular ion concentration conditions, shown in Figure 1.3. In this case, the equilibrium potential has been calculated for the four main ions in a variety of conditions. Critically, it can be seen that a large negative current exists particularly for calcium, mainly because of an extremely low intracellular concentration. As a result, a large driving force exists for calcium (stronger than other ions), and accordingly, it rushes into the cell during action potentials following the opening of voltage-gated calcium channels (Hodgkin and Huxley, 1952). Once inside the cell, free calcium ions act in a number of critical ways, but one central mechanism is binding to calmodulin (CaM) that acts in the CAMKII pathway which has been shown to be critical for synaptic plasticity and learning (Silva et al., 1992). Researchers have leveraged this calcium-calmodulin binding to generate genetically-expressed fluorescent reporters of neuronal activity, known as GECIs (Tian et al., 2009). These come in many different varieties, but for the sake of consistency with Section 1.2, we will consider GCaMP, which is a GFP-derived calcium indicator (Tian et al., 2009). GCaMP fluorescence efficiency is modulated by the presence of calcium in a conformational change dependent fashion, meaning when calcium binds to the CaM domain, the GFP portion of the molecule is brought into a more optimal structure to support fluorescence. This ultimately results in a green fluorescent protein which gets brighter whenever it binds to free calcium, assuming constant illumination conditions (Tian et al., 2009). Since we know that intracellular calcium concentration increases rapidly following action potentials, this enables researchers to get a proxy readout on the activity of neurons, by effectively monitoring the intracellular calcium concentration. While this technique, known as calcium imaging, comes with many advantages, it also creates challenges. Since calcium takes substantial time to buffer and pump from cells following action potentials (100s of ms), and the fact that calcium-GCaMP binding takes more time than the underlying voltage signals (slow rise time) the technique isn't suitable for measuring activity in neurons like Purkinje cells or interneurons with high firing rates (Wagner et al., 2017; Doischer et al., 2008). Additionally, since these methods are only



sensitive to calcium concentration, other important electrical signals that exist between neurons such as subthreshold voltage oscillations or excitatory or inhibitory postsynaptic currents (EPSP or IPSP respectively) cannot be measured. For this, faster methods that rely on direct modulation of fluorescent efficiency based on membrane potential are required (Yang and St-Pierre, 2016). We will touch on this in Part II of the dissertation.

## 1.5 Interim Summary

Hopefully through reading this portion of the dissertation, you have been convinced that optical imaging is a critical tool for studying the brain in new and advantageous ways. Viral methods enable the localization of fluorescent reporters to targeted neuronal subpopulations, which can then be studied with fluorescent microscopy in large cell numbers (depending on density and viral strategy) across multi-day timescales. Calcium indicators that are genetically encoded enable researchers to investigate how these neural populations represent information, function during complex tasks, and change over time with learning. Few other methods lend themselves quite as well to studying the way key subpopulations of cells change in the brain as a function of experience or disease state.

## CHAPTER 2

### 1P Excitation Imaging in Neuroscience

#### 2.1 Core 1P Microscopy Ideology

The fluorescent physical process described in section one is the core operating principle of single photon (1P) imaging. In general, any single photon that is provided to the sample contains enough energy, on its own, to induce a fluorescence event. Such microscopy systems manifest typically in the form of a visible light source (usually a light emitting diode (LED), visible continuous wave laser, or arc-lamp), spectral filters and dichroic beamsplitters, focusing optics like an infinitely-conjugated objective assembly, a image forming tube lens, and an array detector such as a Complementary Metal-Oxide-Semiconductor (CMOS) image sensor. The majority of 1P microscopy systems can be decomposed into two main subsystems, one that generates appropriate photoexcitation into the sample, and one for collecting the fluorescent emission provided by the protein of interest.

##### 2.1.1 Example 1P Microscope Setup and Operational Principles

In the example of a 1P microscope used for GFP imaging, a visible, blue LED of  $\approx 470\text{nm}$  wavelength would be collimated using a short focal length aspheric lens, then spectrally filtered with an excitation filter to remove frequency components outside of a desired pass-band. An excitation filter that is centered at 470 nm with a bandwidth of  $\pm 20\text{nm}$  would be suitable for this purpose. The light would then pass through a simple lens before being reflected on a dichroic mirror. This spectral beam splitter is critical to the operation of the microscope and serves to separate the excitation light (via reflectance)

from the collected fluorescence (via transmission). As such, the dichroic requires specific consideration, and something on the scale of the T495lpxr from Chroma would work nicely. The excitation light will reflect off the dichroic mirror, then enter an infinitely conjugated objective assembly, with the simple lens having focused the light onto the rear pupil plane of the objective. In this configuration, the excitation light being emitted from the objective, into the brain, will intentionally not be focused to a single point, rather it will illuminate the entire focal plane in a wide-field manner. However, because each 470nm photon used for photoexcitation contains enough energy to locally generate a fluorescent event in any GFP molecule it experiences, there is a considerable amount of background fluorescence generated above and below the focal plane of interest. This additional fluorescence contributes background and limits resolution, especially in dense neuronal populations. The fluorescence that is generated will be collected over a fixed numerical aperture (NA) as defined by the objective lens. The equation for numerical aperture is as follows:

$$NA = n \sin \theta \quad (2.1)$$

where  $n$  is the refractive index of the medium in which the lens is working,  $\theta$  is the half-angle of the maximum cone of light that can enter or exit the lens. Once fluorescence is collected, it is transmitted through the dichroic mirror, before being further spectrally filtered with an emission filter. A filter centered at 520nm with a bandwidth of  $\pm 20$ nm, or alternatively a longpass filter beyond 500nm would be suitable. Following spectral filtering, the light that came only via fluorescent emission is then focused by a tube lens to form an image onto an 2D image sensor. The optical resolution of a diffraction limited 1P imaging system depends strongly on numerical aperture, and scales as the following:

$$R_{lateral(1P)} = \frac{\lambda}{2 \cdot NA} \quad (2.2)$$

$$R_{axial(1P)} = \frac{2 \cdot \lambda}{NA^2} \quad (2.3)$$

This is on the assumption that the camera system and effective pixel size in the sample follows Nyquist sampling, which is typically the case in high-magnification imaging systems, but is less common with low magnification arrangements that seek to resolve very large fields of view. These intrinsic optical limitations describe the optical Point-Spread Function (PSF) which is the extent to which a single point-source is spread across a detector as a result of the fixed size of the lenses in the optical system and the laws of electromagnetism. The fixed lens diameter limits the maximum spatial frequency content captured by the system, and thus results in low-pass filtering of the object in the Fourier domain. NA and WD parameters are closely linked to one another through geometry, as described in Figure 2.1.

To further demonstrate the relationships between numerical aperture and resolution, two imaging simulations were conducted, of optical systems resolving a 1D periodic grating with spatial frequency of 1 linepair/ $\mu\text{m}$  in two different NA conditions, 0.15 and 0.8. The “Impulse Response” shows the 2D PSF and a corresponding cross-section through the center shows the “Coherent PSF.” The goal of the simulation is to show the loss of resolution with lower NA for a given wavelength, of a fixed sample, magnification, and wavelength.

## 2.2 Advantages and Disadvantages of 1P Microscopy

These singly photon microscopes are advantageous for many reasons, mainly in their ease of assembly, low cost, and accessibility. However, because each excitation photon provides enough energy to generate a fluorescence event, out-of-focus background is high due to a lack of optical sectioning (we will describe optical sectioning in detail in section 3). Additionally the short wavelengths of visible light used in 1P microscopy generally (470nm

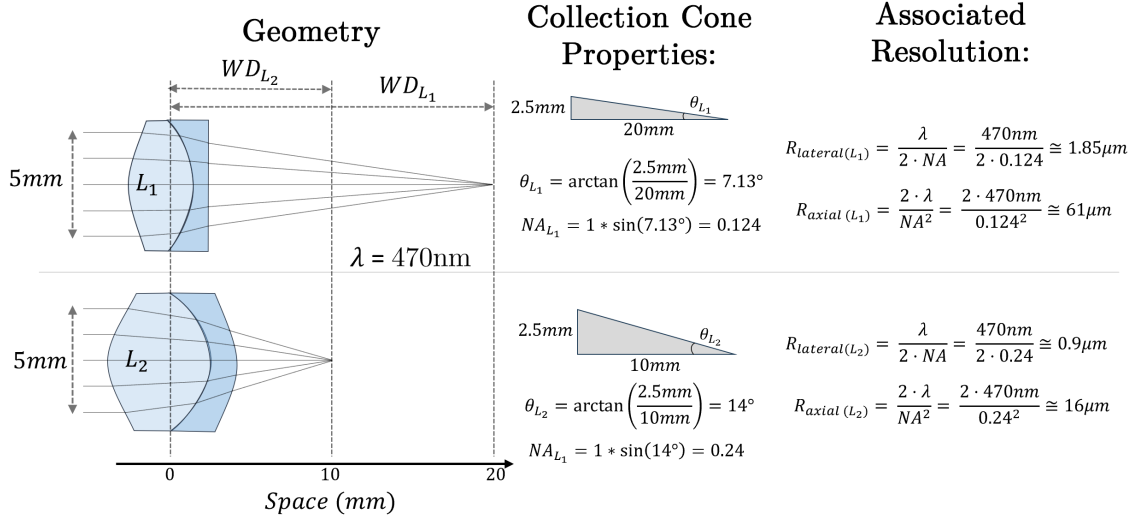


Figure 2.1: **General Properties of Numerical Aperture, Working Distance, and Resolution Interdependencies**

Two doublet lenses of identical diameter, with different numerical apertures. Lens 1 forms a focus at 20mm, which is associated with a 7.13 degree cone angle, and thus an NA of 0.124. Lens 2 however focuses in half that distance (half the focal length), and thus has twice the NA for the same input beam diameter. This ultimately results in a scaling of resolution that is linear in the lateral dimension, but quadratic in the axial dimension.

in our example) scatter through tissue much more severely than longer wavelengths, as Rayleigh scattering is a wavelength dependant process that scales as:

$$\sigma_s \propto \frac{1}{\lambda^4} \quad (2.4)$$

where:  $\sigma_s$  is the scattering cross section, and  $\lambda$  is the wavelength of the incident light. As such, blue light of 470nm scatters through a given material 16x more than near infrared (NIR) light of twice the wavelength, 940nm. This will become important in the next section when we discuss two-photon (2P) methods. Lastly, wide-field 1P microscopy relies on solid-state area-detectors to collect information from the entire two dimensional focal plane, essentially at once (in accordance with readout times, rolling vs. global shutter, etc.), without displacing or otherwise manipulating the excitation light. As a result, many of these systems are primarily temporal bandwidth-limited by the camera that is being

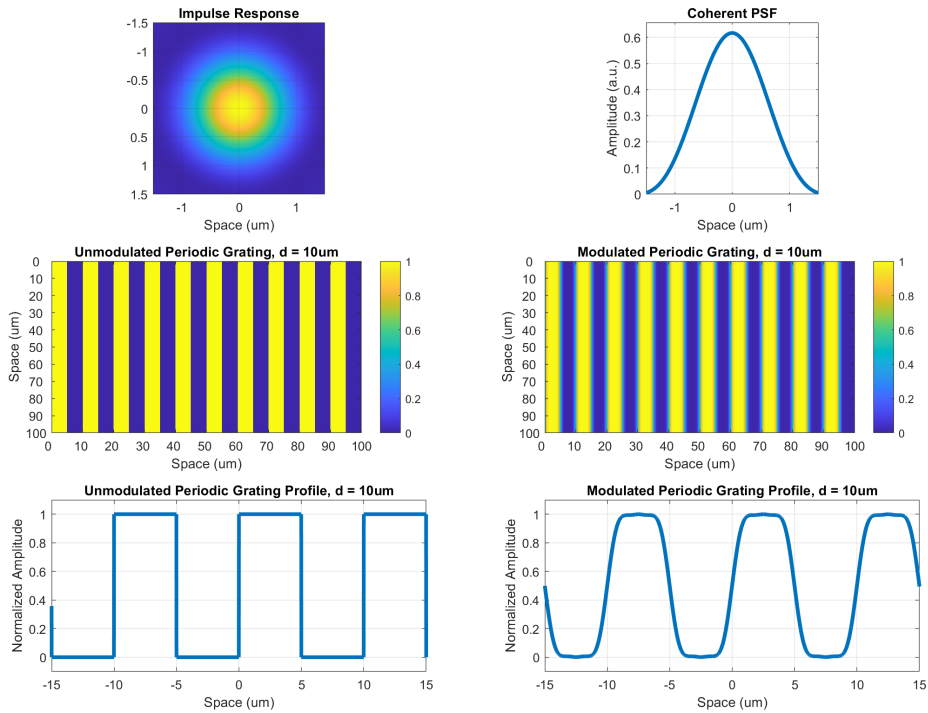


Figure 2.2: **Imaging Simulation at 0.15 NA**

The unmodulated periodic grating is convolved with the impulse response (PSF) thus resulting in a significantly filtered and blurred version of the grating shown on the right.

used and the irradiance levels supplied to the sample. As a result, 1P microscopes can be exceptionally high speed, making the capture of rapid dynamics, such as the beating of a zebrafish heart, flow of individual blood cells in vessels, or ms-scale membrane potential variations possible. In fact, a benchtop 1P microscope system designed to resolve voltage dynamics *in-vivo* over large fields of view is included in this dissertation and formally presented in Chapter 10.

### 2.3 Interim Summary

All together, 1P microscopy is a critical research tool that holds many advantages, along with some optical disadvantages. They are straightforward to assemble, relatively low cost, easy to operate, and very high speed in some cases. However, because of the 1P fluorescent

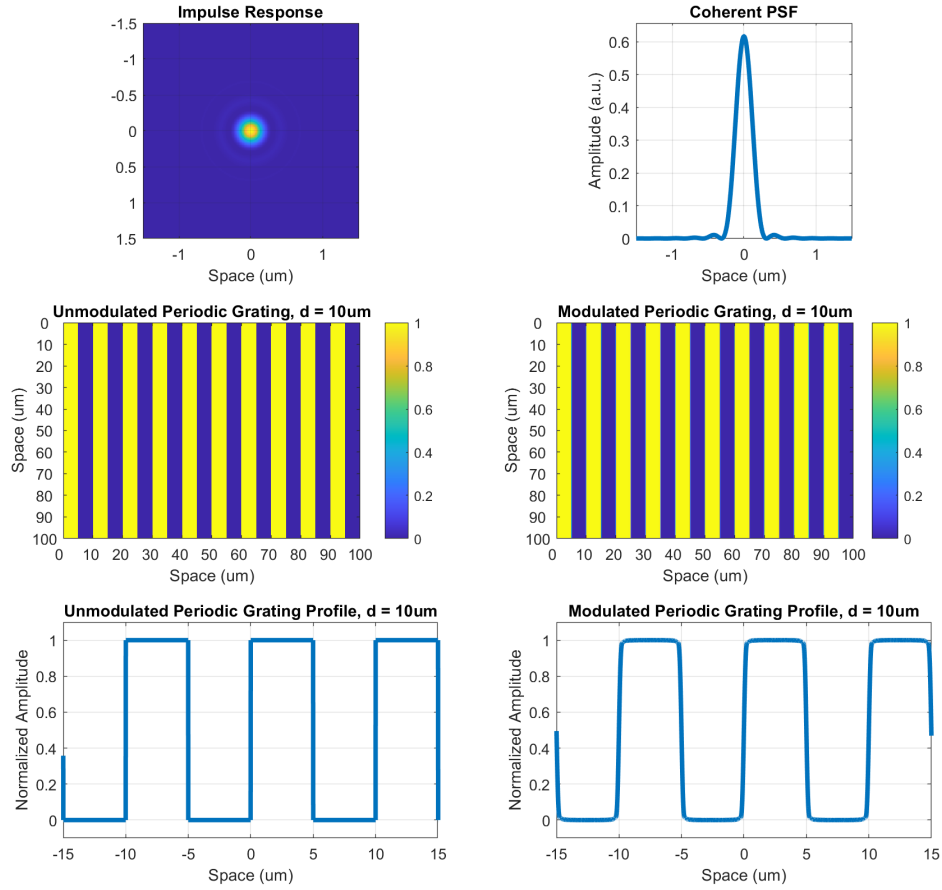


Figure 2.3: **Imaging Simulation at 0.8 NA**

The unmodulated periodic grating is convolved with the sharper impulse response (PSF) thus resulting in a far less filtered, sharper version of the grating shown on the right.

process, resolution is limited due to scattering and the lack of optically constraining where the fluorescence is generated. In the following section, we will describe 2P microscopy, which solves some of these optical challenges, at the cost of a more complex and expensive assembly.

## CHAPTER 3

### 2P Excitation Microscopy in Neuroscience

#### 3.1 Core 2P Microscopy Ideology

Multiphoton absorption is another natural process that generates fluorescence, which relies on the nearly simultaneous absorption of more than one photon. However, in nature this process is much less frequent. In the example of rhodamine-B from earlier, where 1P fluorescence is generated roughly once every second in bright sunlight, a 2P process would occur once every 10 million years (Denk and Svoboda, 1997). As such, special optical geometries are required to create 2P excitation in a controlled and predictable way.

Where 1P microscopes use LEDs, lasers, or arc lamps as their visible light sources, two-photon microscopes rely on NIR lasers which emit ultrafast optical pulses of light, composed of photons with roughly half the energy of photons used 1P setups. Such microscopes classically used titanium-doped sapphire (Ti:Si) lasers that are tunable in output wavelength, and emit pulses generally on the scale of 100fs (1e-13s). For perspective, within the time of a single laser pulse, light, the fastest thing in the universe, can only move forward by  $c * 1e-13s = 0.3\mu\text{m}$ , roughly 1/50<sup>th</sup> the diameter of an average neuron. Ti:Si lasers usually emit pulses with a repetition rate of  $\approx 80\text{MHz}$ , making the duty cycle  $(80\text{MHz} * 1e-13s) / 1s = 8e-6$  meaning the laser is outputting 100fs pulses only 0.0008% of the time. To better understand the mechanisms of generating ultrafast pulses, simulations of the interactions of 200 frequency components in a gaussian distribution (top image, blue curve) centered around 920nm, propagating in a laser cavity were conducted. As you can see, with sufficient frequency bandwidth, the individual oscillation modes (middle



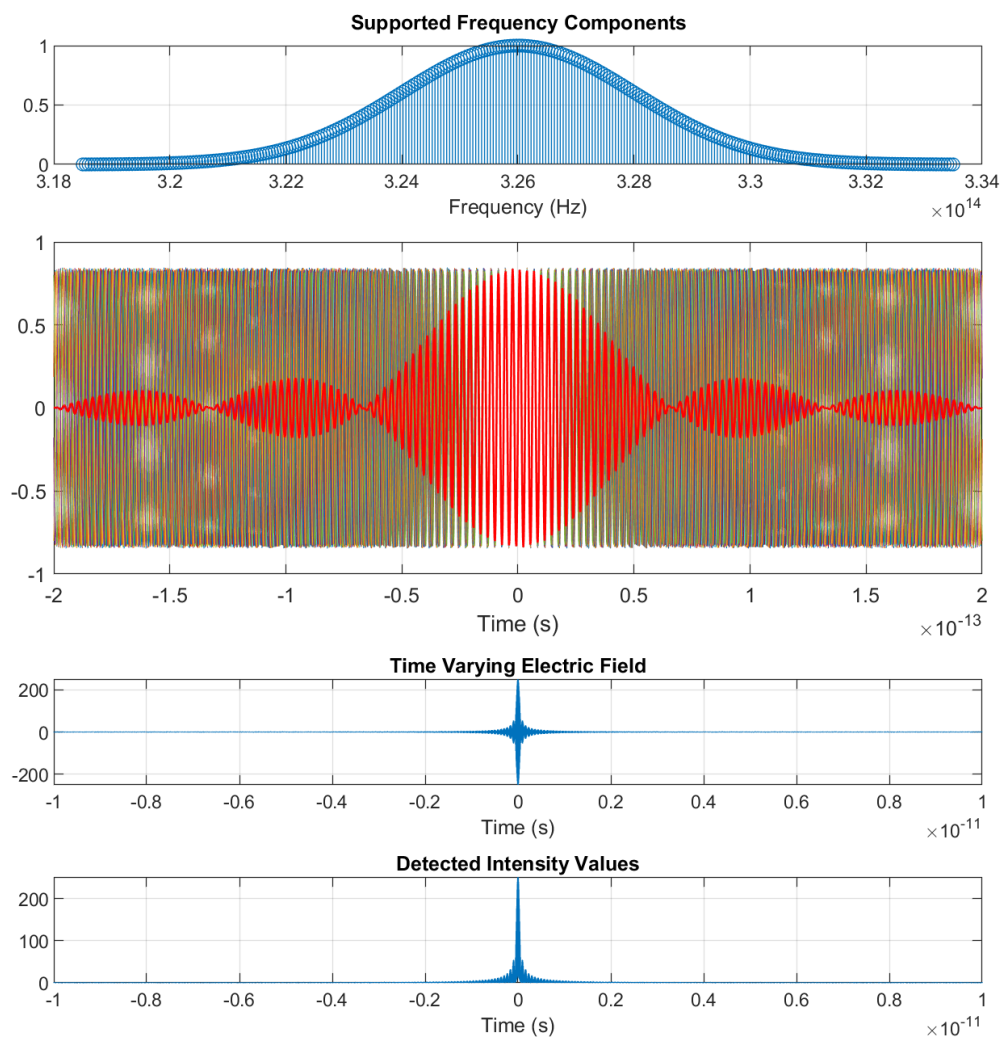


Figure 3.1: **Simulated 2P Optical Pulse Generation**

A superposition of 200 frequency components centered about the 326THz range (corresponding to 920nm wavelength) with a  $\pm 10$ nm bandwidth giving rise to rapid optical pulses approximately 100fs in pulse width.

graph, many colors) are able to interact with one another and give rise to ultrafast periods of time with very large field amplitudes within a  $\approx 100\text{fs}$  range (shown in red) through constructive and destructive interference. The electric field distribution over time is shown below (in isolation) as well as the Intensity distribution of the pulse over time (bottom).

More recently, fixed frequency, non-tunable lasers have been developed that rely on fiber optic resonators to generate similar optical pulse properties at a fraction of the cost and complexity (Srinivasan and Yildirim, 2023). As we will discuss, these ultrafast lasers are necessary to generate the nonlinear 2P absorption needed in multiphoton microscopy applications, in an efficient way which does not disrupt the underlying biology. Since each individual photon contained in the pulse contains approximately half the energy of those used in 1P excitation, the fluorescent process relies on the near simultaneous absorption of two photons by the same molecule, hence the “2P” designation. In the case of GFP, the energy of two 940nm photons need to add together at essentially the same instant, allowing the molecule to transition from ground to the fully photoexcited state. This fundamental difference manifests as fluorescence that is proportional to photon flux, rather than as a purely power-dependent process. As such, 2P microscopes traditionally constrain all of the excitation light to a single tiny volume in accordance with the excitation NA, where the spatiotemporal concentration of NIR excitation photons is intentionally extremely high. The minimum dimensions of this excitation volume are constrained by the diffraction limit (without additional complexity) and thus define the resolution and efficiency of the 2P microscope. The diffraction limit equations for a 2P microscope of NA less than 0.7 (as is the case for the microscope described here) are approximately:

$$R_{l2P} = (2\sqrt{\ln 2}) \cdot \left( \frac{\lambda \cdot 0.320}{\sqrt{2} \cdot \text{NA}} \right) \quad (3.1)$$

$$R_{a2P} = (2\sqrt{\ln 2}) \cdot \left( \frac{\lambda \cdot 0.532}{\sqrt{2}} \right) \cdot \left( \frac{1}{n - \sqrt{n^2 - \text{NA}^2}} \right) \quad (3.2)$$

Where  $R_{l2P}$  is the lateral resolution and  $R_{a2P}$  axial resolution (Lees et al., 2024). Assuming an excitation NA of 0.5 at a 940nm wavelength, the resolution would be  $\approx 0.8 \mu\text{m}$  laterally and  $\approx 6.5 \mu\text{m}$  axially, resulting in an ellipsoid volume of  $\approx 110 \mu\text{m}^3$ , or 110fL, roughly 125x smaller than the volume of a 15  $\mu\text{m}$  diameter neuron. To image neural tissue, average powers on the scale of  $\approx 50\text{mW}$  are needed, which when confined to a single 100fs pulse, result in absurd peak powers of  $\approx 6.25\text{kW}$  distributed within the minute 110fL volume. The energy contained within a single pulse can be described as:

$$E_{\text{pulse}} = \frac{p_{\text{av}}}{f_{\text{rep}}} = \frac{50 \text{ mW}}{80 \text{ MHz}} = 6.25 \times 10^{-10} \text{ J/pulse} \quad (3.3)$$

$$\text{Photons}_{\text{pulse}} = \frac{E_{\text{pulse}}}{h\nu} \approx 3 \times 10^9 \text{ photons/pulse} \quad (3.4)$$

The number of total photons per pulse is  $\text{Photons}_{\text{pulse}}$ , which is confined within a diffraction limited 110fL volume. When considering the volumetric power density  $\Phi$  during a single 100fs pulse, contained within the excitation volume, you arrive at:

$$\Phi = \frac{\frac{E_{\text{pulse}}}{100 \text{ fs}}}{110 \text{ fL}} \approx 5.6 \times 10^{13} \text{ mW/mm}^3 \quad (3.5)$$

These extremely spatiotemporally concentrated instants of very intensity excitation light are by design, in order to maximize the probability with which a single fluorescent

molecule absorbs two photons almost instantaneously. 2P conversion efficiency is inherently related to the 2P cross section  $\sigma$  and quantum yield  $\phi$  of the fluorescent molecule and scales quadratically with excitation intensity  $I$ :

$$P = \sigma \cdot \phi \cdot I^2 \tag{3.6}$$

Up until now, we have described focusing the NIR laser to a single point in space, generating fluorescent events from only one 110fL volume via a multiphoton absorption-based process. In order to form a 2D image in the brain, that point of light must be translated across a focal plane, over time. To accomplish this, 2P microscopes typically employ resonant scanning mirrors and galvanometric scanning mirrors (galvos) which angularly displace the input laser beam in time following a raster scan pattern. Resonant mirrors oscillate only at a single sinusoidal frequency, corresponding to its resonant frequency ( $\approx 8\text{-}16\text{kHz}$ ), unlike galvos which can be driven according to an arbitrary waveform, within a more limited bandwidth ( $\approx 1\text{kHz}$ ). Since resonant scanners are typically able to displace the laser spot faster than galvos can, they usually control the “fast axis” of the raster scan (along the x axis), while a galvo scanner controls the “slow axis” following a sawtooth waveform which moves linearly from the top of the frame to the bottom (along the y axis). As a result, 2P microscopes build images as a function of time, rather than flood-illuminating the entire image field at once, as is done with 1P microscopy. This excitation focal volume is translated using scanning mirrors which build up 2D image planes over time.

As a result of displacing a single volume of photoexcitation in the brain over time, 2P microscopes can make use of highly sensitive photon detectors, rather than more conventional 2D image sensors used in 1P methods. Historically, photomultiplier tubes (PMTs) traditionally used in particle physics have been repurposed to detect signals from 2P microscope systems because of their high gain, ns rise times, low noise, and ability to quantify even single photons, as a result of current multiplication via multiple dynode stages. However, such devices are expensive, typically require kV photocathode bias

voltages, and are prone to degradation and damage over time. More recently researchers have used Si-based detectors manufactured according to a CMOS process which are nearly as sensitive to incident photons, but far more robust, easier to drive, and two orders of magnitude less expensive (Modi et al., 2019).

### 3.1.1 Example 2P Microscope Setup and Operational Principles

Like 1P systems, a standard 2P microscope is composed of an excitation subsystem and an emission subsystem. The excitation portion of the microscope begins with an ultrafast laser source, such as a fixed frequency 920nm laser, emitting 140fs pulses at a 60MHz repetition rate. From here, the laser can be expanded to suit the clear aperture of the scanning mirrors, using a fixed or variable beam expander. From here, the beam reflects off a set of two scanners placed in close proximity, one resonant (8kHz) and one galvo, to control position of the focal volume in two dimensions on the image plane. Following the reflection off these scanners, the light typically passes through a scan lens set (placed one focal length away from the scanner set) which is optimized to generate a flat focal field across the full range of possible scan angles. After the scan lens, the laser passes through a tube lens, placed at the sum of its focal length and the focal length of the scan lens, which re-images the surface of the scanner mirrors onto the rear pupil of the objective in a 4F configuration (Chaigneau et al., 2011). Following the tube lens, a specialized 2P dichroic is used, which reflects the NIR laser, but transmits visible fluorescence. The laser is directed into the objective by the dichroic mirror, making sure that the image of the scanning mirror is focused onto the rear pupil of the objective lens, and the entire rear aperture of the objective is filled with laser light, in order to maximize the excitation numerical aperture of the system, and thus, image resolution and 2P conversion efficiency. After 2P absorption takes place and GFP emits fluorescence, the system uses its emission subsystem to direct and filter the collected light onto the detectors. First, the objective collects that light over the full NA, transmits it through the dichroic beamsplitter and a NIR blocking filter, and onto a short focal length collection lens. This lens then directs the

fluorescent signal onto a PMT or SiPM where it is digitized and transmitted to downstream electronics. In general, the emission subsystem of any 2P microscope should take care to minimize the overall path length between the specimen and the detector as much as possible, in order to collect the most scattered light as possible.

### 3.2 Advantages and Disadvantages of 2P Microscopy

2P microscopes hold clear optical benefits that are particularly advantageous for resolving signals in brain tissue. Because they use NIR wavelengths for photoexcitation, the amount of scattering experienced by an excitation photon is approximately 16x less than in 1P systems (Helmchen and Denk, 2005). This manifests in the fact that 2P microscope systems can resolve fine structures, even hundreds of micrometers into brain tissue, while 1P systems are limited to only  $\approx 75\mu\text{m}$  -  $100\mu\text{m}$  in depth. Additionally, since fluorescence is only generated from one diffraction limited volume/time, the photodetector can integrate all the scattered fluorescence into a single brightness value corresponding to a single position, which is independent of the next pixel position, thereby improving signal to noise ratio (SNR) in scattering conditions. Additionally, since the 2P absorption process is inherently related to irradiance (and not simply power as is the case in 1P) the system generates photoexcitation only from a tiny volume, rather than a widefield column. This effect is known as optical sectioning, since 2P systems do not induce significant photoactivation of fluorescent molecules  $R_{a2P}/2$  above or below the focal plane. As a result, 2P imaging can record from dense, strongly-labeled populations by restricting the depth within which photoexcitation occurs, often less than the diameter of a single neuron. Lastly, despite the high irradiances needed for 2P imaging, the amount of photobleaching induced by 2P microscope systems is significantly lower than that incurred from 1P imaging (Helmchen and Denk, 2005), making imaging for long time periods possible even when reasonably large amounts of excitation power are required. However, 2P imaging systems are significantly more complex and rely on far more expensive hardware compared to 1P microscopes. Ultrafast lasers, scanning mirrors, specialized electronics, and sensitive photodetectors

present substantial barriers to entry for neuroscientists, and as such there is a need to make these systems more accessible. Additionally, 2P microscope frame-rates are defined by the frequency of the “fast-axis” and number of bidirectional lines that are resolved in a single frame, resulting in modest sampling rates of approximately 30Hz. Thus, resolving dynamics from faster physiological phenomenon (such as individual action potentials with voltage indicators) is difficult when trying to maintain a reasonable field of view. Lastly, unlike 1P systems, 2P microscopes are sensitive to pulse broadening due to dispersion, which accumulates with the thickness of the glass elements installed in their optical trains(Helmchen and Denk, 2005). Because of this, adding new elements or making substantial changes to the optical design can impact the pulse width, and thus performance of the 2P microscope. Such dispersive effects would ideally be compensated using additional optics, making the entire assembly even more complex and expensive.

### 3.3 Interim Summary

Multiphoton microscopy is a key method for studying neural circuit structure and function *in-vivo*, although it comes at a higher cost and increased complexity compared to 1P microscopes. Because 2P systems hold several optical advantages in terms of scattering through tissue and optical sectioning ability, they can address scientific questions that 1P systems can not. However, these microscopes are expensive, sensitive to dispersion, and complex, ultimately meaning they fall outside the reach of many labs. Also, while these systems are well suited for imaging at moderate frame-rates of  $\approx 30\text{Hz}$ , there are no clear methods to effectively speed them up for resolving high speed dynamics. As a whole, 2P microscope systems are effective tools for answering important neuroscientific questions. They hold the same inherent advantages (as an imaging technique) as 1P systems, but with key additional utility that comes at the cost of expense and complexity.

## CHAPTER 4

# Miniature Microscopy: The Logic in Making Large Systems Small

One of the major goals in neuroscience is to understand and explain how natural behaviors arise from complex patterns of neural activity. To do so, the field has relied on genetically encoded calcium indicators and the large 1P or 2P microscopes described above to record dynamics of large cellular populations in the brain during behavior. However, due to the size and complexity of traditional, benchtop optical systems, these experiments have necessitated the immobilization of the animal under the microscope during recording sessions. In turn, this imposes limitations on the scope of testable and naturalistic behaviors that can be studied, such as spatial navigation or social interaction. Researchers have turned to developing virtual reality (VR) systems that display visual information which updates as a function of the animals locomotion on a treadmill or 2D ball. While these VR-based systems certainly add utility to the range of experimental conditions that are testable, they still alter neural representations through the lack of vestibular inputs (Acharya et al., 2016) and restrict the overall scope of testable behaviors.

To circumvent these scientific limitations, engineering solutions were developed. One-photon miniature microscopy serves as a means to optically resolve neuronal population activity in mice while allowing the animal to freely move, participate in naturalistic behaviors, and engage in previously validated behavioral assays. A freely behaving animal receives inputs from the vestibular system and is without the stress of head-fixation – two factors which result in recording of neural dynamics that are free of the experimental



confounds which come from immobilization. While one-photon miniature microscopes have been instrumental to numerous scientific advancements in the neuroscience field, they have critical limitations due to the scattering of light through tissue.

## 4.1 1P Miniature Microscopes and the UCLA Miniscope Project

Single-photon epifluorescent miniature microscopes are important tools that have generated numerous neuroscientific advancements for more than a decade. Such microscope systems enable researchers to image neuronal activity from large populations of cells during naturalistic free behaviors in mice and rats, without the restraint of head fixation imposed by traditional benchtop microscopes.

Pioneering work from (Ghosh et al., 2011) realized the miniaturization of 1P microscopes for freely behaving mice, however the designs were not open to the community making replication difficult. The resulting commercial entities that were developed in recognition of the applications of the technology began selling commercial products that were exceedingly expensive and outside the financial range for many groups despite a large amount of demand and research utility. In response to this need in the neuroscience community, the UCLA Miniscope project was created by P. Golshani, A. Silva, and B. Khakh, with instrumental developments from D. Aharoni, to build, use, and share low-cost, open source miniature microscopes that the community could easily adopt and build on top of. Since 2016, the UCLA Miniscope project has designed, developed, and disseminated such 1P miniscopes for the neuroscience community, resulting in thousands of systems being used across hundreds of labs worldwide. These microscopes have been instrumental in studying neuronal dynamics underlying complex naturalistic behaviors ranging from social interactions in autistic models, to dominance behavior, to spatial navigation deficits following epileptic seizures. Due to the open-source nature of the project, dozens of spin-offs have been generated from labs across the world which are specialized for unique applications such as recording activity from zebra-finches or freely

flying bats, thus maximizing overall scientific utility.

While miniature 1P microscopy holds many positive attributes in terms of ease of dissemination, low cost, and straightforward adoption, it holds the same limitations as its larger benchtop counterparts discussed earlier. Since 1P epifluorescent systems generally lack optical sectioning abilities and suffer from increased scattering in neural tissue, resolution and maximum imaging depth are limited compared to multiphoton modalities. As a result, miniature 2P microscopes were designed and built, which are able to circumvent many of these optical limitations, thereby making new scientific questions addressable.

## **4.2 Miniature Microscopes Using More than One Photon, a (not so) Brief History**

### **4.2.1 Foundational 2P Miniature Microscopes in the literature**

Miniature 2P microscopes were demonstrated as early as 2001 by Fritjof Helmchen and Winfried Denk while working at Bell Labs (Helmchen et al., 2001). The microscope weighed  $\approx 25\text{g}$  and was used to resolve capillary blood flow and calcium transients in freely moving rats. In order to accomplish this, the microscope relied on several innovative components, such as a piezoelectric driver to move the distal end of a single-mode optical fiber into a 2D lissajous scan profile (shown in (Delaney and Harris, 1995), originally described by (Lissajous, 1857)). Although the researchers used a grating pair to compensate for group-velocity dispersion, they were limited to 1ps pulse lengths due to non-linear power dependent self-phase modulation (SPM) effects occurring within the optical fiber at transmission powers  $> 10\text{mW}$ . They also were limited in temporal resolution as the mechanical resonance frequency of fiber oscillations occurred below 1kHz, resulting in 2D frame rates of approximately 2 Hz, thus making imaging of cellular activity not possible. Instead, line-scans were used to quantify calcium events in dendrites in head-fixed rats under anesthesia. In addition, this microscope also featured a PMT mounted directly

onto the headpiece itself, thereby resulting in high collection efficiency at the expense of additional weight. Despite some of the technical limitations, this groundbreaking work from more than 20 years ago set the stage for future developments in the space of miniature 2P microscopy and laid an important foundation that indeed it is possible to resolve neural activity *in-vivo*, using multiphoton miniscopes.

In 2009, Winifried Denk and Jason Kerr published a head-mounted 5.5g 2P microscope with the critical added capacity to resolve neuronal activity in awake, freely moving rats (Sawinski et al., 2009). This design made use of a polarization maintaining optical fiber in order to limit the bending-induced fluctuations in 2P absorption efficiency, which proved to be a practical problem with the earlier design. Researchers also replaced the onboard PMT with a high-NA large core optical fiber to transmit the collected fluorescence to remotely positioned PMTs and fluorescence filters, thereby reducing overall system weight at the expense of reduced signal collection efficiency. Scanning was accomplished using a nonresonant fiber scanner, enabling frame rates to be increased to  $\approx 11$  Hz due to slight shifts in drive frequency and using lower pixel counts (64 x 64 pixels) per image frame. Despite having a limited field of view (not explicitly described, approximated as  $\approx 100\mu\text{m}$  x  $100\mu\text{m}$  based on Figure 3) the microscope resolved calcium transients from multiple cells while the rat moved through a semi-circular environment. This was a pivotal moment for 2P miniature microscopes as it demonstrated the ability of such systems to quantify neuronal signals from freely behaving animals.

Around the same time, Wibool Piyawattanametha and Mark J. Schnitzer designed a 2.9g miniature 2P microscope for imaging neocortical vasculature in mice (Piyawattanametha et al., 2009). While this system was unable to resolve calcium dynamics *in-vivo*, it made two critical contributions to the field. The first was the use of a custom-made 2D Micro-Electrical-Mechanical-System (MEMS) scanning mirror to translate the light across a 2D frame, in place of the piezoelectric methods that rely on actuating the end

of an optical fiber. The MEMS-based scanning system used here can be controlled at an arbitrary scan frequency (within bandwidth) resulting in greater experimental flexibility and likely increased experimental durability. Secondly, this system sent the laser light to the microscope using a hollow-core photonic bandgap fiber optic. This component, critically, enables the ultrafast laser pulse to propagate primarily through air, in place of solid glass, resulting in minimal group velocity dispersion and self-phase modulation. The researchers did not even use pulse precompensation optics in their method (at 800 nm excitation wavelength) because of the performance of the photonic crystal fiber, however pulse quality after the fiber was never explicitly described. This microscope did not resolve neural activity, but it did utilize two key components which shaped the way the field thought about and constructed miniature 2P microscopes in the future.

It wasn't until 2017 that the 2P miniature microscope field took a large step forward, with the development of a 2.15g 2P microscope from Weijian Zong and Heping Cheng (Zong et al., 2017). This system used new MEMS scanners which were much faster than those used previously, enabling framerates up to 40Hz (for 256 x 256 pixel frames) making the imaging of neural activity possible. The researchers also integrated new hollow-core fibers that were optimized for the transmission of wavelengths that are ideal for photo-exciting GCaMP or other green fluorescent proteins (920 nm) making the experimental utility of the system very high. However, the initial design had only a mechanical means of focusing, and relied on Gradient Index (GRIN) optics to resolve very small FOVs (150  $\mu\text{m}$  x 150  $\mu\text{m}$ ) with prohibitively short WDs ( $\approx 170$   $\mu\text{m}$ ). Additionally, in place of a single optical fiber, fluorescent signal generated by the system was transmitted through a lossy bundle of optical fibers, which limits overall collection efficiency due to low transmittance through fiber bundles. In response to these limitations, the same group substantially improved their design (in most ways) through the fabrication of custom optical assemblies and the integration of an axial scanning system at the expense of roughly twice the weight (Zong et al., 2021). These microscopes weigh  $\approx 4.2\text{g}$  and are able to resolve

FOVs of high experimental utility ( $420\ \mu\text{m} \times 420\ \mu\text{m}$ ) with the capacity to scan axially over a  $180\ \mu\text{m}$  range, at slower frame rates (10Hz for  $512 \times 512$  pixels). While this system addresses many limitations of their previous design, many key elements are withheld from the community, making adoption and replication by others nearly impossible.

Baris Ozbay and Emily Gibson published a 2P miniature microscope design in 2018, which was the first, to my knowledge, to accomplish scanning off of the microscope head-piece (Ozbay et al., 2018). This was done by using a single coherent optical fiber bundle, which was used for both relaying excitation light and receiving emitted fluorescence over a  $240\ \mu\text{m}$  diameter FOV. Such systems are greatly simplified in terms of the mechanical complexity of the head mounted imaging device, however the coherent optical fiber bundle places strong limitations on the optical system overall. Firstly, the resolution of such a system is inherently related to the core diameter and separation distance of each fiber contained within the coherent bundle, resulting in measured resolution of  $2.6\ \mu\text{m}$  laterally and  $9.9\ \mu\text{m}$  axially. Additionally, transmission variability from fiber-to-fiber within the bundle needed to be measured and compensated to restore uniform brightness in images of homogeneous, invariant test samples. Lastly, since the excitation light is propagating through one (or several) solid glass fibers within the bundle, those ultrafast optical pulses are sensitive to group velocity dispersion and self-phase modulation as in (Helmchen et al., 2001; Sawinski et al., 2009). As such, substantial precompensation optics are necessary to recover transform limited pulses at the sample plane, limiting ease of adoption by users.

#### 4.2.2 3P Miniature Microscopes

In 2020, 3P miniature microscopes came onto the scene with work published by Alexandr Klioutchnikov and Jason Kerr (Klioutchnikov et al., 2020) opening up new possibilities to image deep cortical structures like layer 5 neurons in freely moving rats. These microscopes used new hollow core fibers optimized for dispersion reduction at  $1300\ \text{nm}$ , however a multi-prism precompensation setup was still necessary to correct for third order dispersion

which occurred through the new hollow-core optical fiber. The microscope weighs 5g and thus was used to study neuronal activity in freely moving rats, but critically, since the microscope uses 3P excitation, the study of extremely deep structures is possible (up to 1.12mm below cortical surface) over 200  $\mu\text{m}$  diameter FOVs. This system was further optimized by authors in 2022 by increasing the FOV to 300  $\mu\text{m}$  in diameter and reducing the weight to 2g, thus making it possible to apply these miniature 3P systems to freely behaving mice (Klioutchnikov et al., 2023). Critically, these systems also were the first since (Helmchen et al., 2001) to place an active photodetector onto the miniature microscope headpiece itself. In this case, the authors used silicon-based photomultipliers (SiPMs) on the head of the animal, to directly collect fluorescence without lossy transmission over flexible optical fiber bundles, or with rigid, large diameter solid core fibers. This greatly improves signal collection (especially of highly scattered fluorescence photons deep in the brain) resulting in far more signal for a common excitation input reaching the detector, thus generating higher SNR images. These microscopes represent large contributions to the field and make new recordings of deep structures in the brain possible in freely behaving rats and mice. However, the designs are closed and not made readily available to the community, making replication extremely challenging. Additionally, some of the specialized hardware, such as the low repetition rate, high power 3P laser, is extremely expensive and outside the reach of many labs. As such, the applications and utility of these 3P miniature microscopes remain limited.

### 4.2.3 Current State-Of-The-Art

Perhaps the most influential contribution to multiphoton miniature microscopy came in 2022 when Weijian Zong, May-Britt Moser, and Edvard Moser published a new  $\approx 3\text{g}$  system capable of resolving 420-500 $\mu\text{m}$  x 420-500 $\mu\text{m}$  FOVs even in methodologically challenging brain regions like the medial entorhinal cortex (MEC) (Zong et al., 2022). This microscope represents the third substantial iteration by Zong in the field and holds many advantages. The system was made lighter than (Zong et al., 2021) through the use of a new tunable

lens element assembly which is comprised of a stack of four piezoelectric lens elements operating in series. The introduction of new lenses also enlarged the overall FOV making the microscope more experimentally useful. Critically, these microscopes were also made open-source (for the most part) meaning others could build and design on top of the designs presented. However, specific components, such as the tunable lens assembly, is highly sensitive to alignment and thus necessitate the outside assistance of commercial companies to properly assemble. All the housings are CNC machined from solid PEEK material, making them difficult to produce and expensive. The objective lens assemblies alone contain in some cases 9 optical elements that need to be precisely fabricated and assembled with tight tolerances, making them exceptionally expensive to build by end users and subject to poor performance as a result of even minor misalignments during construction. Additionally, these microscopes also rely on similar fiber bundles (although slightly smaller) as (Zong et al., 2017, 2021) and external PMTs for digitizing fluorescence, and are thus subject to the same corresponding reductions in SNR that come from using photonically lossy fiber bundles. Despite these limitations, the system described in (Zong et al., 2022) is a serious contribution to the field and has inspired many aspects of the system which will be outlined in the rest of the dissertation.

#### **4.2.4 Addressing a clear gap in the field**

Multiphoton miniature microscopes have existed for more than two decades. In that time we have seen tremendous technical advancement in many areas of science, from fiber optic design, to integrated scanning methodologies, optical system configurations, and detection schemes. Extremely capable miniature 2P and 3P microscopes now exist that are able to address many questions in the field, but they each have limitations. Firstly, 2P miniature microscopes from (Zong et al., 2022) are complex, difficult to fabricate, and are composed of many sensitive and expensive optical components. Fabrication of housings and co-linear alignment of many tunable lens elements makes it virtually impossible to fabricate from scratch within a lab, limiting utility for others. Those systems also rely on the external

digitization of weak fluorescent signals from the brain after being transmitted through a lossy fiber optic bundle, resulting in diminished fluorescence collection efficiency compared to local detection methods. 3P systems, such as (Klioutchnikov et al., 2023) have solved some of these issues, at the expense of other parameters and technical aspects. These 3P designs use on-board SiPM detectors to capture fluorescence, but they also rely on low-repetition rate, high power, expensive lasers and almost completely closed, very high NA optomechanical designs to function, making user adoption extremely expensive and difficult. The result is a clear gap in the field, to build an accessible and open source multiphoton miniature microscope with high collection efficiency, at a low cost. The goal throughout the remainder of this section of the dissertation (Part I) is to describe the UCLA 2P Miniscope, designed and fabricated to fill this gap in the field and enable new scientific discovery.



# CHAPTER 5

## Part I: UCLA 2P Miniscope System Development

### 5.1 Initial Versions and Design Trajectory

The system outlined in this chapter is the result of extensive iterative optimization across 49 unique versions of multiphoton miniature microscopes. Some of the incremental revisions were minor, only to change tolerances or alignments between components, while others were fundamental to the architecture of the microscope system. The following section describes the major design revisions and underlying logic associated at arriving at the microscope that will be detailed.

#### 5.1.1 Learning from the Literature

Before constructing a novel optical system, the project began with replicating the work of (Zong et al., 2017), which used an 800 $\mu\text{m}$  diameter scanning mirror, a molded aspheric scan lens, and a multiphoton GRIN lens assembly. The microscope lacked a mechanism to remotely control the focal plane, and the optical FOV was extremely limited. In addition, the WD was approximately the thickness of the glass coverslip used for cranial window implants ( $\approx 100\mu\text{m}$ ) making resolving structures below cortical layer L1 essentially impossible without placing the GRIN directly into brain tissue – certainly not an ideal arrangement for repeated chronic experiments during free behavior. Despite these known limitations, the process of replicating a system that was previously demonstrated in the literature brought tremendous knowledge and experience, making system limitations very

apparent. Through that learning experience, we were able to build a new microscope with capabilities that addressed many challenges we faced directly while imaging. It was clear that we needed a larger FOV, a WD that enabled us to access brain regions of interest, and a way to focus remotely to arrive at a system with significant experimental utility.

### 5.1.2 Innovation by Iteration

With that in mind, we began designing our first versions of a fully custom miniature 2P microscope. Our design targets were as follows:  $750\mu\text{m} \times 750\mu\text{m}$  FOV, a WD of  $720\mu\text{m}$ , an excitation NA of 0.3, and a collection NA of 0.56. These optical parameters became impractical, but regardless we set our design specifications high and did everything we could to achieve them. The first part of the redesign was to consider the scanning mirror, as it defines many parameters of the downstream optical assembly. Initially, we built our microscope around a 2.4mm diameter scanner from Mirrorcle Technologies, that was fabricated within an LCC48 ceramic package. While this package was known to be quite a bit larger than the previous 0.8mm scanners we had used (LCC20 package) we believed the larger beam diameter (and thus excitation NA) the scanner could support was a design trade-off that was worth the incurred weight. We designed custom scan and tube lens assemblies assuming a 2.4mm beam diameter and optimized for a diffraction limited 0.3NA spot in tissue. Additionally, our initial version used a large electro-tunable lens (5.8mm clear aperture) placed between the tube lens and the objective assembly. The large diameter lens was used to ensure minimal fluorescent signal loss on the collection side, as the laser spot was less than half of the clear aperture. This was done for a number of reasons, the first being the consideration that altering the focal power on the excitation side would shift the focal conditions onto the optical fiber bundle we were using, likely changing transmission efficiency. By shifting the focus of both the excitation and emission, we maintain a constant relation to the optical fiber input, which is sensitive to axial misalignment. Doing this resulted in incurring even more weight, and before we knew it

the microscope was substantially heavier than predicted. We were able to achieve all of our optical specifications that we designed for, but the microscope weighed approximately 6.5g, when our goal was closer to 4g. We completed some free behavior experiments with this microscope but determined that it was impeding animal behavior to an unacceptable extent.

We knew the system needed to be miniaturized further, and doing so meant changing the heaviest components, the scanning mirror and tunable lens. The scanner was replaced to the largest diameter model that could fit into an LCC20 package, which happened to be 2mm in diameter. This was certain to impact our excitation NA, and it was predicted to drop from 0.3 to approximately 0.25. While this does not seem like a dramatic reduction in overall NA, it's important to consider that 2P collection efficiency and axial resolution scale quadratically with NA. Regardless, we pressed forward using the 2mm diameter scanner. Simultaneously, we knew that the 5.8mm diameter ETL was simply too heavy for our application, and as a result, we moved to a smaller unit with a 2.5mm clear aperture and placed it only in the excitation beam-path. This was known to generate known issues, as explained above, but we continued in this fashion in order to satisfy perhaps the most important parameter for a microscope that is to be worn on the head of a mouse, weight. This version of the microscope was also constructed and tested carefully. The weight came down dramatically to less than 4g, and the microscope was able to resolve  $800\mu\text{m} \times 800\mu\text{m}$  FOVs, but at the expense of resolution. An excitation NA of 0.25NA is calculated to offer a diffraction limited PSF of  $1.4\mu\text{m}$  laterally and  $24\mu\text{m}$  axially. This greatly diminished optical resolution not only limits the structures visible with the microscope, it also makes the 2P excitation probability far worse. As a result, we were able to successfully resolve some relatively sparse structures in cortex, but large laser powers ( $> 100\text{mW}$ ) were required in order to collect sufficient signal, even for relatively superficial structures. This prompted additional redesigns that prioritized a tradeoff between numerical aperture of the excitation and the total FOV we can resolve. We believed doing so would make our images not only higher resolution but also brighter,

enabling increased biocompatibility over long experimental timeframes.

The next major version introduced two key modifications to make the microscope more photo-efficient. The first was a new set of off-the-shelf scan lenses from ThorLabs which act together as a short focal length achromatic assembly (approximately 5mm focal length). This establishes a difference in focal lengths between the scan lens optics and the tube lens optics, generating a magnification factor of 1.65 on the rear pupil of the objective assembly when in a 4F configuration. As a result, the 2mm diameter scanner is effectively magnified through the lenses, to occupy a diameter of  $\approx 3.3$ mm on the back focal plane. This actually exceeds the specifications we set out to accomplish and generates an effective excitation NA of 0.36. With this, the microscope should demonstrate  $\approx 1\mu\text{m}$  lateral and  $\approx 10\mu\text{m}$  axial resolution with high photo efficiency – which we will demonstrate in the following section. The inherent tradeoff of such an arrangement is that due to conservation of etendue, the field height associated with a given scan angle decreases by the previously described magnification factor. As a result, the FOV is reduced from the initial goal, but with higher optical performance and brighter signal from deep biological structures. Since signal strength was a primary concern during this design iteration, we also began thinking about the way in which the signal was relayed from the microscope and collected by conventional PMTs. The vast majority of systems rely on bundles of optical fibers which are flexible enough to prevent massive behavioral interference in mice wearing the headpieces. The issue with this configuration, however, is that the packing efficiency of many individual cylindrical cores (with associated cladding) is low. There is a substantial fraction of space (across the bundle face) which is unable to transmit light at all. As a result, these fiber bundles typically are about 50% transmissive, meaning half of the precious signal we collect is lost just by transmitting it through the optical fiber bundle itself. Additionally, since miniature microscope systems that use these bundles still require conventional large filter sets, collimation lenses and benchtop photomultiplier tubes, there is substantial path length (and loss of non-ballistic photons) through each step of the

detector assembly. We took design inspiration from (Modi et al., 2019; Klioutchnikov et al., 2023) which demonstrated impressive results and high performance from small, low cost, integrated Si-based photodetectors both in benchtop, and miniature 3P applications respectively. As such, we decided to place the detectors on the microscope itself, as was done in the first miniature 2P microscope (Helmchen et al., 2001) albeit with a different type of detector. The benefits of digitizing the fluorescence on the head of the animal are threefold. First, they remove cumbersome fiber bundles that while flexible can still impact behavior. In their place is a simple coaxial cable that is roughly the diameter of a piece of dental floss. Second, the microscope does not throw away 50% of the generated fluorescence due to the lossy nature of packing cylindrical optical fiber cores and classing up against one another. And third, the path length from 2P fluorescent generation to digitization at the SiPM detector takes place over no more than 2.5cm, resulting in an extremely sensitive optical device that can resolve signals hundreds of microns deep.

### 5.1.3 The Iterative Optimizer

The microscope that will be described through the rest of this chapter is the result of this iterative optimization and learning, going from replicating past work to innovating and solving engineering problems as they arose. Along with each of these major revisions came updated and modified mechanical housings, circuit boards, and optical elements. The entire process will not be described at length here, but rather a set of 5 key design principles that were followed. They are as follows:

#### 1. Start from a comprehensive optical model

In order to ensure the design will meet the optical requirements, begin with an extensive sequential optical model of the microscope system. This will enable optimization via merit function definition and enable the best possible performance from the imaging system. It is far easier to modify the simulation than it is to change the hardware after performance is lacking.

## 2. Design mechanical housings around the optical model

The next step is to build mechanical housings around the optical model. Whenever possible, extract a CAD model from the optical design software and bring that into your 3D modeling software of choice. When all optical surfaces and ray traces are defined in 3D space, it is straightforward to build housings which index lenses in precisely the correct orientations and spacing. At this stage, do not optimize for weight, simply worry about putting the elements in the correct places.

## 3. Validate performance of the assembly in the real world

Once the lenses and optical surfaces are correctly positioned within the assembly, resolve known specimens like pollen grains, corn stem, or fluorescent microspheres. First confirm performance in broad terms, like measuring the symmetry of the image field, strength of background noise, the working distance, and the dimensions of the FOV (specifics in Chapter 6 and Section 6.1). If the initial measurements are in agreement with the simulation, proceed to measuring more detailed parameters, such as the Point-Spread Function (PSF) and axial displacement range of the microscope (detailed in Sections 6.3 and 6.2 respectively). Should these results be substantially different than the optical model, stop and understand *why* that is the case. In my case, multiple large discrepancies between model and measurement occurred, necessitating teardown of the assembly and detailed characterization of problems. In one case, the tube lens shifted downward towards the objective, bringing the WD to something prohibitively short, like 40 microns. This necessitates going back to step 2 and updating tolerances and dimensions to ensure stable and reliable operation. Only when the parameters measured from the optical assembly on the bench are in close agreement with the optical model should you continue to step 4.

## 4. “Simplify, then add lightness”

Because you now know the optical elements are properly positioned and performing in the intended fashion, the mechanical housings and other components can now be optimized to be as simple and lightweight as possible without sacrificing function

or experimental durability. The process I took was to essentially strip away all unnecessary material from the rough design defined in step 2 assuming a wall thickness of 500µm. That seemed to be a reasonable optimum between strength and weight for the SLA-based resin we are using to construct the microscope housings. Generally, there are some design liberties that were taken to increase this thickness in key areas, such as the interface between the main housing and the scanner, where any flex would result in misalignment. Similarly, the thickness of the mounting surfaces of the lower housing was increased since it mechanically interfaces with the baseplate and is thus subjected to torque and other mechanical loads that the rest of the system does not experience. In general, this step embodies the spirit of British aeronautic design engineer Colin Chapman, who took the philosophy of “simplify, then add lightness” into building vehicles for motor racing.

#### 5. **Break it, fix it, break it again**

These complex (*at least in my view*) optomechanical systems are ultimately built to be placed on the head of a mouse which, with a high degree of likelihood, will nearly immediately bang it against various surfaces and objects within its environment. With this in mind, generally speaking, the microscope should never be on a design knife-edge, where wall thickness are just barely thick enough to be feasible. For example, a system in which the slightest vibration or mechanical displacement, or a small flex of the housing, results in complete loss of performance is deeply sub-optimal. Rather, the system designed throughout these steps should follow a high degree of tolerance to ensure experimental reliability without incurring unnecessary weight. This being said, to understand experimental durability, experiments must be done in the first place. Put the microscope on the head of a mouse and assess how close to a knife-edge the system really is. Can the microscope deal with being routinely abused by mice that are oblivious to the effort that went into its creation? If not, the design needs to be updated, with consideration of each observed vulnerability addressed. Once the system is able to be used for months at a time across different

animals, delivering the expected results, the optimizer is complete.

The output that results from the completion of this iterative process is a microscope system that is known to perform as intended and meet all technical specifications during in the intended use case. Moreover, the microscope is designed to deliver high quality results in a reliable and robust manner despite being mounted to the head of a mouse. Generally speaking, succeeding in such a development effort requires many rounds of optimization, often resulting in large changes of design direction. This was the case for this project, ultimately resulting in 49 redesigns, some of which were small and some of which were fundamental. The latest version, the ultimate output of the iterative optimizer, will be described now.

## 5.2 Optical System Design

### 5.2.1 Excitation Path

We designed the UCLA 2P miniscope to be lightweight, with minimal tethering complexity, and to enable sustained imaging of dynamics from deep structures during free behavior. The microscope’s full optical simulation can be seen in Figure 5.4 A and optomechanical design and beam-path are shown in Figure 5.5 A. Ultrafast laser pulses are launched to a hollow-core photonic bandgap fiber (NKT HC-920) with a 3-axis fiber launch and a coupling aspheric lens (ThorLabs, C230TMD-B). The light is delivered to the microscope headpiece via the thin flexible fiber, at which point it is collimated with a molded aspheric lens (Newport Photonics, KGA170-B). An electro-tunable lens (ETL) (Varioptic A-25H1) converges or diverges to the collimated beam according to a supplied electrical signal, remotely controlling the depth of the focal plane (nominal  $WD = 720\mu\text{m}$ ) of the imaging system by  $\pm 75\mu\text{m}$ . Following the tunable lens, the light is scanned on an integrated 2mm diameter 2-D MEMS scanner (Mirrorcle Tech, A7M20.2-2000AL). A set of two 10mm focal length doublets are positioned near one another to form a scan lens set (ThorLabs, AC050-010-B), with their exact positions defined by hard stops located within



Surface Type	Comment	Radius	Thickness	Material	Coating	Clear Semi-Dia	Chip Zone	Mech Scr	Conic	TCE x 1E-6	Par 1	Par 2	Par 3(unused)	Par 4	Par 5	Par 6	Par 7
0 OBJECT	Standard	HC-920 Fiber Tip	Infinity	4.300				0.000 U	0.000	0.000	0.000						
1	Standard	Lens voltage: 41.0000 Volts	Infinity	0.000				0.586	0.000	0.586	0.000						
2 (aper)	Standard	Collimation Asphere KGA170	19.164	3.480	ECOS50			2.050 U	0.000	2.350 U	0.000						
3 (aper)	Even Asphere		-4.255	0.500				2.050 U	0.000	2.350 U	-0.000	0.000	-0.000	-3.000	1.547E-05	-0.000	-0.000
4	Standard	Lens voltage: 40.4500 Volts	Infinity	0.000				0.836	0.000	0.836	0.000						
5	Standard	Cap thickness	Infinity	0.100				1.700 U	0.000	2.000 U	0.000						
6 (aper)	Standard	Cap Glass Window	Infinity	0.550	D263TECO			1.700 U	0.000	2.000 U	0.000						
7 (aper)	Standard	Conductive phase	Infinity	0.352 Z	PC427A			1.700 U	0.000	2.000 U	0.000						
8 (aper)	Standard	Oil bodycone	137.661 Z	0.248 T	H572A			1.550 Z	0.000	2.000 U	0.000						
9 (aper)	Standard	Oil cylinder	Infinity	0.100	H572A P			1.250 U	0.000	2.000 U	0.000						
10 (aper)	Standard	Bodycone Glass Window	Infinity	0.300	D263TECO			1.250 P	0.000	2.000 U	0.000						
11 STOP (aper)	Standard	^^^(Varioptic ETL) ^^^	Infinity	4.500				0.836	0.000	2.000 U	0.000						
12	Coordinate Break	MEMS Angle	0.000	V				0.000	-	-		0.0	0.0	30.000	0.0	0.0	(
13	Coordinate Break	MEMS Scan Angle	0.000	-				0.000	-	-		0.0	0.0	0.000	0.0	0.0	(
14 (aper)	Standard	MEMS mirror (2.4mm)	Infinity	0.000	MIRROR			1.000 U	0.000	1.000	0.000	0.000					
15	Coordinate Break	MEMS Scan Reset	0.000	-				0.000	-	-		0.0	0.0	0.000	P	0.0	0.0
16	Coordinate Break	MEMS Angle Reset	-4.000	-				0.000	-	-		0.0	0.0	30.000	P	0.0	0.0
17 (aper)	Standard	Thorlabs AC050-010-B	-6.550	-2.200	N-LAK22	THORB		2.500 U	0.000	2.500	0.000						
18 (aper)	Standard		5.250	-1.600	N-SF6HT			2.500 U	0.000	2.500	0.000						
19 (aper)	Standard		24.890	-1.750		THORBSLAH64		2.500 U	0.000	2.500	0.000	0.000					
20 (aper)	Standard	Thorlabs AC050-010-B	-6.550	-2.200	N-LAK22	THORB		2.500 U	0.000	2.500	0.000						
21 (aper)	Standard		5.250	-1.600	N-SF6HT			2.500 U	0.000	2.500	0.000						
22 (aper)	Standard		24.890	-5.000		THORBSLAH64		2.500 U	0.000	2.500	0.000	0.000					
23	Coordinate Break	Dichroic Angle	0.000	-				0.000	-	-		0.0	0.0	-45.000	0.0	0.0	(
24 (aper)	Standard	Dichroic Beam Splitter	Infinity	0.000	MIRROR			4.000 U	0.000	4.000	0.000	0.000					
25	Coordinate Break	Dichroic Angle Reset	4.570	-				0.000	-	-		0.0	0.0	-45.000	0.0	0.0	(
26 (aper)	Standard	Tube Lens Element 2	14.413	1.000	N-SF4			3.000 U	0.000	3.000 U	0.000						
27 (aper)	Standard	Tube Lens Element 1	3.642	3.400	N-LAK22			3.000 U	0.000	3.000 U	0.000						
28 (aper)	Standard		-7.744	2.000				3.000 U	0.000	3.000 U	0.000	0.000					
29 (aper)	Standard	Objective Element 1	5.020	2.500	N-LAK22			2.380 U	0.000	2.380	0.000						
30 (aper)	Standard	Objective Element 2	-3.467	0.500	N-SF4			2.060 U	0.000	2.380	0.000						
31 (aper)	Standard		-38.184	0.100				1.840 U	0.000	2.380	0.000	0.000					
32	Standard	Internal Stop	Infinity	3.244				1.760 U	0.000	1.760	0.000	0.000					
33 (aper)	Standard	Objective Element 3	1.448	1.300	N-SK5			1.144 U	0.000	1.144	0.000						
34 (aper)	Standard		Infinity	0.400	SEAWATER			0.770 U	0.000	0.770 U	0.000						
35	Standard	Cover Glass (Approx. #0)	Infinity	0.100	N-BK7			0.083	0.000	1.144	0.000						
36	Standard		Infinity	0.220	SEAWATER			0.059	0.000	1.144	0.000						
37 IMAGE	Standard	Water at Focal Plane	-1.300	-	SEAWATER			0.700 U	0.000	1.144	0.000						

Figure 5.1: ZEMAX Model for Excitation Laser Scanning and Electronic Focusing Subsystem

Optical prescription for the entire excitation optical system, from the optical fiber to the tissue in the brain. ETL function is simulated as well within the multi-configuration editor by altering the value for “Lens Voltage” shown on surface 4.

the microscope housing. A dichroic beam-splitter (Chroma, ZT775sp-2p-UF1) directs the laser beam, which underfills a custom fabricated 6mm diameter doublet and 3-element objective assembly (Optics Technology, USA) thereby focusing the light into the brain. The excitation path is designed to be diffraction-limited at the numerical aperture of approximately 0.36 over the 445µm x 380µm image field of view.

## 5.2.2 Emission Path

Once 2P excitation is generated, fluorescent photons are collected through the objective utilizing its full NA ( $\approx 0.56$ ), and relayed through the tube lens and dichroic mirror, to a collection head fitted with on-board silicon detectors. The collected light is spectrally filtered to reject laser components using two emission filters (Chroma, ET750sp) and directed with a 4.5mm focal length plano bi-convex collection lens (Edmund, 47-895).

	Surface Type	Comment	Radius	Thickness	Material	Coating	Clear Semi-Dia	Chip Zone	Mech Semi-Dia	Conic	TCE x 1E-6	Par 1(unused)	Par 2(unused)
0	OBJECT	Standard	1.300	0.220	SEAWATER		0.354	0.000	1.144	0.0...	-		
1	Standard	Cover Glass (Approx. #0)	Infinity	0.100	N-BK7		0.439	0.000	1.144	0.0...	-		
2	Standard		Infinity	0.400	SEAWATER		0.482	0.000	1.144	0.0...	-		
3	(aper)	Standard	Infinity	1.300	N-SK5		0.770 U	0.000	0.770 U	0.0...	-		
4	(aper)	Standard	Objective Element 3	-1.448	3.244		1.144 U	0.000	1.144	0.0...	0.000		
5	STOP	Standard	Infinity	0.100			1.760 U	0.000	1.760	0.0...	0.000		
6	(aper)	Standard	38.184	0.500	N-SF4		1.840 U	0.000	2.380	0.0...	-		
7	(aper)	Standard	Objective Element 2	3.467	2.500	N-LAK22		2.060 U	0.000	2.380	0.0...	-	
8	(aper)	Standard	Objective Element 1	-5.020	2.000		2.380 U	0.000	2.380	0.0...	0.000		
9	(aper)	Standard	7.744	3.400	N-LAK22		3.000 U	0.000	3.000 U	0.0...	-		
10	(aper)	Standard	Tube Lens Element 1	-3.642	1.000	N-SF4		3.000 U	0.000	3.000 U	0.0...	-	
11	(aper)	Standard	Tube Lens Element 2	-14.413	4.570		3.000 U	0.000	3.000 U	0.0...	0.000		
12	(aper)	Tilted	1mm*root(2)	1.414	N-BK7		1.750 U	-	-	-	-	0.000	1.000
13	(aper)	Tilted		0.000			1.750 U	-	-	-	0.000	0.000	1.000
14	Coordinate Break			1.900	-		0.000	-	-	-	-	0.000	-0.332
15	(aper)	Standard	First ET750sp-2p8	Infinity	1.000	N-BK7		2.000 U	0.000	2.000	0.0...	-	
16	Standard		Infinity	0.100			1.290	0.000	2.000	0.0...	0.000		
17	(aper)	Standard	6.580	2.600	N-LASF44	EO_VISO_717	2.025 U	0.225	2.250	0.0...	-		
18	(aper)	Standard	-6.580	0.250		EO_VISO_717	2.025 U	0.225	2.250	0.0...	0.000		
19	(aper)	Standard	Second ET750sp-2p8	Infinity	1.000	N-BK7		2.000 U	0.000	2.000	0.0...	-	
20	(aper)	Standard	Infinity	1.600			2.000 U	0.000	2.000	0.0...	0.000		
21	Coordinate Break			0.000	-		0.000	-	-	-	-	-0.150	0.000
22	(aper)	Standard	Infinity	0.000	MIRROR		2.000 U	0.000	2.000	0.0...	0.000		
23	(aper)	Tilted		0.000			2.000 U	-	-	-	0.000	0.000	0.000
24	Coordinate Break			-2.500	-		0.000	-	-	-	-	0.220	0.000
25	(aper)	Standard	Infinity	0.200			1.500 U	0.000	1.500	0.0...	0.000		
26	IMAGE	Standard	GREEN SiPM Detector	Infinity	-		1.500 U	0.000	1.500	0.0...	0.000		

Figure 5.2: ZEMAX Model of Green SiPM Detector Channel

Optical prescription for the emission system, from the fluorescence emitted by the brain to the green SiPM channel (following reflection off the 1P dichroic mirror).

Green and red components are split with another 1P dichroic mirror (Chroma, T550lpxr) and corresponding signal is collected on fast, sensitive, and low-cost Hamamatsu MPPC detectors (S13360-3075PE) located on the collection head.

### 5.2.3 Complete System Path

Both the excitation subsystem shown in Section 5.2.1 and emission paths shown in Section 5.2.2 are integrated into a single 3D ZEMAX model which enables the function of the entire microscope to be simulated at once. Once all of the optical elements were arranged into positions which generated the highest performance, the model (along with ray tracing results) was exported as a .STEP file into SolidWorks 2020. Bringing the optics into CAD space enabled the design of mechanical housings which were sure to position all the lens elements in the correct places without resulting in clipping of any rays.

	Surface Type	Comment	Radius	Thickness	Material	Coatin	Clear Semi-Dia	Chip Zone	Mech Semi-Dia	Conic	TCE x 1E-6	Par 1(unused)	Par 2(unused)	Par 3(unused)	Par 4(unused)
0	OBJECT	Standard	1.300	0.220	SEAWATER		0.354	0.000	1.144	0.0...	-				
1		Standard	Infinity	0.100	N-BK7		0.439	0.000	1.144	0.0...	-				
2		Standard	Infinity	0.400	SEAWATER		0.482	0.000	1.144	0.0...	-				
3	(aper)	Standard	Infinity	1.300	N-SK5		0.770	U 0.000	0.770	U 0.0...	-				
4	(aper)	Standard	-1.448	3.244			1.144	U 0.000	1.144	U 0.0...	0.000				
5	STOP	Standard	Infinity	0.100			1.760	U 0.000	1.760	U 0.0...	0.000				
6	(aper)	Standard	38.184	0.500	N-SF4		1.840	U 0.000	2.380	U 0.0...	-				
7	(aper)	Standard	3.467	2.500	N-LAK22		2.060	U 0.000	2.380	U 0.0...	-				
8	(aper)	Standard	-5.020	2.000			2.380	U 0.000	2.380	U 0.0...	0.000				
9	(aper)	Standard	7.744	3.400	N-LAK22		3.000	U 0.000	3.000	U 0.0...	-				
10	(aper)	Standard	-3.642	1.000	N-SF4		3.000	U 0.000	3.000	U 0.0...	-				
11	(aper)	Standard	-14.413	4.570			3.000	U 0.000	3.000	U 0.0...	0.000				
12	(aper)	Tilted	1mm*root(2)	1.414	N-BK7		1.750	U -	-	-	-	0.000	1.000		
13	(aper)	Tilted		0.000			1.750	U -	-	-	0.000	0.000	1.000		
14		Coordinate Break		1.900	-		0.000	-	-	-	-	0.000	-0.332	0.000	0.000
15	(aper)	Standard	Infinity	1.000	N-BK7		2.000	U 0.000	2.000	U 0.0...	-				
16		Standard	Infinity	0.100			1.215	U 0.000	2.000	U 0.0...	0.000				
17	(aper)	Standard	6.580	2.600	N-LASF44	EO...	2.025	U 0.225	2.250	U 0.0...	-				
18	(aper)	Standard	-6.580	0.250		EO...	2.025	U 0.225	2.250	U 0.0...	0.000				
19	(aper)	Standard	Infinity	1.000	N-BK7		2.000	U 0.000	2.000	U 0.0...	-				
20	(aper)	Standard	Infinity	1.600			2.000	U 0.000	2.000	U 0.0...	0.000				
21		Coordinate Break		0.000	-		0.000	-	-	-	-	-0.150	0.000	0.000	45.000
22	(aper)	Standard	Infinity	1.000	N-BK7		2.000	U 0.000	2.000	U 0.0...	-				
23	(aper)	Tilted		2.500			2.000	U -	-	-	0.000	0.000	0.000		
24		Coordinate Break		-2.000	-		0.000	-	-	-	-	-2.750	0.000	0.000	-45.000
25	(aper)	Standard	Infinity	0.200			1.500	U 0.000	1.500	U 0.0...	0.000				
26	IMAGE	Standard	Infinity	-			1.500	U 0.000	1.500	U 0.0...	0.000				

Figure 5.3: ZEMAX Model of Red SiPM Detector Channel

Optical prescription for the emission system, from the fluorescence emitted by the brain to the red SiPM channel (following transmission through the 1P dichroic mirror).

### 5.2.4 Silicon Photon Counters

As detailed in section 5.1.2, the microscope uses a class of silicon photon detectors that are not conventionally used for 2P microscopy. This is large part due to the extreme sensitivity and low noise of GaAsP PMTs (they have been used for decades) coupled with a lack of necessity to miniaturize the complete microscope assembly. However, more recently groups have turned their attention to these sensors because of their impressive specifications, unparalleled durability and availability, small size, and affordable cost (Modi et al., 2019). As a result of these advantages and in combination with surmounting the issues that are associated with relaying the fluorescence off the head of the animal, we decided to add two SiPM detectors to the microscope itself. The optical paths for the green and red SiPM channels are shown in Figures 5.2 and 5.3 respectively.

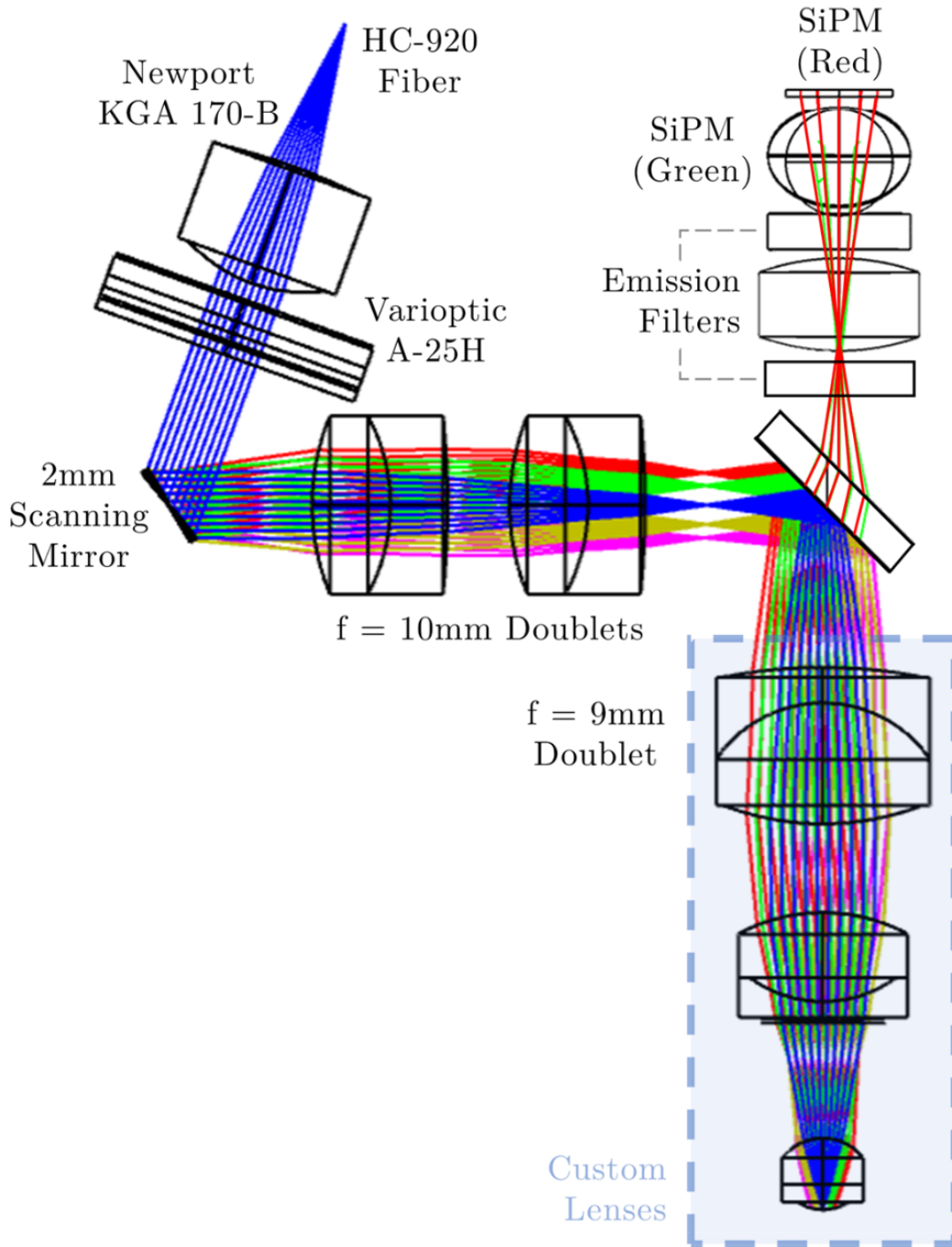


Figure 5.4: **UCLA 2P Miniscope Full Optical System Design**

Full-system optical simulation and optimization in Zemax. All lenses, mirror surfaces and filters were simulated to ensure high optical performance once constructed and assembled. The detector path was simulated separately and superimposed here to demonstrate the full system as a combination of both optical paths.

## 5.3 Mechanical System

### 5.3.1 Optomechanical System Design

To support and appropriately orient all of the optical components simulated in Figure 5.4, a custom-made mechanical housing was designed in SolidWorks 2021 and fabricated using SLA-based resin 3D printers. The microscope’s optomechanical design can be seen in Figure 5.6 and is composed of four sub-systems. First, a collimator assembly, which supports the optical fiber ferrule and a collimation aspheric lens. The electro-tunable lens is positioned between the collimator and the main body of the microscope, secured in place via four thread-forming torx screws. The screws also provide a clamping force between the electrodes of the UCLA 2P Miniscope flex-PCB and the electro-tunable lens, making for a reliable and secure electrical connection. The electronics subsystem, described in detail below, is fixed to the main housing using UV adhesive (Norland 68). The main scope body contains the scan lens set, the custom-made tube lens, and 2P dichroic mirror. The lower scope body assembly secures the custom objective lens to the microscope, and interfaces with the baseplate on the head of the animal. Lastly, the detector head press-fits into the main scope housing and can be secured with a small amount of UV adhesive.

### 5.3.2 Fabrication

Housings are entirely 3D printed using readily available SLA-based machines (Formlabs Form 3) using standard, black V4 resin. STEP files of all mechanical parts, as well as ready-to-print .form files with build resolution, orientation and support configuration will be uploaded to the UCLA 2P Miniscope GitHub repository following peer review, as a reference for users. After printing and standard curing of the parts using 99% isopropyl alcohol (30 minutes) and UV light exposure (30 minutes at 60C), the internal bores are lightly touched up using chuck reamers, either 1.8mm (collimator bore, MSC, 55451678), 5mm (scan lens bores McMaster Carr, 8851A18) or 6mm (tube lens bore McMaster Carr, 8851A21). These tools are fitted to a t-handle tap wrench and spun lightly by-hand into

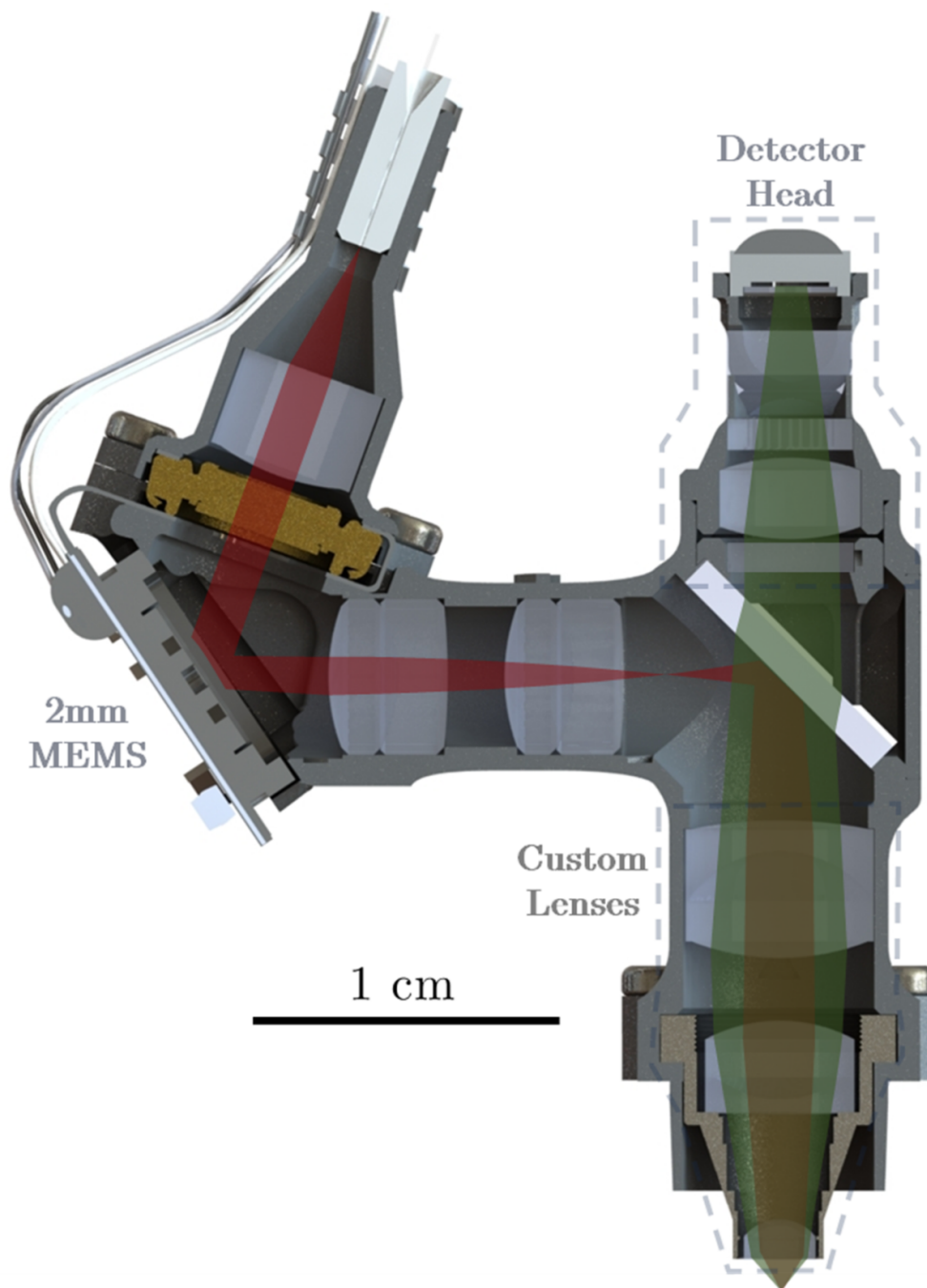


Figure 5.5: **UCLA 2P Miniscope Optomechanical Drawing**  
Optomechanical design of the system, including all housings, lenses, optical filters, and on-board PCBs in cross-section. The red beam denotes the 920nm excitation, and the green beam path describes the fluorescent collection onto the detector head.

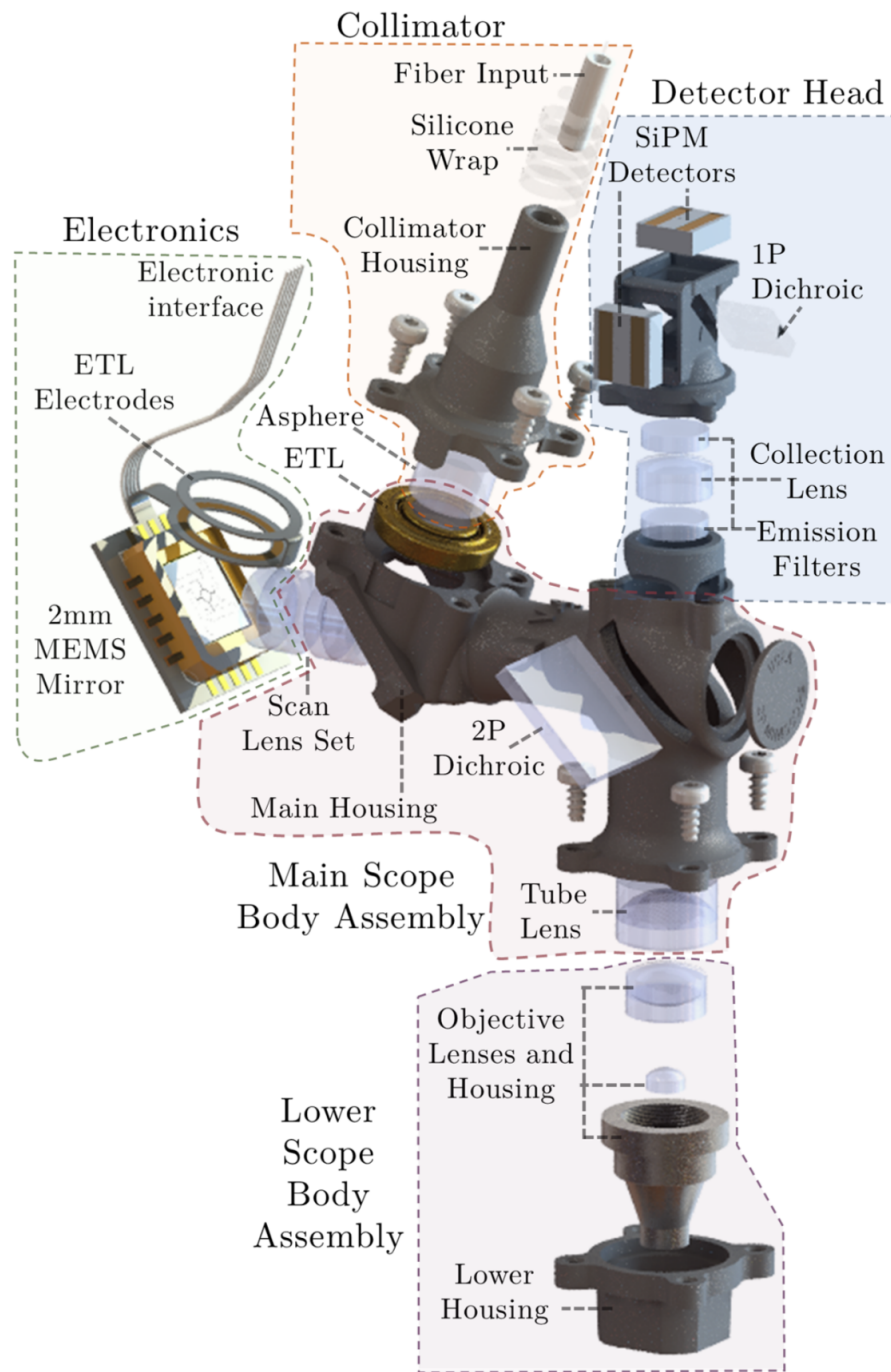


Figure 5.6: **UCLA 2P Miniscope Exploded View**

Exploded view of the UCLA 2P Miniscope, describing the various sub-assemblies that work together, and the individual parts that comprise them.

the bores of the collimator or microscope housing to remove any excessive material left behind from the 3D printing process. Components are then airbrushed in 3-5 coats of matt-black acrylic airbrush paint (50/50 blend with 99% isopropyl alcohol) to reduce light from the environment that can penetrate through thin aspects of the microscope housings. Baseplates and cannular window implant rings are made from sintered titanium and sourced from an online metal 3D printing house (Protolabs, Maple Plain, MN).

### **5.3.3 Assembly**

Miniature microscopes were assembled following a straightforward set of steps. A precise building tutorial and step-by-step instructions will be made available on the UCLA 2P Miniscope GitHub repository after peer review, to assist others in building these microscopes. For a familiar user, a microscope headpiece will take approximately 30-45 minutes to assemble once all the housings are prepared and the assembled Flex-PCBs are sourced. Additionally, tutorials for launching the 2P laser onto an optical fiber, collimating the output of the optical fiber, and others will be provided, ensuring users are able to not only assemble the microscope headpiece, but the rest of the system as well.

## **5.4 Electronic System**

### **5.4.1 General Overview**

Control of all microscope functionality is accomplished with several custom PCBs which relay control signals to one another. Off the animal, there is a signal interface PCB, seen in Figures ??, which combines inputs from an I2C controller (NI, USB 8451 OEM), Hamamatsu SiPM drivers, an analog MEMS amplifier (Mirrorcle BDQ PicoAmp, Analog), and other equipment into a single connector that can be easily accessed for experimentation. The miniature microscope PCB itself, shown in Figures ??, connects to the signal interface PCB over a thin and flexible set of coaxial cables. This allows for control of the scanner position, as well as on-board driving of the electrotuneable lens using the I<sup>2</sup>C data protocol.



The circular, flexible electrodes on the PCB wrap around the electrotuneable lens and deliver the appropriate signals from the ETL driver to the lens body. Altogether these PCBs work alongside traditional electronics for controlling benchtop 2P microscopes, and enable straightforward and reliable driving of the miniature 2P system. The miniature microscope hardware is mainly controlled by ScanImage (MBF Bioscience, free version) a commonly used software and user interface in the field of multiphoton microscopy. All machine configuration and user configuration files are available to users for direct implementation and ease of use. Running alongside ScanImage, a custom MATLAB script is used to control ETL position using the NI I<sup>2</sup>C controller (USB 8451 OEM) fitted on the signal interface PCB, and a free MATLAB hardware support package (National Instruments NI-845x I<sup>2</sup>C/SPI Interface).

#### **5.4.2 Flex-PCB Design**

Custom electronics integrated into the microscope headpiece were required to control key functions like the scanner mirror position, and electronically tunable focal depth. They are based on a 160 $\mu$ m-thick 2-layer flex-PCB to minimize weight, allowing the LCC20 package of the MEMS scanner to stabilize the PCB itself.

## FLEX-PCB (On Microscope)

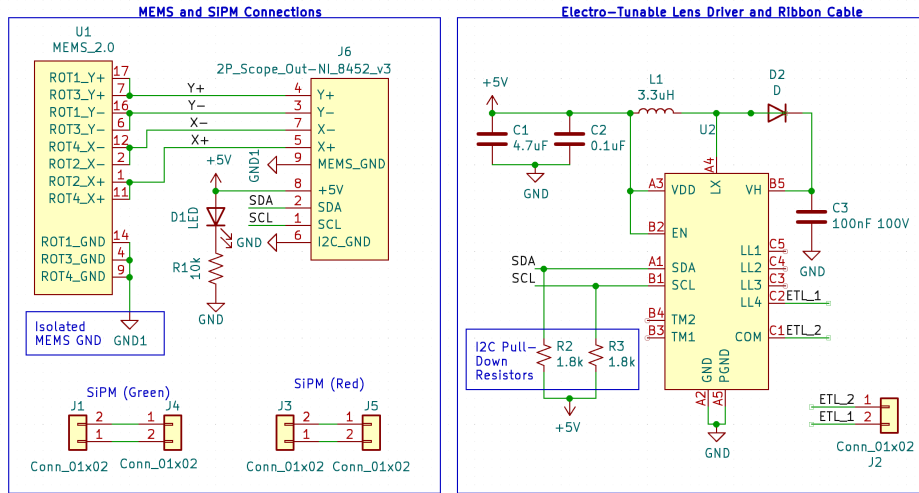


Figure 5.7: UCLA 2P Miniscope Flex-PCB Schematic

This PCB accomplishes two main functions for the microscope. First, this PCB delivers the correct drive signals to the MEMS scanner, thus enabling 2D imaging (left panel). Secondly, the flex board establishes I<sup>2</sup>C communication with the electro-tunable lens control IC, making axial scanning possible.

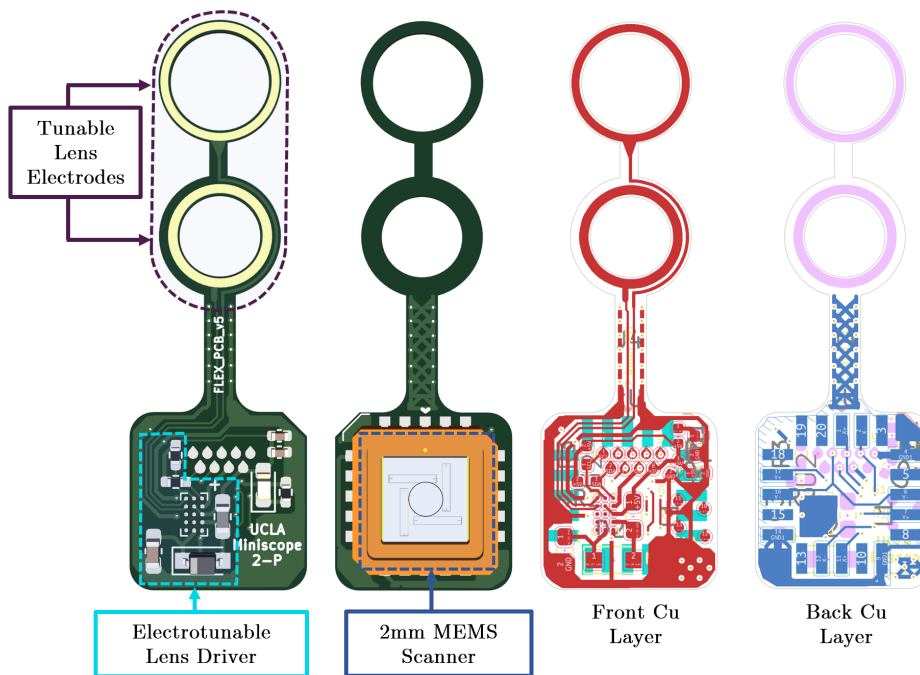


Figure 5.8: UCLA 2P Miniscope Flex PCB design

## MEMS Interconnect Board (Separate GNDs, SiPM V3)

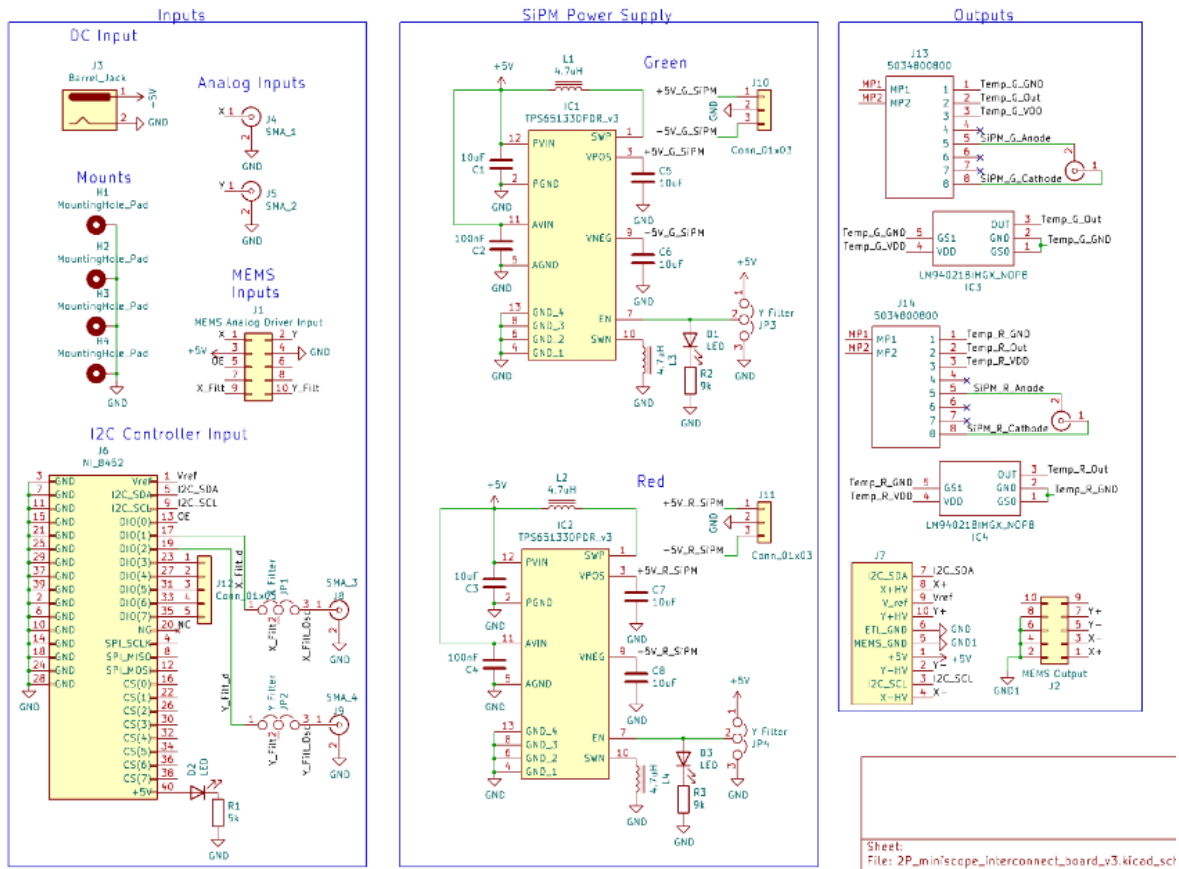


Figure 5.9: UCLA 2P Miniscope Signal interface Schematic

### 5.4.3 Signal Interface PCB Design

The second custom-made PCB is a signal interface motherboard which is responsible for integrating signals from different sources and daughter boards and packing them into a clean single connector for integration into the miniature microscope system. When assembled, the signal interface PCB is comprised of four main subsystems. There is an I<sup>2</sup>C interface, Hamamatsu Multi-Pixel Photon Counter (MPPC) drivers, SiPM power supplies, and an analog MEMS driver. These things take signals from multiple sources and combine it to output to a single "2P Miniscope Output" connector J7. More information can be seen in the schematics and drawings in the following figures.

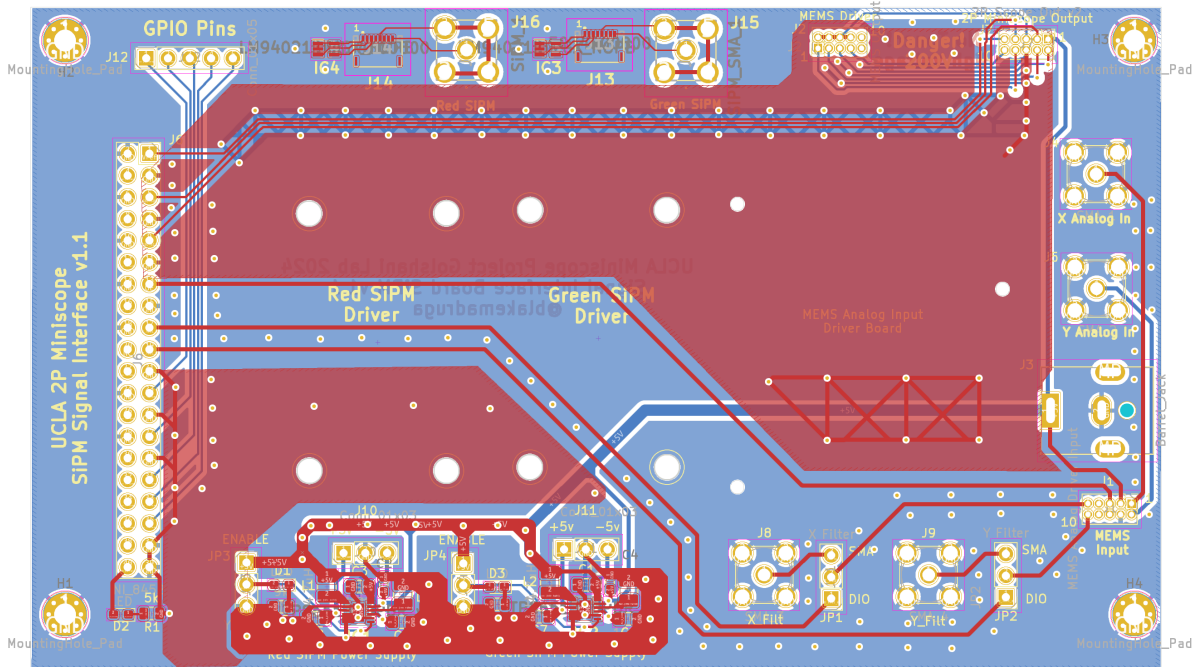


Figure 5.10: UCLA 2P Miniscope Signal interface PCB

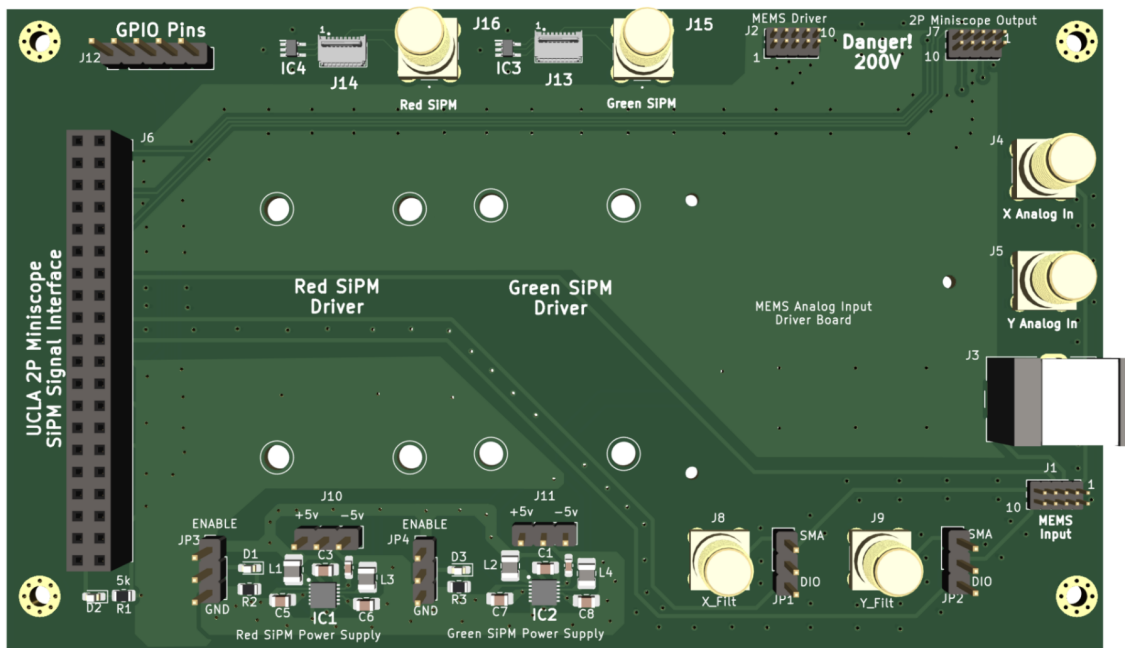


Figure 5.11: UCLA 2P Miniscope Signal interface PCB 3D Rendering

#### 5.4.4 Complete System and Wiring Diagram

Figure 5.12 demonstrates the entire control system responsible for generating and controlling the multiphoton miniature microscope. A data acquisition control PC is used to control three main devices, a Digilent Analog Discovery 3, ScanImage compatible electronic system (NI or vDAQ), and the UCLA 2P Miniscope Interface electronics. Together these components generate the drive signals to the miniature microscope and resolve the fluorescent signal from it.

### 5.5 Software System

The control software for the microscope is built on top of ScanImage (Free version, MBF Bioscience) which runs inside of MATLAB. ScanImage is a commonly used and well respected software for the control of commercial and custom made scanning microscopy systems. The software interfaces with control electronics (either from National Instruments, or MBF Bioscience) to generate analog waveforms and reconstructs 2D images from the 1D detector data stream. In order to control the custom electronic components, a GUI was written in MATLAB that runs alongside ScanImage which enables the manipulation of parameters which are specific to the miniature microscope system.

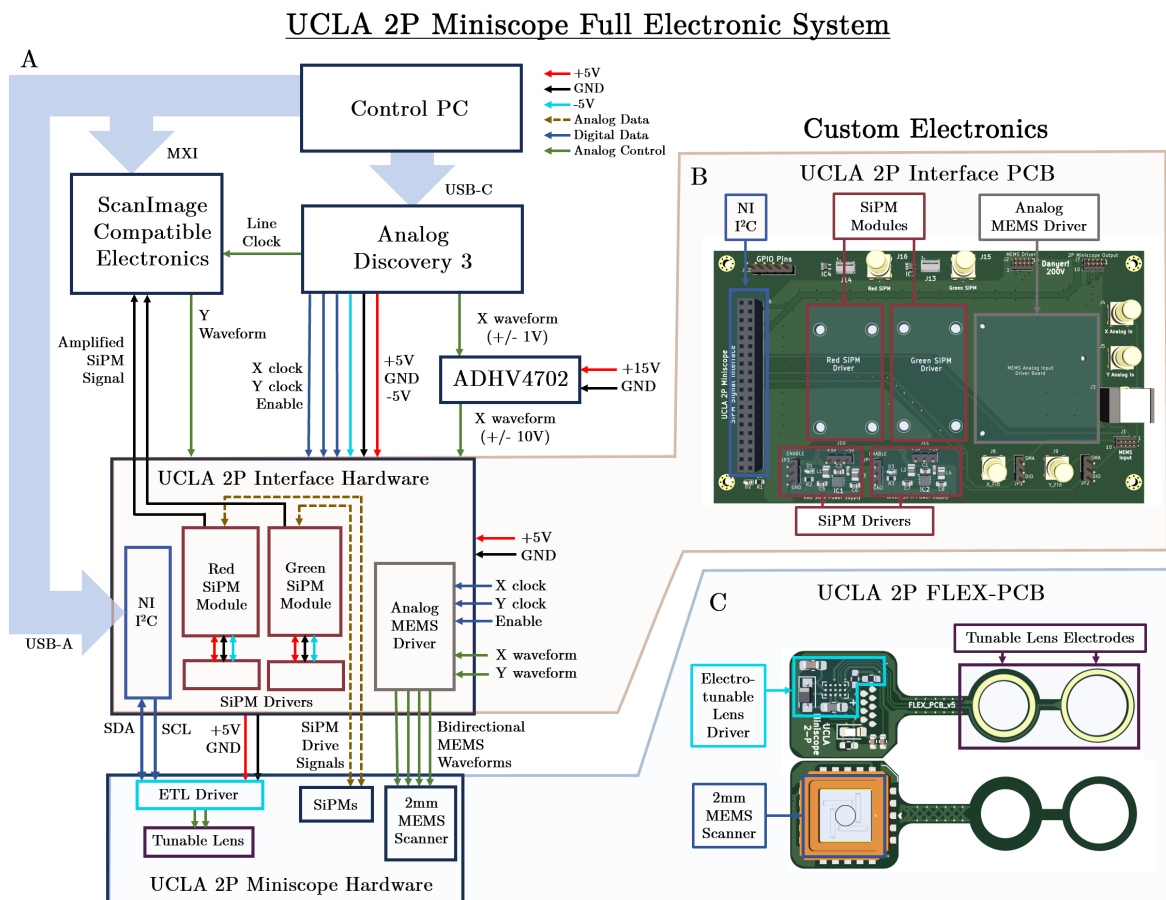


Figure 5.12: **UCLA 2P Miniscope Electronic Circuitry**

(A) Simplified block diagram of the custom and off-the-shelf electronic components. The custom PCBs communicate with one another via thin coaxial cables and the specifics of the connections can be seen. (B) UCLA 2P Miniscope interface PCB. This single low-cost 2 layer PCB integrates electronic signals from various sources and packages it into a single connector; the microscope plugs into this connector. This interface PCB receives four daughter boards: two SiPM drive modules (Hamamatsu), an I<sup>2</sup>C controller (NI), and the MEMS amplifier (Mirrorcle). The interface PCB receives inputs from ScanImage-compatible electronics and additional hardware. (C) UCLA 2P Miniscope flex PCB. These electronics are a fundamental part of the headpiece and are used to control the MEMS scanning mirror and electro-tunable lens.

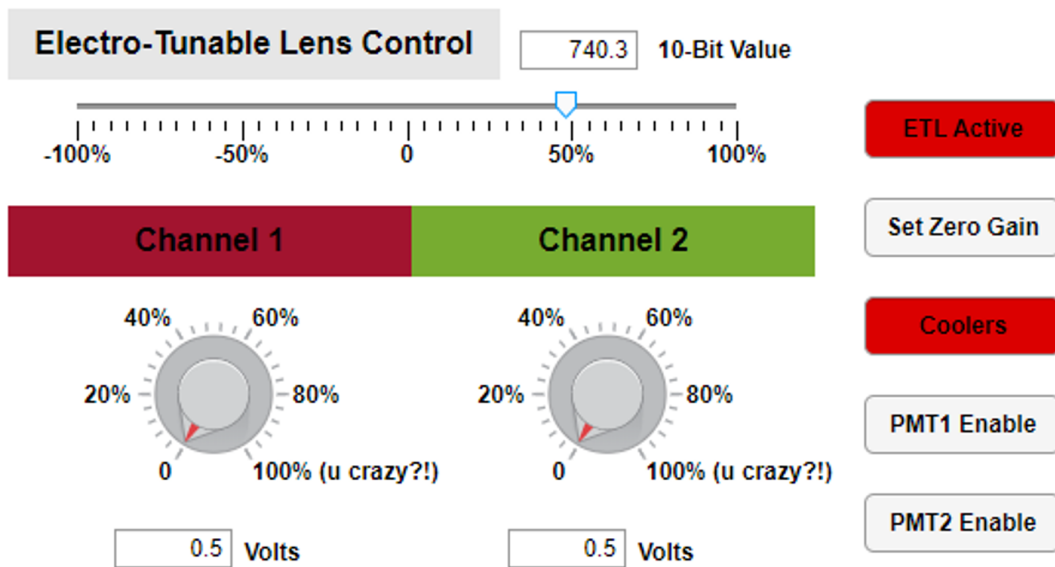


Figure 5.13: MATLAB Control User Interface

## CHAPTER 6

# UCLA 2P Miniscope: Optical Performance Assessments

### 6.1 Field of View Measurements

The UCLA 2P Miniscope was first tested on several imaging specimens to assess resolution and performance prior to use in animal experiments. First, fluorescent microspheres (Invitrogen, TetraSpeck Fluorescent Microspheres Size Kit, T14792) of various diameters were imaged to tune parameters like drive waveform frequency amplitude, bidirectional phase offset, and clock filter frequencies. The FOV was measured by displacing a 4 $\mu$ m bead (T14792, position #1) from one edge of the image field to the opposite edge using an electronically controlled linear stage with high precision and digital readout. Measurements were taken for each independent lateral axis.

### 6.2 Electronic Focus Range Measurements

We then assessed the axial range of the ETL with a piezoelectric actuator that was calibrated using a commercial z-stage from a benchtop 2P microscope system. Digital commands were sent to the ETL, thereby offsetting the focal plane in depth, and the piezo was adjusted manually to bring the focal plane back to the original view. Required displacements of the piezo to restore focus were recorded for each ETL set point, resulting in a total displacement of 150 $\mu$ m.



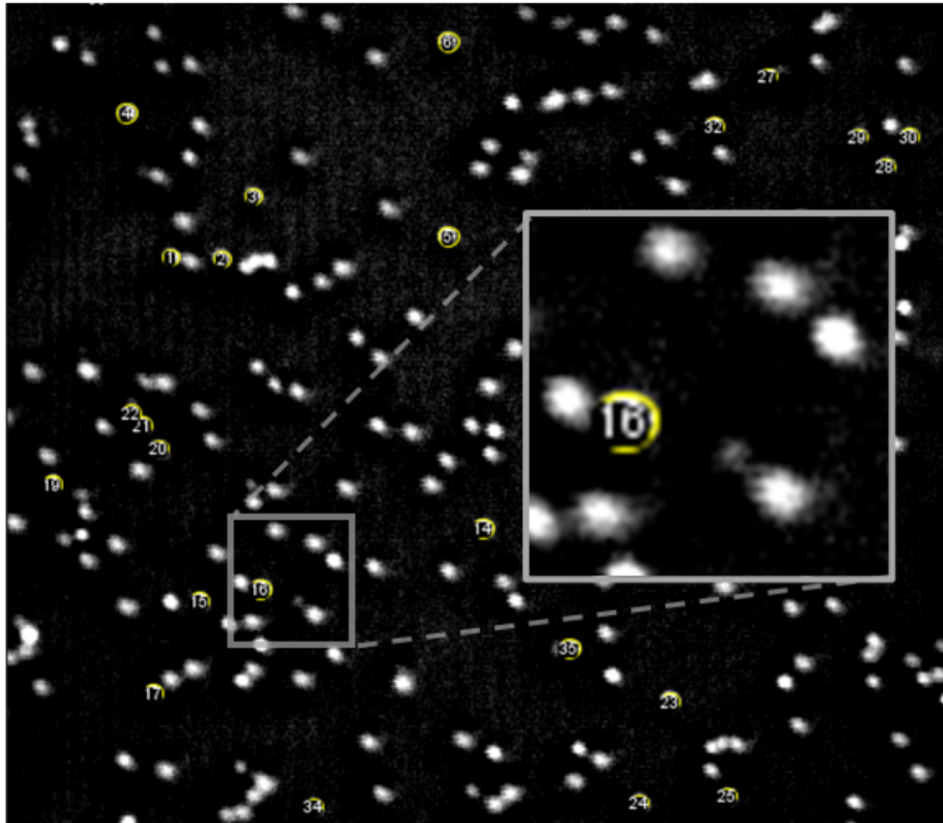


Figure 6.1: Resolving 4 $\mu$ m Microspheres for FOV and Z-Range Measurements

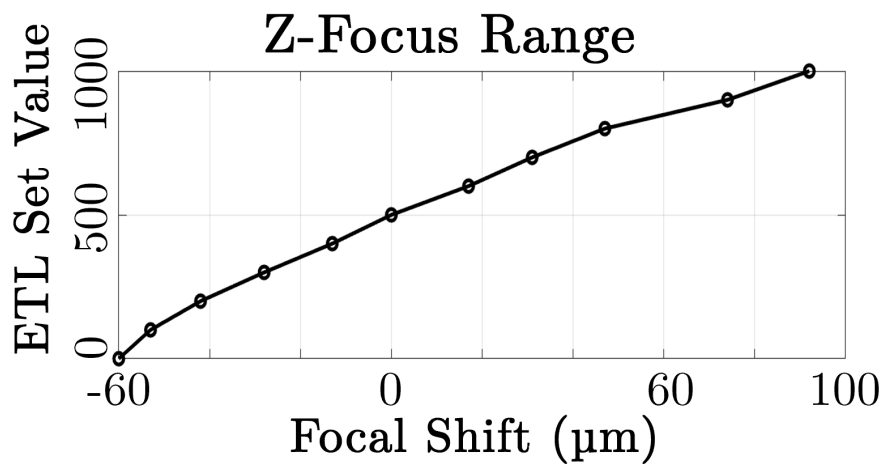


Figure 6.2: Measured Axial Focus Range Provided by the Electro-Tunable Lens

### 6.3 Point-Spread-Function Measurements

Once the basic imaging parameters were assessed using 4 $\mu\text{m}$  microspheres, the optical resolution was characterized with sub-diffractive 200nm fluorescent microspheres (T14792, position #4). First, the drive waveforms were reduced in amplitude to effectively zoom the FOV to 50 $\mu\text{m}$  in each direction, as verified with the high-resolution translation stage. Then, individual 200nm microspheres were brought into view with the ETL set to the digital value 500 (no appreciable focal power) and adjusted axially maximize bead diameter. 50-frame image sequences of 512 x 512 resolution were acquired, making the per-pixel sampling rate 97.5nm in the lateral dimension. Frames were averaged together to reduce noise prior to taking line-profile measurements through the centroid of the bead. For axial measurements, we used a calibrated, high-resolution piezoelectric actuator to displace the imaging slide by  $\pm 20\mu\text{m}$  about the focal plane over approximately 40 seconds. The displacement of the slide and the onset of the microscope recording were time-synchronized using external electronics (Digilent, Analog Discovery 3). In the axial direction, 400 images were collected per stack, grouped mean projections of 10 images were calculated, resulting in the final axial measurement stack of 40 frames with an axial displacement of 1 $\mu\text{m}$  between frames. A circular ROI is drawn which encircles the bead and the mean value of the pixels within the ROI are computed for each image in the stack. The Z-axis profile was used to assess the changes in mean value across the 40 $\mu\text{m}$  displacement, and thus, axial resolution. The final measurement included  $>10$  beads for each direction (lateral and axial) which were then shifted relative to each other as to align their maximum values, accounting for any misalignments in experimental setup. These measurements were then averaged over all beads, and a gaussian function was fit for each direction (Figure ??D).

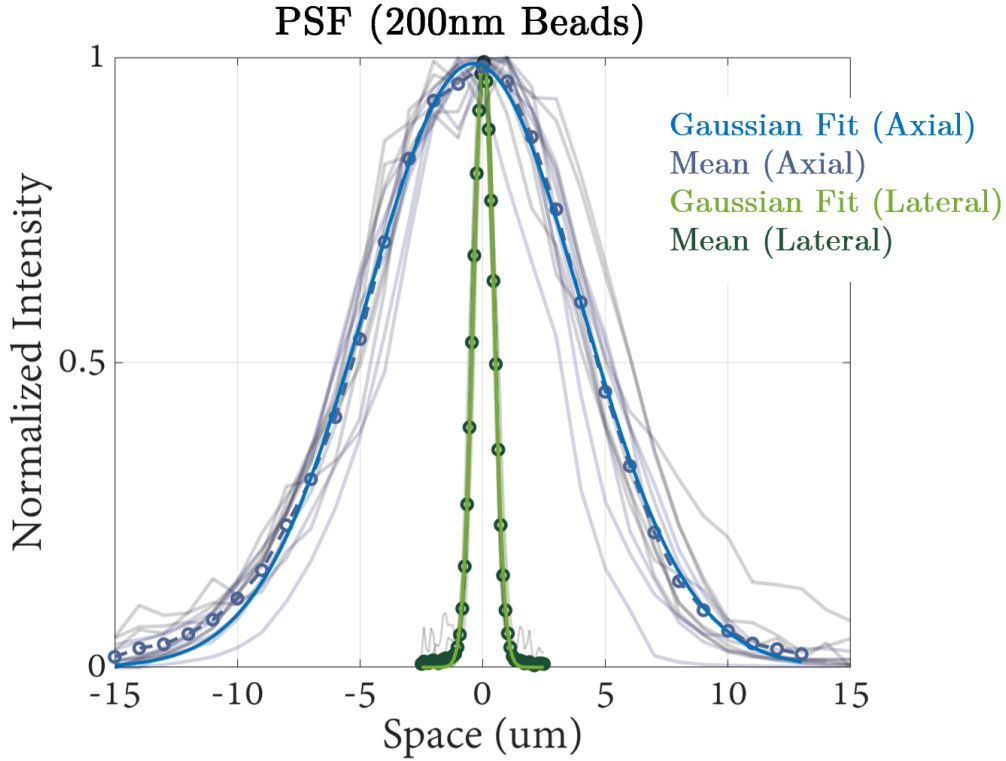


Figure 6.3: Measured Lateral and Axial Point-Spread Function (PSF)

Lateral PSF is 980nm full-width at half maximum (FWHM), axial is 10.18 $\mu$ m FWHM.

The FWHM of the gaussian fits were used to describe the resolution of the microscope, which was found to be 980nm in the lateral dimension, and 10.18 $\mu$ m axially. These numbers are in close agreement with our optical simulations and suggest an effective excitation NA of  $\approx 0.36$  (Lees et al., 2024) which matches the predicted NA of 0.36.

## 6.4 Comparison Between Zemax Optical Simulation and Measurements

Once the optical performance from the microscope system was measured on the benchtop, it was possible to return to the initial Zemax simulation and assess the degree of similarity between the two. We find that the main system parameters are quite nicely aligned between the measurements and the output of the model, namely the lateral PSF and the

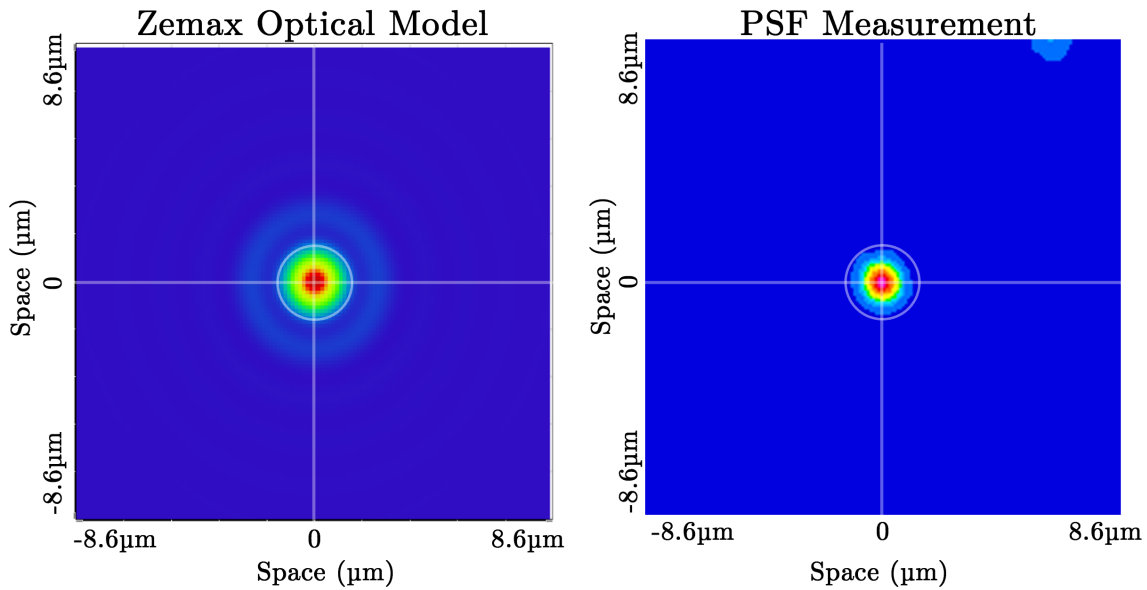


Figure 6.4: **2D PSF comparisons Between Zemax Simulations and Measurements** The 2D Huygens PSF exported from the optical simulation (left) compared directly to an observed 200nm fluorescent microsphere (right). Spatial scales were adjusted to be identical and a 2-pixel gaussian smoothing kernel was applied to the PSF measurement. The white circle is approximately  $2.5\mu\text{m}$  in diameter for comparison purposes. Notice the suppression of the outer rings present in the Zemax model due to the nonlinear multiphoton effect suppressing the side lobes of the PSF.

dimensions of the FOV. This suggests that the optical system is performing in ways that we we expect, and thus can go forward with a high degree of confidence in our measurements, to study biological tissue.

## 6.5 Resolving Biological Tissue

Following PSF measurements, *ex-vivo* tissue slices expressing GCaMP6f were visualized, in order to assess detection sensitivity as a function of excitation laser power. Slides were imaged under  $\approx 30$  mW of laser power, clear cell bodies and processes were observed, confirming that the microscope can generate sufficient signal from physiological concentrations of fluorescent molecules of interest.

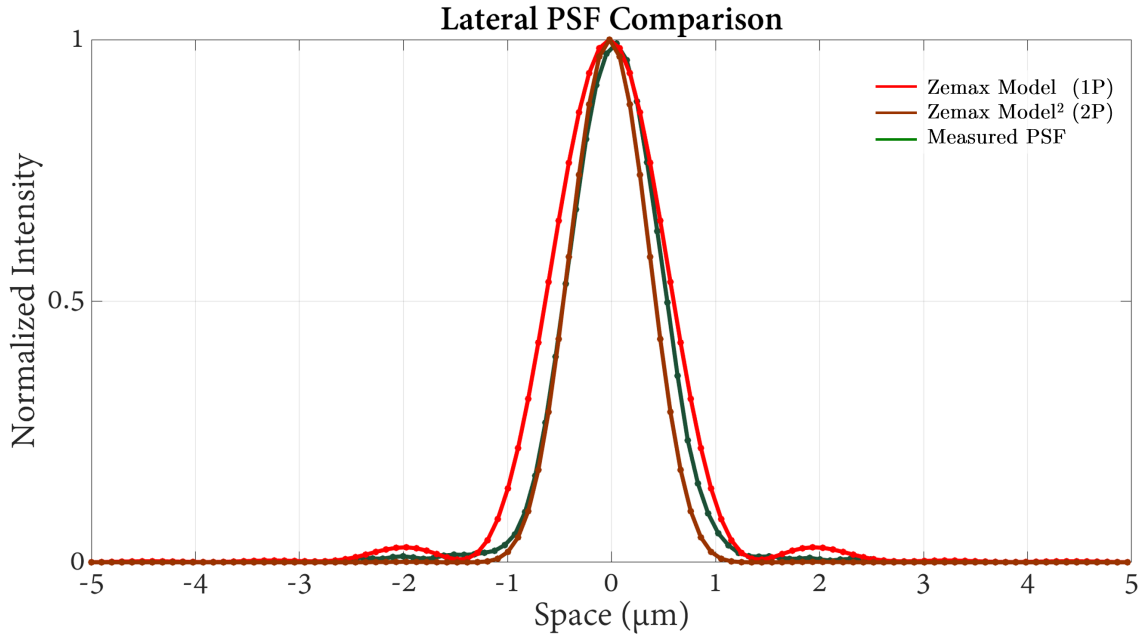


Figure 6.5: **Lateral PSF Cross-Sections from Optical Model and Measurements**

The gaussian fit to the measured lateral PSF (green) shows a 980nm FWHM and outperforms the native Zemax model (red) conducted at a 920nm laser wavelength with approximately a 1.3 $\mu$ m FWHM. Squaring the intensity profile (deep red) approximates the 2P effects on resolution, however the 870nm FWHM is below the diffraction limit. Simply calculating the diffraction limit with Equation 3.1 for 920nm source at 0.36NA yields a FWHM of 963nm, which is only 1.8% different between simulation and measurement.

Following tissue slice recording, we tested the imaging ability of the microscope *in-vivo*, with head-fixed animals expressing various GCaMP varieties, including 6f, 7f, and 8f. Animals were implanted with a cranial window over cortex or a canular implant above hippocampus (described in detail in the Methods). Neural activity was captured in multiple experimental conditions (Figures 7.1, 7.2, 7.3) verifying the microscope’s capacity to resolve neural dynamics *in vivo*.

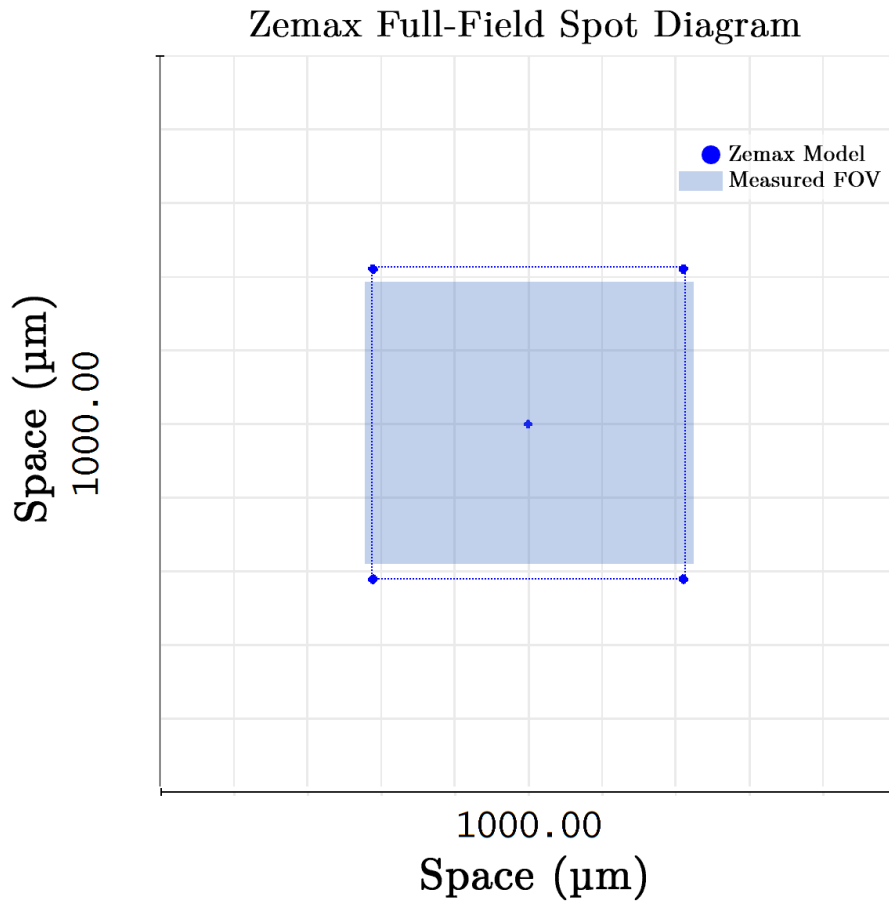


Figure 6.6: **FOV Predictions and Results from Measurement**

The Zemax model results from simulation of the constraints of the FOV are pictured. The dark blue points represent focal locations at the sample plane at the extremes of the MEMS scanner angular travel (5.2 degrees simulated). The FOV agrees well in the x dimension because of the resonant behavior and lack of a large spatial fill fraction within acquisition software. The limitations in the y field height come from the flyback behavior of the vertical axis imposing high frequency noise in the images, which necessitates a short settling time, thus constraining the usable FOV in the vertical direction.

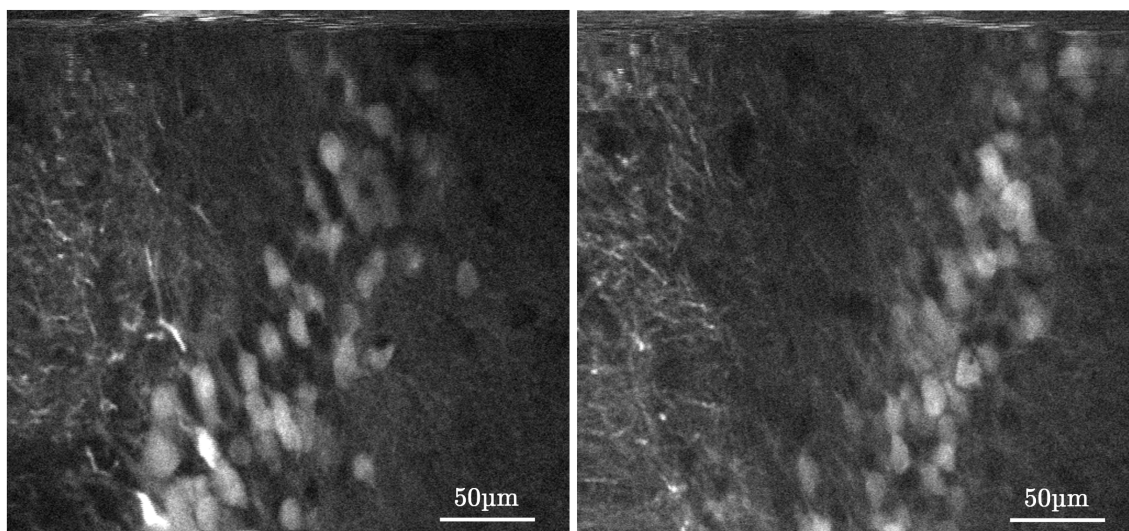


Figure 6.7: **GCaMP6f *Ex-Vivo* Slice Recording**

Measuring biologically-relevant concentrations of fluorescent signal. Axial displacement between left and right frames accomplished using only the electro-tunable lens.

## CHAPTER 7

### UCLA 2P Miniscope: *In-vivo* free behavior recordings

#### 7.1 Animal Protocols and Well-Being

All experiments were conducted per National Institute of Health (NIH) guidelines and with the approval of the Chancellor's Animal Research Committee of the University of California, Los Angeles. Imaging experiments used to validate the performance of the UCLA 2P Miniscope were conducted on both male and female adult (>P60) mice. Animals were anesthetized with isoflurane during the entire surgical procedure. Exposed fur on the skull was trimmed away in a sterile manner, and animals were thermally maintained using a homoeothermic temperature control blanket and controller from Harvard Apparatus. The animal was secured in a stereotaxic frame and subcutaneously administered local anesthetic (lidocaine at 1.5mg/kg and carprofen at 5.5mg/kg) 30 minutes before the scalp was removed using a scalpel. The skull was scraped to facilitate effective bonding between the skull and the implanted optical window. For CA1 and DG recordings, a 3.6mm circular craniotomy was made in the skull just above PPC using a precision dental drill, taking care as to not damage the underlying dura. Cortical experiments used a 4mm x 4mm square craniotomy. Following the removal of the section of skull, the site was flushed with cortex buffer (NaCl = 7.88g/L, KCl = 0.372g/L, HEPES = 1.192g/L, CaCl<sub>2</sub> = 0.264g/L, MgCl<sub>2</sub> = 0.204g/L, at a pH of 7.4) until all bleeding subsided. A viral injection of AAVs to express GCaMP6f, GCaMP7f or GCaMP8f was completed at a rate of 1nL/sec into the targeted structure using a Nanoject injector (Drummond Scientific). For hippocampal CA1 recordings, a unilateral 1000nL injection of pGP-AAV-syn-jGCaMP7f-WPRE (Addgene: 104488) was performed. Dentate gyrus recordings used 500nL of pGP-AAV-syn-jGCaMP8f-



WPRE (Addgene: 162376) delivered unilaterally. Animals used for RSC imaging received a mixture of AAV1.Syn.GCaMP6f.WPRE.SV40 virus (Addgene: 100837), AAV1.cFos-tTA and AAV1.TRE.mCherry at 20 to 120 nL/min into dorsal cortex using stereotactic coordinates -1.7 and -2.3mm posterior to bregma, 0.5mm lateral to midline, and -0.8mm ventral to the skull surface. For cortical experiments, a thin #0 optical cover-glass (4mm x 4mm) was placed onto the surface of the brain and secured to the skull using cyanoacrylate and dental cement. This results in an exposed area of approximately 3.5mm x 3.5mm spanning the midline. When imaging sub-cortical structures like hippocampus or dentate gyrus, overlying cortex was slowly aspirated, taking care to not damage the alveus. A custom-made titanium cannular plug (implanted portion: 3.5mm diameter x 1.315mm depth; flange above skull: 5.7mm diameter x 0.285mm thick) was fitted with a sterile 3mm #0 glass coverslip using optical adhesive (Norland 68) and secured using a UV-light gun. This plug assembly is lowered into the craniotomy and secured to the skull with a thin layer of cyanoacrylate glue and dental cement. Any residual tangential space between the surface of the skull and the flat base of the cannular plug was filled using dental cement and allowed to harden completely. In all cases, the animals also have a stainless-steel head-bar fixed to the skull that enables researchers to lower the microscope easily and find an optimal FOV for recording. Following surgery, animals were given carprofen subcutaneously at 5.5mg/kg every 12-24 hours to minimize pain and inflammation over the first 48 hours post-op. Animals were also provided amoxicillin-treated water at 0.5 mg/mL concentration over 7-days and were allowed to rest for an additional 7-days to allow for full recovery and to ensure the cover-glass had cleared. After 14 days, expression levels were assessed using a benchtop 2P microscope (Scientifica VivoScope) fitted with a Nikon 16x/0.8NA water immersion objective. Once expression levels and overall tissue health was confirmed, animals received a baseplate. First, the animal was head-fixed and approximately 1mL of distilled water is added to the surface of the cranial window. Then, the UCLA 2P Miniscope was lowered over the cover glass, with the baseplate already fitted to the lower microscope housing. The position of the miniature microscope was

controlled using a manual 3-axis stage and adjusted while imaging, until an optimal FOV was found. Once the image field was identified, the baseplate was fixed using dental cement and allowed to fully cure. The miniature microscope was then removed, and a small 3D printed window cover, the exact shape of the lower microscope housing, is placed into the baseplate itself, to help mitigate the ingress of dust and debris onto the recording area. This cover is very light (approximately 0.335g) and was fixed in place with two small screws in the same way as the microscope itself. The animal was then removed from head fixation and returned to its home cage.

## 7.2 CA1 - Resolving Dense Neuronal Populations During Free Behavior

The optical sectioning ability of 2P microscopy allows imaging of activity from dense neuronal populations) with high spatial resolution. To understand how the 2P miniature microscope performed at imaging dense populations, we recorded neurons expressing GCaMP7f in the pyramidal layer of CA1. We recorded from populations of neurons expressing  $\text{Ca}^{2+}$  indicators while the mouse freely navigated an approximately 38cm x 28cm chamber over periods ranging from 24-60 minutes. The position and locomotion of the mouse was recorded by a behavioral camera positioned roughly 50cm above the chamber recording at 30 frames per second (FPS). Positional information was extracted using DeepLabCut (Mathis et al., 2018). Image data from the miniature microscope was processed using Suite2P (Pachitariu et al., 2016) to perform non-rigid motion correction, segment individual neurons, and extract calcium traces. On average from 6 free-behavior recording sessions, we resolved dynamics from  $110 \pm 8$  active neurons in CA1 within the field of view, following processing with Suite2P. The exact parameters for the analysis are included with the rest of the control software, in the form of an ops file that can be easily referenced or deployed by users. Figure 7.1 demonstrates an example CA1 recording session where an approximately 20g female mouse can be seen navigating throughout

the chamber while neural activity is recorded. Over the 20-minute session, the median speed of the mouse was  $\approx 4.1$ cm/s which is similar to previous results regarding the impact of microscope weight on median animal speed (Zong et al., 2022) when considering the system weighs  $\approx 4$ g. Within one recording session, we observed more than 32 cells with spatial firing preference (highlighted in E, F, G, H of Figure 7.1), suggesting that the UCLA 2P Miniscope is able to resolve the activity of place cells in CA1 over behaviorally relevant timeframes.

### **7.3 Retrosplenial Cortex (RSC) - 2-Color Dendritic Calcium Signals During Free Behavior**

1P miniature microscope systems are largely constrained to studying activity patterns from relatively superficial somas near the implanted window or GRIN lens largely due to scattering and fluorescent background in neural tissue. Multiphoton systems, on the other hand, are able to resolve calcium events in fine cellular structures such as dendrites and axons, hundreds of microns below the surface of the brain. One major goal in the development of our miniature 2P microscope was to build an imaging system with sufficient resolution and sensitivity to study dendritic patterns of activity, since the mechanisms by which neural inputs are integrated during free behavior is largely understudied in the field. To assess the system’s ability to detect activity from dendrites, we recorded AAV-GCaMP6f in layer 2/3 neurons in retrosplenial cortex (RSC) during free behavior on the first color channel, along with cFos-expressed mCherry on the second detector channel. Because RSC is such a medial structure, cortical layers are rotationally oriented such that the apical dendrites of pyramidal cells are within the same imaging plane as the cell bodies. We leveraged this anatomical feature to our advantage to study dynamics not only from somas, but their corresponding apical dendrites as well, during free behavior. To gain optical access to RSC, a 4mm x 4mm cortical window was placed over

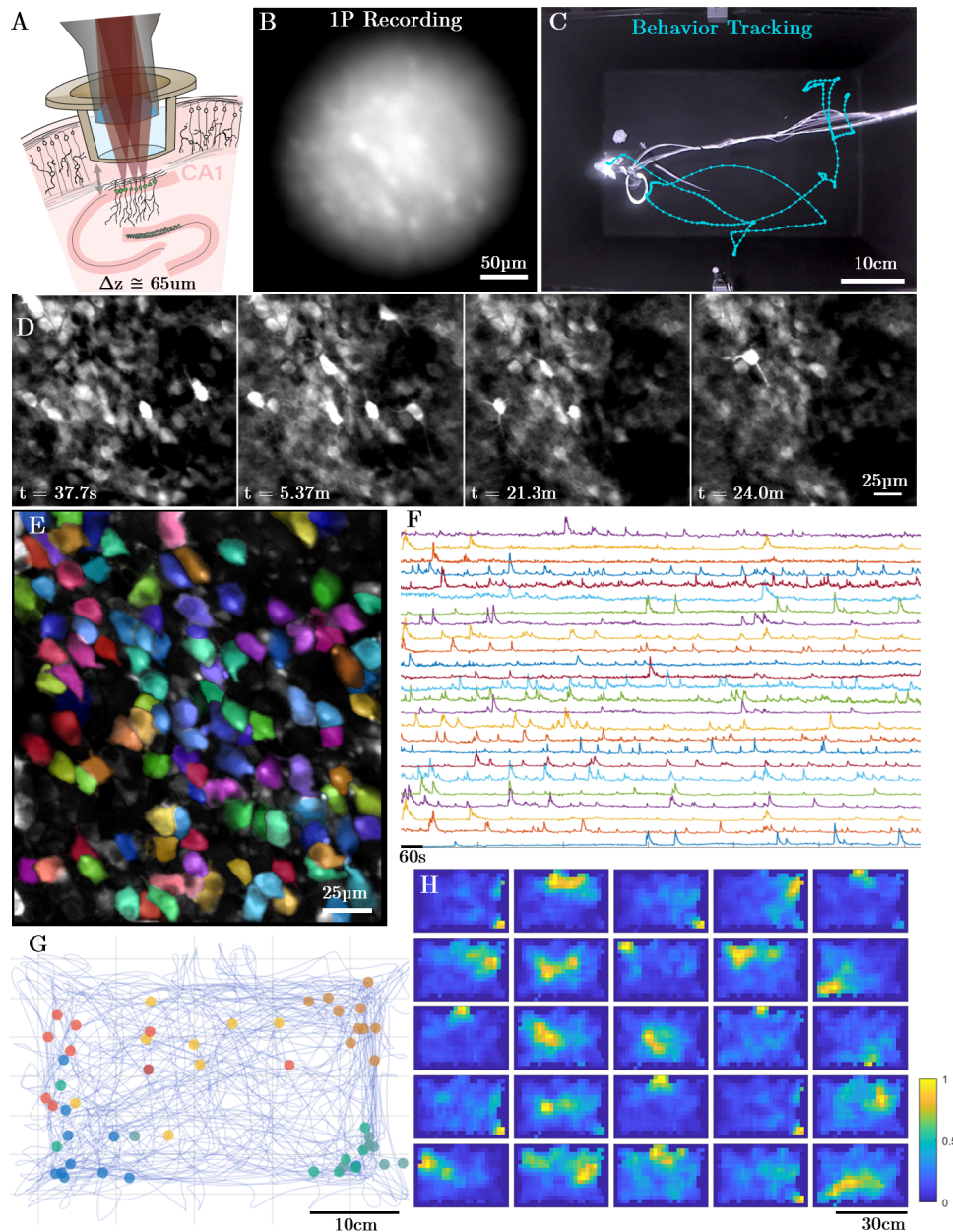


**Figure 7.1: Resolving Densely-Labeled CA1 Neurons During Free Behavior**  
 (A) Schematic drawing of the imaging conditions, including the titanium cranial window implant and the objective lens from the UCLA 2P Miniscope. (B) 1P image collected in the same animal, in the same brain region on the same day as all other panels except E. (C) Experimental mouse in the behavioral chamber, during the > 20-minute imaging session. Light-blue line shows a subset of the animal trajectory in the chamber over time. (D) Imaging results from the microscope system over the course of the free behavior experiment. (E) Extracted footprints of the active neurons within the FOV (randomly-colored) following motion correction. (F) Neuropil subtracted activity from the neurons in G and H. (G) Firing locations of a subset of neurons from F and H plotted within the behavioral arena. (H) 25 example statistically significant place cells.

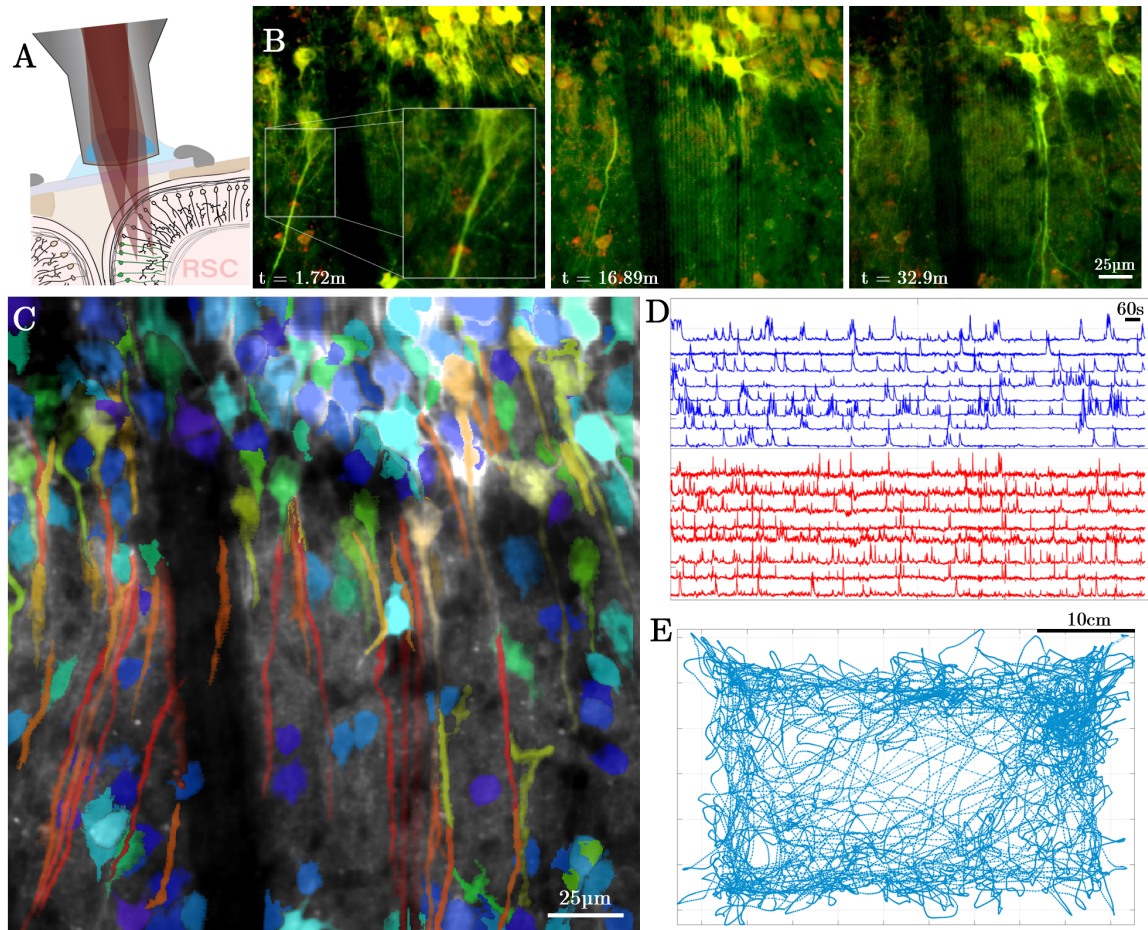


Figure 7.2: **Dendritic 2-Color Imaging in Cortex During Free Behavior**  
 (A) Schematic drawing of the experimental preparation used to record from RSC and the curvature of the cortical column that makes resolving long dendrites in the cortex possible. (B) Time-course of still frames over the course of the 30-minute recording, highlighting the axial stability of the system and ability to reliably track single projections over substantial timeframes. (C) Pseudo-colored image exported from Suite2P which colors ROIs by their aspect ratio. This is superimposed on the mean of the entire recording. (D) Calcium signals from somatic (blue) and dendritic ROIs (red) plotted separately. (E) Animal trajectory over the 30-minute experiment.

the region (details in Methods). While this window was larger than optically required, it provided experimental flexibility and the ability to locate an FOV where dendrites and somas are both coplanar and clearly visible. Figure 7.2 shows the results of an RSC experiment, including the image data, mouse position, and activity traces from both cell bodies and dendrites. The high degree of correlation between the activity of the RSC somas and proximal regions of apical trunk dendrites suggests that the majority of the events resolved are global calcium events activating both soma and dendrites in the FOV. Over 30-minute recording sessions, individual dendrites remained stable within the image field (especially in the z dimension) with no need to remove any portions of the recording where dendrites were lost due to motion. Therefore, the UCLA 2P miniscope is ideal for studying dendritic and potentially axonal dynamics during free behavior in mice.

## 7.4 DG - Imaging Neurons Hundreds of Microns Deep

The dentate gyrus (DG) is a critical region within the hippocampal formation and tri-synaptic circuit with extensive and direct connections to other hippocampal subfields and the entorhinal cortex. The principal cells of the DG, dentate granule cells, have been implicated in spatial navigation, episodic memory formation, and discrimination learning (Hainmueller and Bartos, 2020). The DG is also a key site for adult neurogenesis in the mammalian brain, including humans (Moreno-Jiménez et al., 2021; Eriksson et al., 1998; Johnston et al., 2016; Gonçalves et al., 2016). Studying dentate granule cell activity *in-vivo* through electrophysiological methods has proven challenging due to their extremely sparse but highly salient activity (Tuncdemir et al., 2019), which complicates accurate spike sorting in these neurons. More recently, groups have turned to calcium imaging, which directly visualizes spiking neurons, in order to study the dynamics of granule cells during spatial navigation. However, the current use of calcium imaging in the DG still has significant limitations. In the dorsal hippocampus of the rodent brain, the DG sits deep to CA1 and other subfields within the tri-synaptic circuit. Ideally one would like to maintain

the integrity of all the hippocampal subfields and their connections when measuring activity in the DG. The depth of the dentate granule cell layer lies ( $\approx 500\text{-}650\mu\text{m}$ ) below the surface of the hippocampus (alveus), precluding the use of single photon methods to image the DG within the intact hippocampus. Researchers have relied on the use of GRIN lenses and aspiration and disruption of the overlying CA1 to gain optical access to the DG and resolve dentate granule cells using 1P miniature microscopes (Stefanini et al., 2020). Capitalizing on the ability of multiphoton microscopy to image several hundred micrometers into tissue, others have conducted multiphoton imaging studies in head-fixed animals using surgical approaches that maintain the structure of the full hippocampus. However, these studies rely on virtual or floating environments to study spatial navigation (Hainmueller and Bartos, 2018), which lack vestibular and other important inputs that can modulate place cell activity (Ravassard et al., 2013). To address these limitations, we tested the ability of the miniature 2P microscope to resolve granule cell activity in freely behaving mice exploring a novel environment. Sparse dynamics were captured from  $\approx 50$  granule cells over the approximately 20-minute recording interval. Figure 4 displays the imaging results from an example imaging session, as well as extracted neuronal footprints and activity traces. Taken together, these results demonstrate the capacity of the UCLA 2P Miniscope to resolve calcium transients even from deep neuronal populations during free behavior.

## 7.5 Analysis Methods

Microscope images were processed using Suite2P (Pachitariu et al., 2016) version 9.2 to correct for motion artifacts, perform segmentation, and calculate activity traces over time. Suite2P deconvolved the slower calcium dynamics according to the specific GCaMP being used in a particular experiment, generating a spks matrix used for downstream analysis. Animal locations were calculated from a time-synchronized behavioral video using a trained neural network via DeepLabCut (Mathis et al., 2018). To evaluate the spatial firing properties of neurons, a MATLAB script was written which follows methods

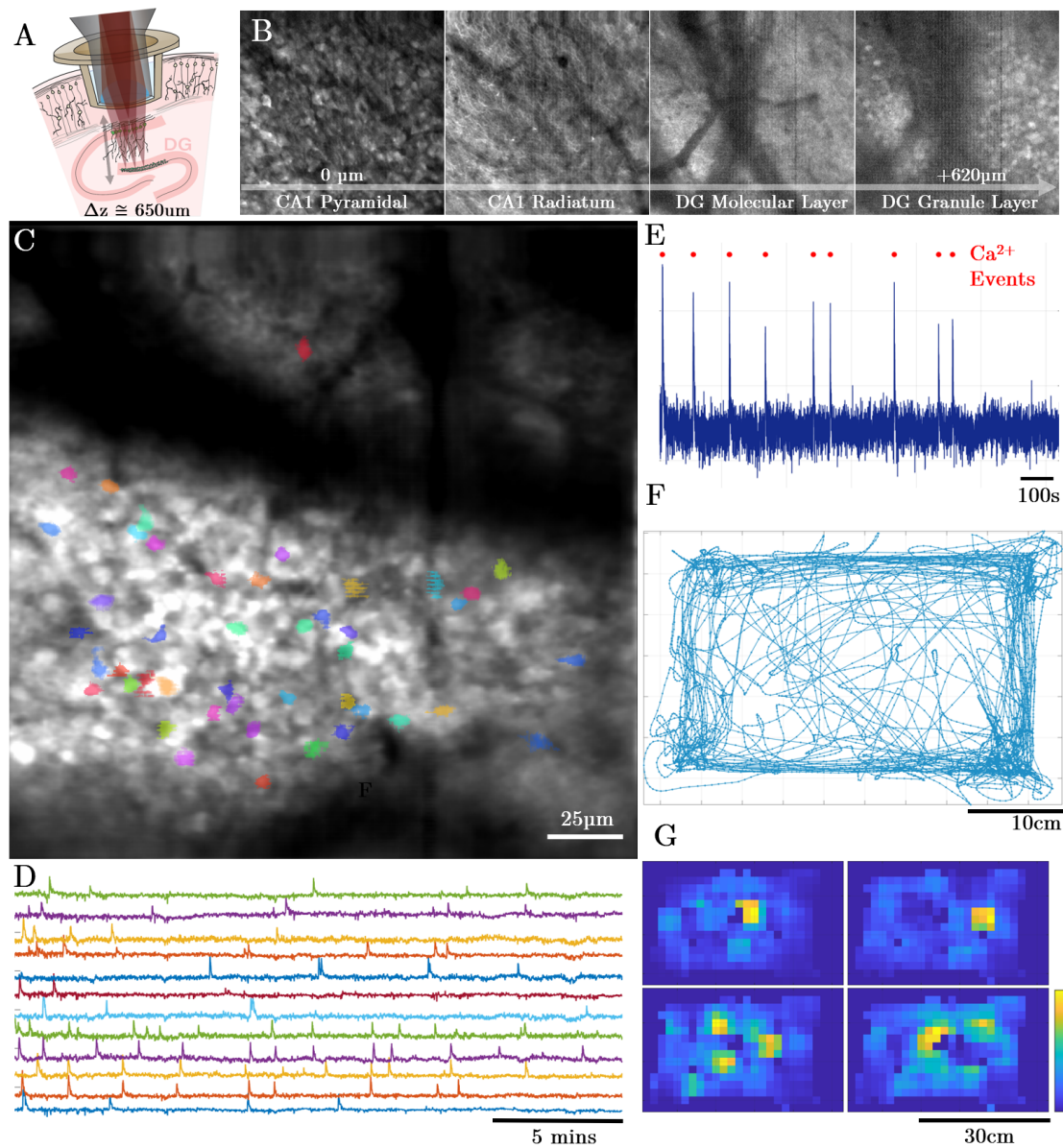


**Figure 7.3: Recording Calcium Dynamics from Dentate Granule Cells Through an Intact Hippocampus During Free Behavior**

(A) Schematic drawing describing the placement of the titanium cannula and cover-glass assembly relative to the image field in DG. (B) Montage of frames from a continuous z-stack in a head-fixed mouse expressing GCaMP8f. (C) FOV from DG, during a 20-minute free behavior experiment. Colored cells were identified as active using Suite2P. (D) Activity traces from a subset of the identified active neurons shown in C. (E) A single example neuron activity trace with a high number of events compared to the average. Calcium peaks identified from the deconvolved signal are plotted as red dots above the neuropil-subtracted activity. (F) Animal trajectory over the 20 minute experiment. (G) Statistically significant spatial activity plots for a subset of the cells displayed in C.



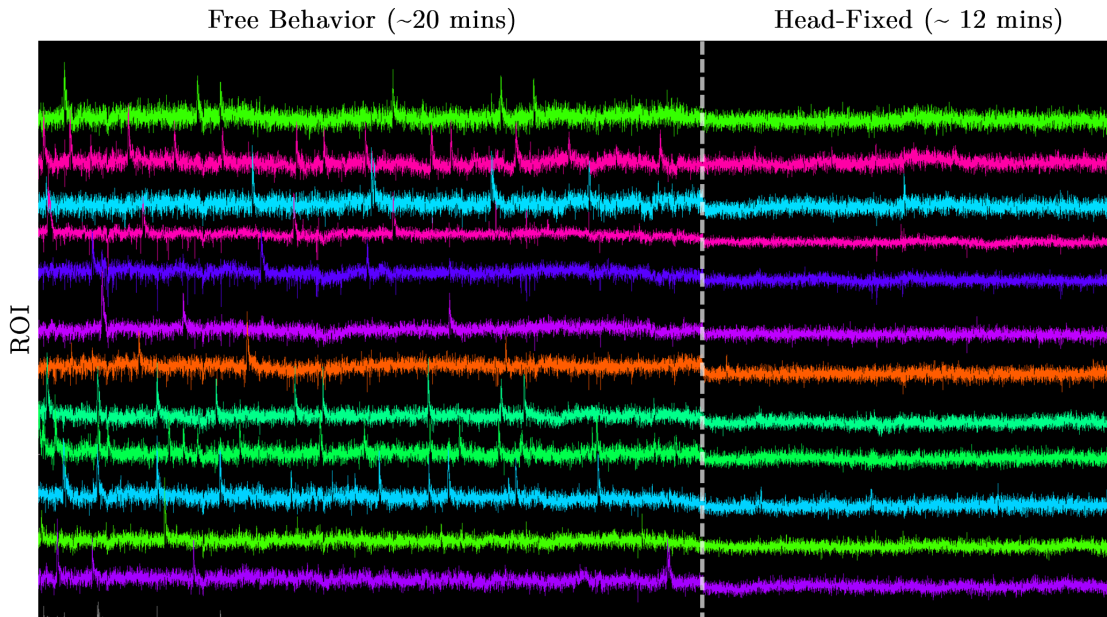


Figure 7.4: **Granule Cell Dynamics Between Head-Fixed and Free Behavior**  
Clear differences between calcium dynamics in granule cells before (left) and after (right) head fixation

previously published (Guo et al., 2023). Position information was down sampled to the same number of time points as there are behavioral frames throughout the experiment. Space within the frames was discretized into 2.08cm x 2.08cm spatial bins for CA1 and DG recordings. A speed threshold of 2cm/s was applied to restrict consideration of data while the animal was immobile. An occupancy matrix was constructed by summing the number of samples spent in each spatial bin, and a spatial neural activity matrix was calculated as the sum of all deconvolved activity for each spatial bin. Each of these matrices were smoothed using a 2D gaussian kernel with a sigma of 6cm. After filtering, the smoothed spatial neural activity matrix was divided by the smoothed occupancy matrix to arrive at a spatial neural activity rate for each neuron. Shannon Information, ( $I$ ), was calculated for each neuron using the Kullback-Leibler Divergence formula, as implemented in (KM-Lab, 2020).

$$I = \sum_i \left( \frac{\lambda_i}{\bar{\lambda}} \log_2 \left( \frac{\lambda_i}{\bar{\lambda}} \right) p_x \right)$$

Such that  $\lambda_i$  is equal to the rate of neuronal activity at bin ( $i$ ) and  $\bar{\lambda}$  is the mean neural activity rate (Guo et al., 2023). Statistical significance was assessed using circular shifting. Neural activity traces were offset by a random number of samples in time, ranging from one sample to the total number of samples within the recording such that the end of the neural activity vector is circularly wrapped to the beginning. This effectively shuffles the relationship between the animal's position and the extracted neural activity. Information content was calculated for all 500 shuffles, across each identified ROI. Only the ROIs whose information content was significantly greater than chance (  $P > 0.95$  ) were considered place cells and plotted in Figures 7.1 and 7.3.

## CHAPTER 8

# UCLA 2P Miniscope: Design Philosophy and Filling a Gap in the Field

### 8.1 A cost-effective 2P Miniature Microscope

We developed the UCLA 2P Miniscope to be cost effective without significantly compromising performance. Our entire microscope headpiece can be built for less than \$7.5k USD currently with low production numbers and likely with scaling can be reduced to approximately \$5k USD each. The majority of the cost comes in the form of the custom optical assemblies which are assembled, coated, and tested individually by Optics Technology in New York, USA. With scale, we predict these assemblies to drop in cost and further lower barriers of entry to labs hoping to use miniature 2P microscopes to study neural dynamics in freely behaving animals. To our understanding, this is the first miniature 2P microscope that is open sourced and able to be built for less than \$10k USD.

### 8.2 Prioritization Given Towards Ease of Assembly

Our goal is to make miniature 2P microscopy as accessible to as many users as possible, while pushing the technical limits of what such systems are capable of achieving. Intentional design tradeoffs were made throughout the engineering process which ultimately prioritized user adoption over absolute performance. One example of this is the tunable lens. Other microscope systems use stacks of piezoelectric tunable interfaces to generate sufficient optical power to translate the focal plane by respectable amounts. (Zong et al., 2022)

Component	Manufacturer	Quantity	Cost	Subtotal
Objective Lens	OT, Custom - 1	1	\$4000	\$4000
Tube Lens	OT, Custom - 2	1	\$1100	\$1100
Scan Lens	ThorLabs, AC050-010-B	2	\$51	\$102
Aspheric Lens	Newport, KGA170-B	1	\$104	\$104
Collection Lens	Edmund, 47-895	1	\$62	\$62
2P Dichroic	Chroma, ZT775sp-2p	1	\$540	\$540
1P Dichroic	Chroma, T550lpxr	1	\$112	\$112
2P Emission Filter	Chroma, ET750sp	2	\$150	\$300
MEMS Scanner	Mirrorcle, A7M20.2-2000AL	1	\$591	\$591
Electrotunable Lens	Varioptic, A-25H1	1	\$135	\$135
Mechanical Housings	Custom Made	4	\$10	\$40
PCBs	PCBWay, Custom Made	1	\$50	\$50
SiPM Detectors	Hamamatsu, S13360-3075PE	2	\$52	\$105
				<b>\$7243</b>

Table 8.1: **Cost breakdown for the UCLA 2P Miniscope microscope headpiece**  
 These costs are as of March 2024 when components were purchased at small scale. Please note that these expenses do not include key additional hardware, such as laser and traditional 2P microscope acquisition electronics

While these elements are extremely lightweight (0.06g) and seem to perform very well, they are difficult to align together into a colinear, stacked assembly and install into the microscope body, resulting in a barrier to entry for users. In contrast, we use off-the-shelf Varioptic lenses which are substantially heavier (0.36g) yet are easy to source and install. This intentional decision was made not due to performance, but to achieve increased user friendliness and adoption capability. We believe that these benefits outweigh the cost associated with the modest increase in weight of the UCLA 2P Miniscope compared to other similar systems.

### 8.3 Designed to Be Sensitive to Dim Signals

The UCLA 2P miniscope also uses on-board Si-based detectors, similar to those used in 3P applications (Klioutchnikov et al., 2023). Such a detection scheme substantially improves collection efficiency of the microscope and thus makes resolving dynamics from

deep structures like DG possible, at the expense of added weight. The microscope in its current form uses two detectors, to record from red and green channels, as well as collection optics and spectral filters to isolate colors onto discrete detectors. Because of this, the microscope incurs some additional weight, at the benefit of being able to record deep and challenging brain areas in two colors.

## 8.4 Designed to Be Shared

We developed the UCLA 2P miniscope as an open-source, easy to assemble miniature multiphoton microscope with high resolution and frame rates optimized for calcium imaging experiments. From the start of the project, lowering cost and maximizing ease of user dissemination has been a critical focus, and we have carried these priorities into each aspect of the microscope design. Custom-made lens assemblies are limited to a modest number of lens elements, for a high degree of mechanical tolerance during assembly and general affordability. The majority of components are off-the-shelf components and easy to procure, in order to lower barriers of entry to labs interested in using this technology. The housings are made using low-cost resin-based 3D printers (all files are uploaded to the Git repository) and can be made easily in large batches. We integrated silicon-based detectors onto the collection head of the microscope similar to 3-photon miniature systems in the literature for rats and mice (Klioutchnikov et al., 2020, 2023) to remove cumbersome and photonically lossy fiber bundles. In addition, we designed electronic interfaces to be plug-and-play and easy to interface with. Initial, fully functional versions of these electronics are uploaded to an open Git repository, and newer, even easier-to-implement versions are nearly complete for user implementation, complete with a standalone python-based GUI. Those designs will be uploaded soon, following peer review. The result is a  $\approx 4$ g miniature 2P microscope system with sub-micron lateral resolution over large image fields, useful for studying neural dynamics of deep structures or fine features in freely behaving animals.

## 8.5 Designed to Be Experimentally Robust

Lastly, the optical design is rather simple, and the mechanical housings are intentionally robust. We know from experience that imaging devices used in freely behaving animal experiments are subject to great abuse, during which housings can break, or optical misalignments may occur. By simplifying the number of components and interfaces, we not only made the optical tolerances forgiving, but we also made the device reliable. Despite this simplicity, the microscope is able to resolve sub-micron features in neural tissue. In key portions of the mechanical housings, the wall thickness is deliberately thick, resulting in components resilient to knocks, bumps, and drops. This increases weight, but ultimately improves useability by researchers and ensures the device works in realistic environmental conditions, which is of paramount importance. Altogether, the UCLA 2P miniscope is a high-performance microscope intended to be set up and used by other labs. Decisions were made throughout the design process which included known sub-optimizations, which in turn impose limitations on performance. In each circumstance, these tradeoffs were made to the benefit of user adoption and reducing the barriers to entry as much as possible. We believe most labs with 2P microscopy experience will be able to set up the UCLA 2P miniscope hardware for approximately \$5k USD when produced at reasonable scale.

## CHAPTER 9

# UCLA 2P Miniscope: Dissemination Efforts and Future Directions

### 9.1 GitHub Repository

One central goal of this project from the start was ensuring that each aspect of the design was made available to the community. With that in mind, every design file required to replicate and use the microscope was uploaded to the UCLA Golshani Lab [GitHub repository](#). A screenshot of that is shown below. A screenshot of that is shown below. This includes all mechanical housing files, the electronic GERBERs, ZEMAX simulations, and Matlab control scripts. Additionally, we have included pre-trained DeepLabCut image classifiers and Suite2P parameters to make the analysis of the data as straightforward as possible for users. We will continue to expand on this repository over time as we include additional assembly tutorials, videos, and other resources.

### 9.2 Workshops

Ensuring that research labs are well equipped to deploy and utilize the open-source hardware presented in this dissertation is extremely important. One effective avenue for making sure that this is the case is through virtual and in-person workshops. The UCLA Miniscope Project has a long history of conducting very impactful workshops to help users not only gain familiarity with the equipment, but also with analyzing datasets. Our goal is to continue this, and we have already held one workshop to date at the University of

blakemadruga Update README.md · 3 weeks ago · 2 Commits


Control Software	Main Upload	last month
Electronic Designs	Main Upload	last month
Images	Main Upload	last month
Mechanical Designs	Main Upload	last month
Suite2P Ops	Main Upload	last month
Trained DeeLabCut Model	Main Upload	last month
ZEMAX Optical Designs	Main Upload	last month
LICENSE	Main Upload	last month
README.md	Update README.md	3 weeks ago

README GPL-3.0 license

## UCLA 2P Miniscope

UCLA miniature multiphoton microscope resources and design files.

The UCLA miniscope project is an open-source initiative to design open-source miniature microscopes for neuroscience. Here, we present a multiphoton miniature microscope developed at UCLA which is able to record from fine structures like dendrites, or several hundred microns into tissue.



In this Git repository, we openly share all of the design files for this microscope with the community, these include:

- Mechanical Design Files (in .STEP format)

**UCLA Multiphoton Miniature Microscope**

- Readme
- GPL-3.0 license
- Activity
- Custom properties
- 4 stars
- 1 watching
- 0 forks
- Report repository

**Releases**

No releases published

**Packages**

No packages published

**Languages**

- MATLAB 100.0%

Figure 9.1: UCLA 2P Miniscope Github Page

California, Irvine, during the Center for Neural Circuit Mapping Bootcamp (August 23, 2023). We plan to hold additional workshops in the future, as well as upload links to videos of the workshops to the GitHub repository for sharing.



## 9.3 Future Directions

### 9.3.1 Extending Current Technology

The most straightforward approach to thinking about future developments within miniature microscopy is to begin with incremental improvements that come from the onset of new and innovative technology that have yet to make its way to the field. To my view, these include: new scanner technologies for autonomous vehicle applications, methods that utilize the new support of polarization maintenance in hollow-core photonic crystal fiber, integration with off-the-shelf freeform miniature lens assemblies and the utilization of diffractive optical elements (DOE).

#### **Piezoelectric scanner technologies:**

Beam steering has massive applications not only in microscopy but in other areas of research and technology. One massive field is LIDAR (Light Detection And Ranging) which holds ubiquitous applications in the mapping of 3D space for geographic satellite surveying, atmospheric physics, and self-driving vehicles (both on Earth and Mars). Other methods of LIDAR scanning exist today (such as phased arrays), but one more common approach is to use MEMS scanning systems to translate a pulsed IR laser beam across 3D space following a specified scan path to generate a depth-map of 3D space surrounding the sensor. To date, the field has largely relied on comb-drive style actuators, which rely on generating force through relatively high voltages ( $\approx 200\text{V}$ ) placed across a large surface area and ground. These are called comb-drives because they look like two interleaved, but not touching, hair-combs, with a high bias placed between them. The resulting electric field generates a force which ultimately results in the displacement of a mirror surface located at the center of two equal, but opposed comb-drives. When one pushes, the other repels, thus generating a net torque on the mirror surface and displacing the laser beam angularly. While these comb-drives have many inherent benefits, they have clear limitations as well. The actuators take up substantial surface area, and they are limited in the total force production before

dielectric breakdown. One advance seen in the LIDAR field is to generate these scanning mirrors with piezoelectric technology, which does away with the complex geometry of comb drives all together and relies on advanced materials which directly compress or elongate as a result of applied voltage. The result of this arrangement is a much more compact actuator with higher deflection angles for a given drive voltage. Ultimately this creates a scanner with higher resonant frequencies and larger mirror diameters, which both act in unison to improve the performance of miniature 2P microscope systems. One difficulty is that the majority of such scanners are unable to be operated through conventional raster scanning means, and as such, new methods would need to be developed. Regardless, turning to older scanning techniques of the past, such as (Helmchen et al., 2001) with cutting edge piezoelectric LIDAR scanning technology, could be a beneficial and innovative combination.

#### **Polarization maintenance strategies:**

New hollow-core optical fibers are not only beneficial for limiting the amount of group-velocity dispersion felt by an optical pulse propagating along its length, they also have polarization maintaining properties. This is to say that a 2P miniature microscope could be built using plate polarization beam splitters and waveplates to utilize the entire clear aperture of the scanner surface. Currently, because we are not utilizing the polarization maintaining properties of the fiber, input light is reflected at an angle relative to the scanner, resulting in a smaller effective beam diameter that scales as  $1/\cos(\theta)$  where  $\theta$  is the incident angle of the laser on the scanning mirror. To utilize the full mirror angle would mean improving the excitation NA and thus 2P conversion efficiency. In addition, this methodology could be used to integrate further equipment into the same beam path more efficiently in combination with some additional mirror surfaces, such as 1P lasers for optogenetic stimulation.

#### **Off-the-shelf Freeform Miniature Lens Assemblies:**

Lens assemblies designed and manufactured for use in portable camera systems have superb

optical performance over extremely large image fields. One significant explanation for this is their use of freeform optical assemblies consisting of many molded lenses consisting of complex, non-spherical surfaces. While these lens arrangements are difficult to design and produce, there is a case to be made for deploying these assemblies, with some modifications, for use in miniature microscopy. Some designs have been fabricated in the literature, including (Wan and Tao, 2021), however designs that have been used to study neural circuit function *in-vivo* are yet to be realized. I believe that leveraging existing optical designs with often superb optical performance and low cost, could be an avenue for future development. For 2P applications, specific optical coatings may be required to achieve peak performance, but that is a relatively straightforward modification to an otherwise highly optimized piece of hardware.

### **Integration of Diffractive Optical Elements:**

Diffractive optical elements hold the capacity to shape light on the sub-wavelength length scale through the formation of fine surface features that interact with the wavelike nature of light. Some of these elements include typical lenses like fresnel lenses, (Fresnel, 1819), but more elaborate geometries like fraxicons (Golub, 2006), and beam multiplexers (Kazanskiy et al., 2020) can be designed. Additionally, because these structures are completely flat (with the exception of extremely small surface features) multiple optical elements can be stacked in very close proximity to one another. Additionally, multiple beam shaping profiles, such as a prescribed astigmatism as the combination of cylindrical lens shapes of different power, can be accomplished using a single optical element which would be very difficult to fabricate otherwise.

### **9.3.2 Learning From Large Systems**

Another fruitful way to think about future directions is to consider what can currently be done in large form factors, but not yet in miniscopes. Several that come to mind are: Temporal and Spatial Multiplexing, SCAPE, Bessel Scanning, Topographic Methodologies,

and Scan Multiplexing. These are described in detail below.

### **Temporal and Spatial Multiplexing of the Optical Pulse:**

2P microscopy relies on ultrafast pulsed lasers to spatiotemporally confine large NIR photon fluxes to create efficient multiphoton stimulation at MHz repetition rates. Typical lasers emit pulses in the 60-80MHz range, but this isn't strictly required for imaging and some would argue that lower repetition rates are advantageous. Due to the distinct temporal differences in low repetition rate lasers used in some 2P photoexcitation systems (say 5MHz, corresponding to 200ns between pulses) and the fluorescence lifetime of many proteins ( $\approx 6$ ns for GCaMP), there is a world of unutilized dead time which can be leveraged to improve throughput in exciting and experimentally advantageous ways. One method is to split a single low rep rate laser into multiple beams and temporally delay them relative to each other. Since these beams are now spatially and temporally separate, additional optics can be used to add differing degrees of divergence or convergence to each beam path separately, thus generating four individual focal planes which can be addressed from one single detector (Cheng et al., 2011). Other groups have taken this concept to extremely impressive limits with sophisticated cavity designs, generating 30 individual foci which are temporally and axially offset (Demas et al., 2021) allowing for the recording of 10s of thousands of neurons simultaneously across many cortical layers. While building a full "Light Bead" microscope that fits on the head of a mouse is impossible, integrating some of those ideas to enable extended functionality is certainly possible. For example, by transmitting four optical fibers (each carrying a temporally offset beamlet) to a miniature microscope, it would be possible to axially offset and record from four distinct focal planes simultaneously, something that would not only massively enhance experimental throughput but also enable new studies in freely behaving animals. This is currently underway and a future direction that is very important in my view.

### **Swept Confocally-Aligned Planar Excitation:**

Swept confocally-aligned planar excitation (SCAPE) microscopy is a single-objective light sheet imaging system that enables rapid volumetric imaging without the need for sophisticated, high-speed piezoelectric objective collars. Because SCAPE relies on sweeping a planar excitation source (positioned at an angle relative to the objective’s native focal plane) across a sample in 1D, it generates inherently 3D volumetric images at very high speeds (300 volumes/s) (Voleti et al., 2019). While other miniscopes exist that are able to capture volumetric data *in-vivo* (Skocek et al., 2018) they rely on light-field methods which inherently function through a trade-off between lateral and axial resolution. In addition, light-field methods often rely on complex and computationally demanding reconstruction algorithms which make analysis difficult for users. A method like SCAPE, for example, would generate native images which could be quickly analyzed through conventional methods like NoRMCore and Suite2P without extensive preprocessing. Additionally, a SCAPE arrangement could enable the use of a multiphoton excitation light sheet, whereas light-field means could not. Regardless, all SCAPE systems rely on remapping the tilted excitation focal plane onto another set of objective lenses, positioned at a prescribed angle relative to one another, thus compensating and removing the impact of the original tilted lightsheet in the sample before being captured by an image sensor. Doing this whole process on the head of an animal seems unlikely unless there are sophisticated sets of custom optical elements involved in remapping the focal plane of interest. One likely avenue which brings its own challenges is the use of relaying the fluorescence over a coherent optical fiber bundle to downstream bench optics that employ the conventional method for remapping the focal plane onto the image sensor. One issue that arises from this method is the minimum core-to-core distance defining the resolution of the imaging system, since any spatial information that may exist within the diameter of a single fiber core is lost following transmission to the detector end of the coherent bundle. Such bundles are also photonic lossy (as described in section 8.3) and thus the SNR of the collected data is likely to be low. However, perhaps with DOEs or sophisticated MEMS solutions new ways of remapping the

focal plane onto an on-board image sensor would be possible, making volumetric recordings possible at near volume imaging rates, which would be extremely impactful to the field.

### **Bessel Scanning:**

Non-diffractive optical beams, such as Bessel beams, hold inherent performance advantages when compared to traditional Gaussian beams, especially when considered in the multiphoton domain. Bessel beams specifically are generated as a result of interference phenomenon taking place between plane waves propagating along conical vectors (think of a relatively thin ring in k-space) (Ren et al., 2021). The resulting beam is far longer, more homogeneous, and thinner than a traditional gaussian beam with “self-healing” properties. However, significant energy is contained outside of the main beam as a result of the interference necessary to the generation of a Bessel beam. Such energy would contribute a large amount of background in 1P configurations, however because of the irradiance dependence on 2P excitation, the impact of the side-lobes are greatly reduced when using multiphoton approaches. Some light-sheet and upright microscopes have been designed and built which utilize these advantageous beams in new and innovative ways (Gao et al., 2014; Fahrbach et al., 2010; Rodríguez et al., 2018; Chen et al., 2022). For applications in miniature microscopy, the most straightforward application would be an arrangement which intentionally elongates the axial PSF to make recording of long dendritic segments (which span 50-75 $\mu\text{m}$  in depth for example) possible. Modifying the current microscope presented in the dissertation to do this is relatively straightforward either with a diffractive optical element or a small single negative axicon lens. Ideally the length of the Bessel beam would correspond to the 50-75 $\mu\text{m}$  length of the dendritic segments of interest. The resulting 2D images would essentially take the form of a maximum projection of the 3D tissue scanned by the elongated axial PSF.

### **Resonant Scan Multiplexing:**

Imaging the same fields of view in less time is a large goal for microscopists the world

over, because of important and exciting applications that involve measuring rapid, salient signals in the brain like individual action potentials or glutamate release in single dendritic segments. Since 2P methodologies are generally bandwidth limited by scanning technology, optical means to surpass inertial limits have been developed. One study used a microlens array and retroreflector to essentially convert a single sweep of a raster scanner (half-period) into a set of  $n$  periods, where  $n$  is the number of microlenses being swept across a single half-period of the raster scan (Xiao and Mertz, 2022). Using a set of 12 microlenses, for example, would multiply the effective scan rate of a microscope system by a factor of 24, thereby converting a 10kHz scanner to one that generates 240 scan lines/s, thereby making kHz frame rates possible. Integrating the optical scan multiplexing hardware within a miniature device is a clear technical challenge due to the path lengths and polarization optics required. Also, since MEMS scanners are limited in bandwidth compared to large benchtop resonant scanners, the relative gains in speed are less impressive. However, these scanning methods and associated gains in speed can be accomplished relatively quickly when approaching a miniature 2P microscope from a coherent fiber approach, as done in (Ozbay et al., 2018). These methods suffer from clear optical limitations due to the core-to-core distance between individual fiber cores, as detailed in section 4.2.1. Despite these hurdles in optical resolution, it would be possible to leverage scan multiplexing to resolve neurons in the brain at kHz rates in freely behaving animals - a clearly massive technical accomplishment for the field.

### **Topographic Methodologies:**

Recent developments around building microscope systems that rely on topographical concepts have proven to be impactful and exciting for the field. Such systems utilize line-scanning in combination with prior-image constrained compressed sensing reconstruction algorithms (PICCS) to circumvent the main rate-limiting step in 2P microscopy, point-scanning with resonant scanners (Kazemipour et al., 2019; Podgorski et al., 2023). Such methods are capable of achieving multiphoton frame rates in the kilohertz due to

the sampling methodology minimizing the number of tomographic projections required to reconstruct the object with sufficient detail for neuroimaging applications. The potential associated with this methodology is huge, but so is the technical challenge in building it, even on a large optical bench. Reducing the dimensions of such a setup to fit on the head of the mouse is potentially more than just ambitious, however, perhaps taking some inspiration from tomographic approaches could be integrated into miniature 2P systems in the future. I could imagine scanning a line-focus in the brain at various angles using a quasistatic MEMS scanner in combination with a powell-lens. It is not clear to me how projections are required to build a sufficiently high resolution image through reconstruction, but if this number is in the realm of 50 - 75 projections, the framerate of the 2P miniscope presented here could be significantly improved to enable recordings approximately 8.5x faster than raster scanning.

## 9.4 Conclusions

Miniature microscopy is a critically important optical tool for neuroscientists studying neural circuit mechanisms that underly many naturalistic behaviors. Specifically, miniature microscopes allow for the study of cells involved in behaviors that cannot be replicated sufficiently within head-fixed contexts, like spatial navigation or social interaction. While these tools have immense power, the majority of miniature microscopes are single photon in nature, and thus, suffer from scattering and a lack of optical sectioning ability. As a result, 1P systems are only able to resolve somas that are within a few microns from either a cranial window or implanted GRIN lens. To overcome these limitations and study dynamics from deep cellular networks or fine cellular projections like dendrites and axons, multiphoton approaches are necessary. The open-source miniature 2P microscope presented here extends the capabilities of the UCLA Miniscope Project and enables the rest of the community to build and use the hardware and software described for minimal expense. The UCLA 2P Miniscope costs less than \$10k USD, has submicron resolution and optical sectioning abilities that make it able to address new scientific questions in



freely behaving animals. We used it to resolve dendrites in freely behaving animals, as well as resolving dense, tightly packed granule cells hundreds of microns into tissue. Altogether, this innovative tool will contribute to scientific discoveries and further our understanding of how neural dynamics encode behavior in a number of experimental contexts.

## CHAPTER 10

### Part II: Spatially-Confined 1P Excitation Voltage Imaging Microscope

#### 10.1 Introduction to Voltage Imaging

Calcium imaging is undoubtedly an important research tool for characterizing and understanding the dynamics of neuronal networks involved in cognition. However, calcium imaging is fundamentally a proxy for neural activity, since individual cells communicate not through the flow of calcium, but through brief impulses of electrical potential. These rapid events were described in section 1.4 of the dissertation and are known as action potentials. Such events occur on the millisecond timescale and involve a sequence of well characterized ion channels opening and closing, resulting in rapid exchanges of ions across the cell membrane, producing fast electrical signals that propagate across the neuron. These impulses by large are what drive cognition, produce movements, and result in the formation of new memories with mechanisms like Hebbian Plasticity and Long-Term Potentiation. Resolving such rapid events requires high sampling rates in order to prevent aliasing of the true underlying signal, typically in the 10s of kHz for electrophysiology experiments. Building imaging systems that can capture the kinetics of new genetically encoded voltage indicators (GECIs) is clearly a challenge for the field, but one with massive opportunity. In Part II a new, simple 1P microscope is constructed to do so.

### 10.1.1 Constraints on Parameter Space

A central goal of neuroscience is to understand how networks of neurons represent information, and how those representations are updated with new learning or experience. To do so, new voltage indicators have been engineered that operate across a host of functional mechanisms. Only now have these indicators become optimized enough to provide widespread scientific utility, although difficulties on building suitable imaging systems still persist. The voltage indicators of interest still temporally low-pass the single action potentials, so 10kHz frame rates are not strictly required. The consensus of the field seems to be that there is an optimum around 400-500 FPS in terms of signal integration time and the mitigation of spike aliasing. Now since the fluorescent signal of interest from a GEVI only exists across the surface area of a membrane and not throughout a full cytosolic volume as with a GECI, the total amount of space that fluorescent molecules can reside is far lower, likely also reducing the amount of fluorescent signal generated. Additionally, because we need to record approximately 20X more frames per second than with GECIs, the maximum possible exposure time is reduced by that same factor. This ultimately means that the amount of signal contained within a single frame for voltage imaging is quite low, making pulling signal from noise difficult. Lastly, for the two reasons mentioned above, high irradiance powers are needed for voltage imaging to generate sufficient signal, typically an order of magnitude more than for calcium-based imaging experiments.

So then, an ideal voltage imaging experiment would involve recording as many neurons within a single FOV (ideally would be on the 250 $\mu$ m x 250 $\mu$ m scale for utility reasons) at high frame rates (500Hz - 1kHz) as possible. This generates exceptionally large datasets (approaching 1GB/s) and necessitates custom optical arrangements as no commercial options currently exist.

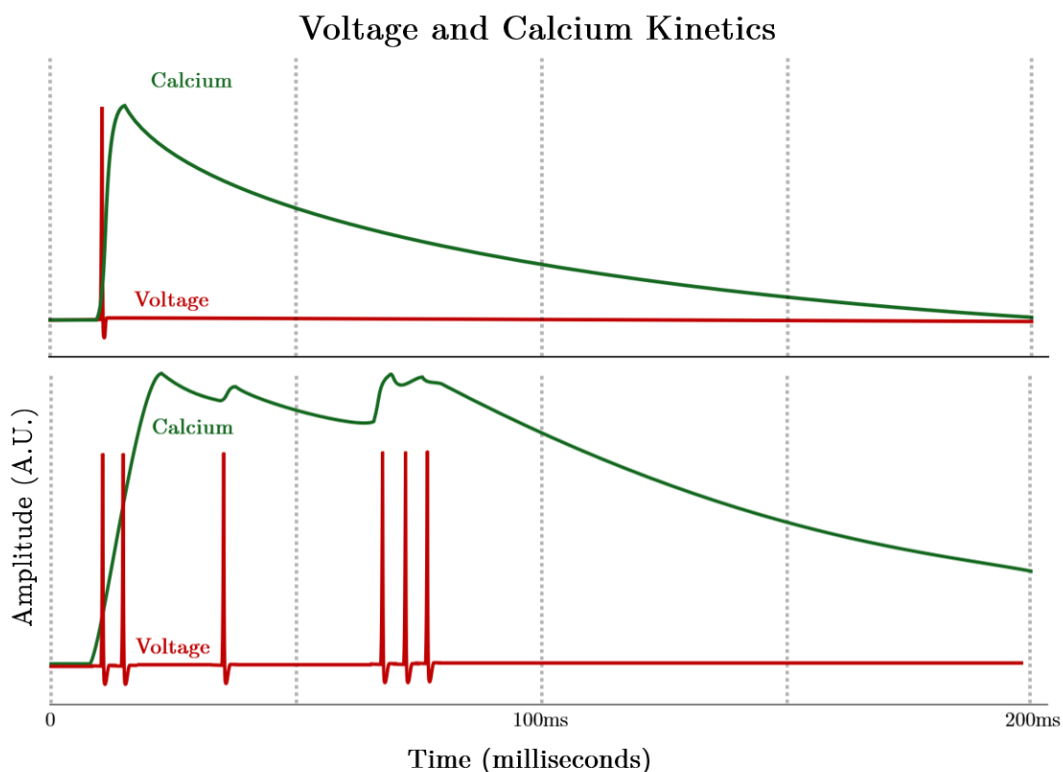


Figure 10.1: **Comparison Between Voltage and Calcium Kinetics**

Green traces shows the slow decay of calcium transients over 100s of ms, red is a single action potential on the 1ms time scale. Each image frame (space between the dashed lines, for a 20FPS system) integrates photo information over the course of the exposure time. In the case of a 20Hz frame-rate, calcium signals would be well resolved since they decay on the slowly, but a single action potential only exists for about 2% of a single image frame, meaning that frame integrated 2% signal, and 98% noise. As such, faster imaging systems are needed to sufficiently capture the kinetics of individual action potentials.

### 10.1.2 Existing Methodologies

Researchers have been working to optically resolve voltage dynamics in the brain for years now. The systems that have been described to successfully do so are often extremely elaborate and built from hundreds of thousands of dollars worth of high power lasers, digital micromirror devices, and custom fabricated optical elements. These methods, while technologically impressive and impactful to the field generally, are also completely outside the reach of most researchers; many of whom could benefit from incorporating voltage imaging into their research. There exists then, a clear opportunity in the field to build

simple, minimal-cost 1P voltage imaging microscopes that can be built and used by anyone. I will now describe a microscope that I believe fills this need of the community.

### **10.1.3 Need For Simple Solutions**

Here I present a custom-made high speed 1P microscope that records voltage *in-vivo*. It is built almost entirely of off-the-shelf components and spatially confines the excitation light to minimize background fluorescence and unnecessary photobleaching. In addition, the microscope features a tiltable objective assembly and a gonimetric stage to make aligning and recording from even tilted FOVs possible in head-fixed mice. The system is equipped with motorized degrees of freedom, making finding exact FOVs possible day after day, and tracking exact depths of the focal plane for each recording relative to the cranial window surface. When considered as a whole, this low cost microscope can enable many researchers to set up a powerful entry point into what I believe is the future of bioimaging, all-optical physiology.

## **10.2 Spatially Confined 1P Excitation Voltage Imaging Microscope**

Here a custom-made high speed 1P microscope that records voltage *in-vivo* is presented. It is built almost entirely of off-the-shelf components and spatially confines the excitation light to minimize background fluorescence and unnecessary photobleaching. In addition, the microscope features a tiltable objective assembly and a gonimetric stage to make aligning and recording from even tilted FOVs possible in head-fixed mice. The system is equipped with motorized degrees of freedom, making finding exact FOVs possible day after day, and tracking exact depths of the focal plane for each recording relative to the cranial window surface. When considered as a whole, this low cost microscope can enable many researchers to set up a powerful entry point into what I believe is the future of bioimaging, all-optical physiology.

### 10.2.1 Need For High Irradiance

Because approximately 20x more frames need to be acquired per second to adequately capture the rapid dynamics of voltage in neurons compared to calcium dynamics, exposure times are limited with voltage imaging. In the case of 25FPS calcium imaging, a single frame is allowed to integrate fluorescent signal over approximately 40ms, building charge on each pixel over the duration of that exposure, thus creating a strong SNR image where features of interest (that are fluorescent) are significantly brighter than background. By reducing that integration time in an extreme way, say by a factor of 20 to 2ms, the total amount of signal present on the image sensor is reduced by the same factor, bringing the SNR of the final image down substantially. As a result higher illumination irradiances are used as a means to surmount the low integration times. In voltage imaging, irradiance is an often used metric to describe the amount of light supplied to an image field per unit area during a given recording. Early systems relied on high power lasers and DMDs to direct 5-10mW of laser energy onto a single neuron, suggesting irradiances in the range of  $10\text{W}/\text{mm}^2$  for average sized cells (Adam et al., 2019). These almost inconceivable irradiances are many orders of magnitude greater than those used routinely in calcium imaging (approximately  $25\text{mW}/\text{mm}^2$ ) and as such result in massive photobleaching which limits the total length of viable recordings to less than 30s. Since that time, voltage indicators have rapidly improved in terms of sensitivity and response magnitude, with many generating suitable levels of fluorescent response within reasonable irradiances of  $1\text{-}150\text{mW}/\text{mm}^2$ . As a result, voltage imaging systems need to generate strong photoexcitation in order to collect the rapid voltage signals from the membrane in a millisecond or two.

### 10.2.2 Necessity of Restricting Excitation Light

Providing light to only the region of tissue that is being recorded is crucial to maximize experimental utility. Because the required irradiances are high, photobleaching is prevalent in modern voltage imaging experiments. Spatially confining the excitation, so as to mitigate any activation of unresolved neurons, presents itself as a logical means to extend the experimental viability of each animal. Since the region of interest that the camera can resolve (discussed in more detail in the next section) is far smaller than the optical FOV of the imaging system, the need to shape the light to suit a given ROI is ideal. The discussed system is able to do just that.

### 10.2.3 Consideration of qCMOS Architecture

Quantitative CMOS (qCMOS) image sensors are incredibly sensitive and fast detectors capable of resolving photon counts. While sCMOS cameras are used widely in bioimaging to collect fluorescent signals from spatially resolved 2D planes, qCMOS cameras offer higher sensitivity and lower noise. Additionally, the qCMOS image sensor was constructed on the semiconductor level with a parallel architecture that emphasizes readout efficiency and line speed. The specific camera used in this work is the Hamamatsu Quest (C15550-22UP) which is equipped with a highly parallelized, back illuminated image sensor capable of reading one full pixel row (4096 pixels) at approximately 272.4kHz. As a result, long, 4096 x 512 pixel ROIs can be resolved at 532Hz, making the visualization of high speed voltage signals possible across very long rectangular FOVs. Since the image sensor architecture is highly parallel along the line such that each pixel has its own analog to digital converter, the amount of time associated with imaging a single frame only depends on the number of vertical pixels and does not depend at all on the number of horizontal pixels (i.e. a 4096 x 512 ROI takes the same time to read out as a 512 x 512 ROI). As a result, we can collect signal from a far greater number of cells (within reason) if we design an imaging system

that can make use of rectangular FOVs and restrict the illumination as described in the previous section to mitigate photobleaching effects.

### **10.3 Optomechanical System**

The microscope is built of four main subassemblies. First is the photoexcitation which is configured to generate spatially defined strips of known size in the brain referred to from here on as the “strip excitation module.” Next is the main scope body that includes the dichroic beam splitter and mounts for the motorized stages. There is also a “tiltable objective module” that enables the microscope to resolve planes of neural tissue that are at non-orthogonal angles relative to the microscope base. This degree of freedom is critical for some regions of interest, such as CA1 where the pyramidal cell layer is often positioned at an angle relative to the dorsal axis. Next the collected fluorescence is imaged onto the qCMOS through an adjustable z-stage and a high efficiency detector subsystem. Each of these subsystems are detailed below.

#### **10.3.1 Strip Excitation Module**

To best suit the architecture of the image sensor, an excitation module which maps an adjustable rectangle onto the brain was developed. This system uses a high-power 470nm LED which is collimated by two 16mm aspheric collection lenses. The collimated beam is then spatially shaped by two adjustable slits that can be adjusted by the user to fit the exact imaging ROI as defined by the image sensor. The image of the strip is then relayed via a 50mm doublet onto the sample of interest, after passing through the tiltable objective assembly. Irradiances in the 250mW/mm<sup>2</sup> range are easily achievable for FOVs that are within the image sensor bandwidth for 500FPS recordings.



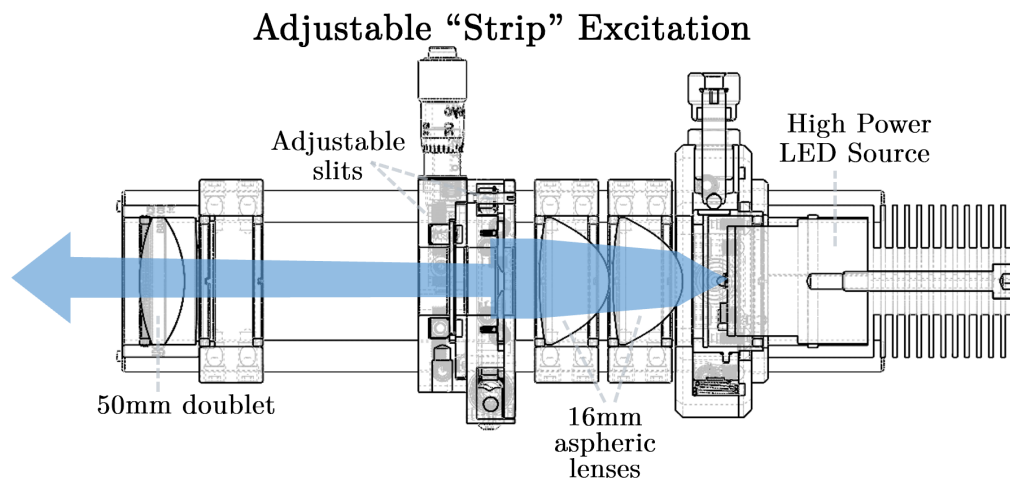


Figure 10.2: **Strip Excitation Module Schematic and Optomechanical Diagram** Demonstrates the collimation and spatial filtering of the light before being re-imaged on the sample plane.

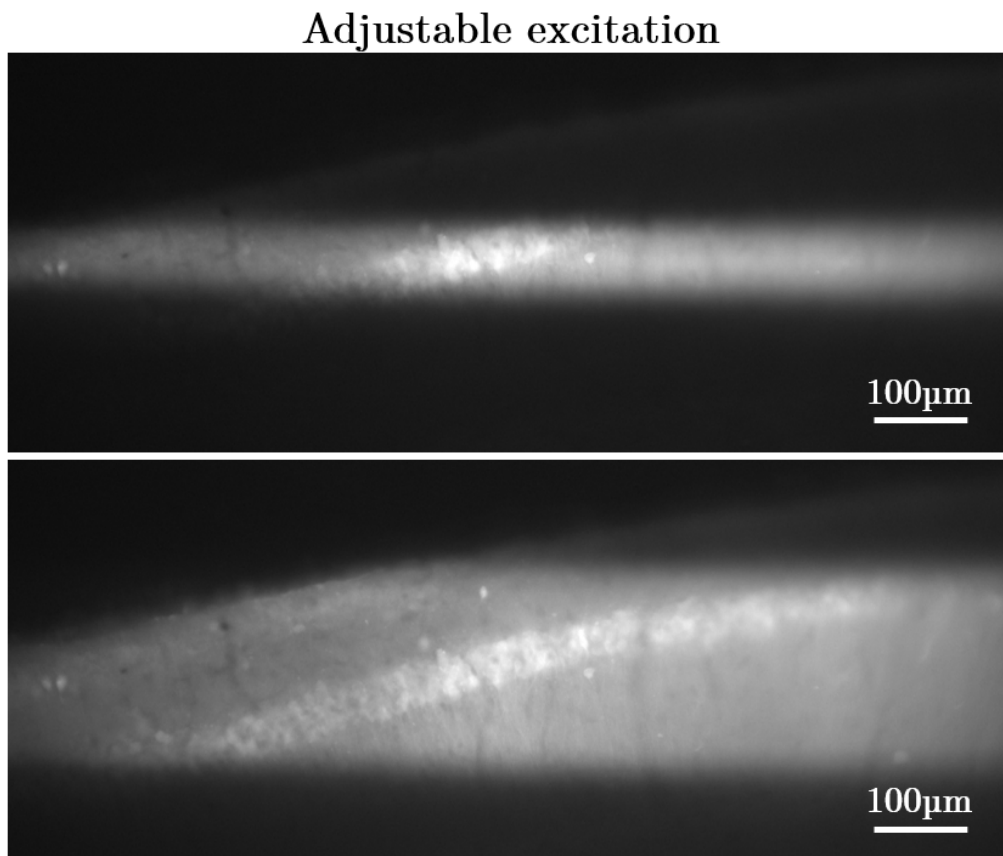


Figure 10.3: **Example Excitation Conditions for a Narrow and Wide Strip**  
Adjustable slits enable the control over the shape of the excitation light.

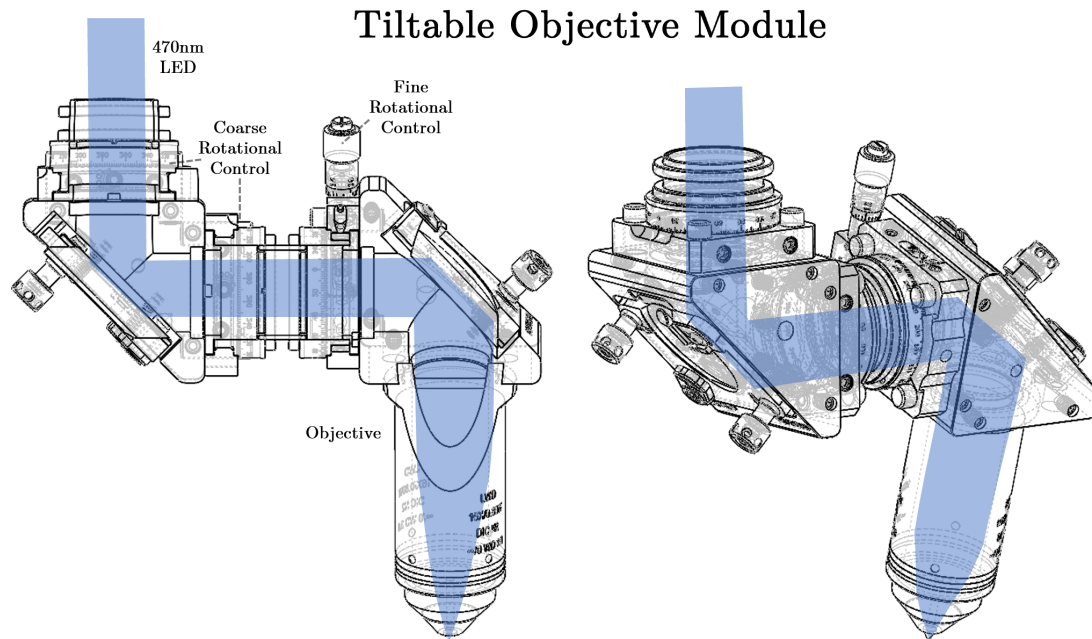


Figure 10.4: **Tiltable Objective Module Optomechanical Diagram.** Schematic demonstrating the beam path and rotational degrees of freedom that enable recording from non-orthogonal image planes.

#### 10.3.1.1 Tiltable Objective Module

The tiltable objective module enables optical access to image planes which are non-orthogonal to the microscope base without significant manipulation of the animal's angular position. It is constructed from 90 degree turning mirrors, rotational 25mm cage mounts, optical construction rails and SM1 coupling rings. An M32 x 0.75 threading adapter is also used to enable the use of common objective lenses like the Nikon 16x/0.8W and ThorLabs 10x/0.5 air. The figure depicts the system with the 16x Nikon lens. All together it enables easy and repeatable access to the same optimal imaging plane even when it is at a specific non-orthogonal angle relative to the optical table surface.

### 10.3.2 High Efficiency Collection and De-Magnification

Light that is collected by the microscope is transmitted through the tiltable objective assembly and relayed through a 1P dichroic mirror before being focused onto the qCMOS image sensor. Because the image sensor has a relatively large pixel size ( $4.5\mu\text{m}$ ) it was ideal to de-magnify the image from the objective onto the image sensor, thus increasing the maximum FOV. To do this, a 0.5x camera tube was used, which contains a 100mm focal length tube lens. This brings the spatial sampling rate to  $4.6\mu\text{m} / 8 = 0.6\mu\text{m}$  for the 16x objective and  $4.6\mu\text{m} / 5 = 0.9\mu\text{m}$  for the 10x lens. When considering the FOVs possible, this corresponds to a  $2.45\text{mm} \times 307\mu\text{m}$  FOV for the 16x and a  $3.68\text{mm} \times 460\mu\text{m}$  FOV for the 10x objective respectively, at a framerate  $> 500\text{Hz}$ .

### 10.3.3 Complete Voltage Imaging System

Each of these subassemblies are integrated together into a low-cost, highly capable 1P voltage imaging microscope using almost completely off-the-shelf parts. Two of these microscopes exist, one at UCLA and one at the SickKids Research Institute (Toronto, CA). The design shown in Figure 10.5 is set up at SickKids, and a slightly different version, pictured in Figure 10.6 is located in the UCLA Neurology department. The main difference between the two systems are the mechanical components responsible for generating fine and repeatable lateral and axial movements of the microscope hardware relative to the sample. In order to adapt the hardware to implement electronic motorized stages, the SickKids version of the imaging system includes several custom-machined stainless steel mounts (ProtoLabs) that enable mechanical interfacing with off-the-shelf electronically controlled stages. Additionally, a light-blocking bellows is installed on the SickKids version, to enable axial displacement of the excitation and tiltable objective assemblies for focusing reasons. The UCLA version of the hardware does not include this complexity as it is controlled using purely mechanical stages. As such, the version pictured in Figure 10.6 does not require the custom components for construction and control.



Figure 10.5: **Spatially Confined Excitation Voltage Imaging Microscope**  
The system as configured at the University of Toronto. The UCLA version of the system is slightly different with the same fundamental operating principles.

# UCLA 1P voltage microscope

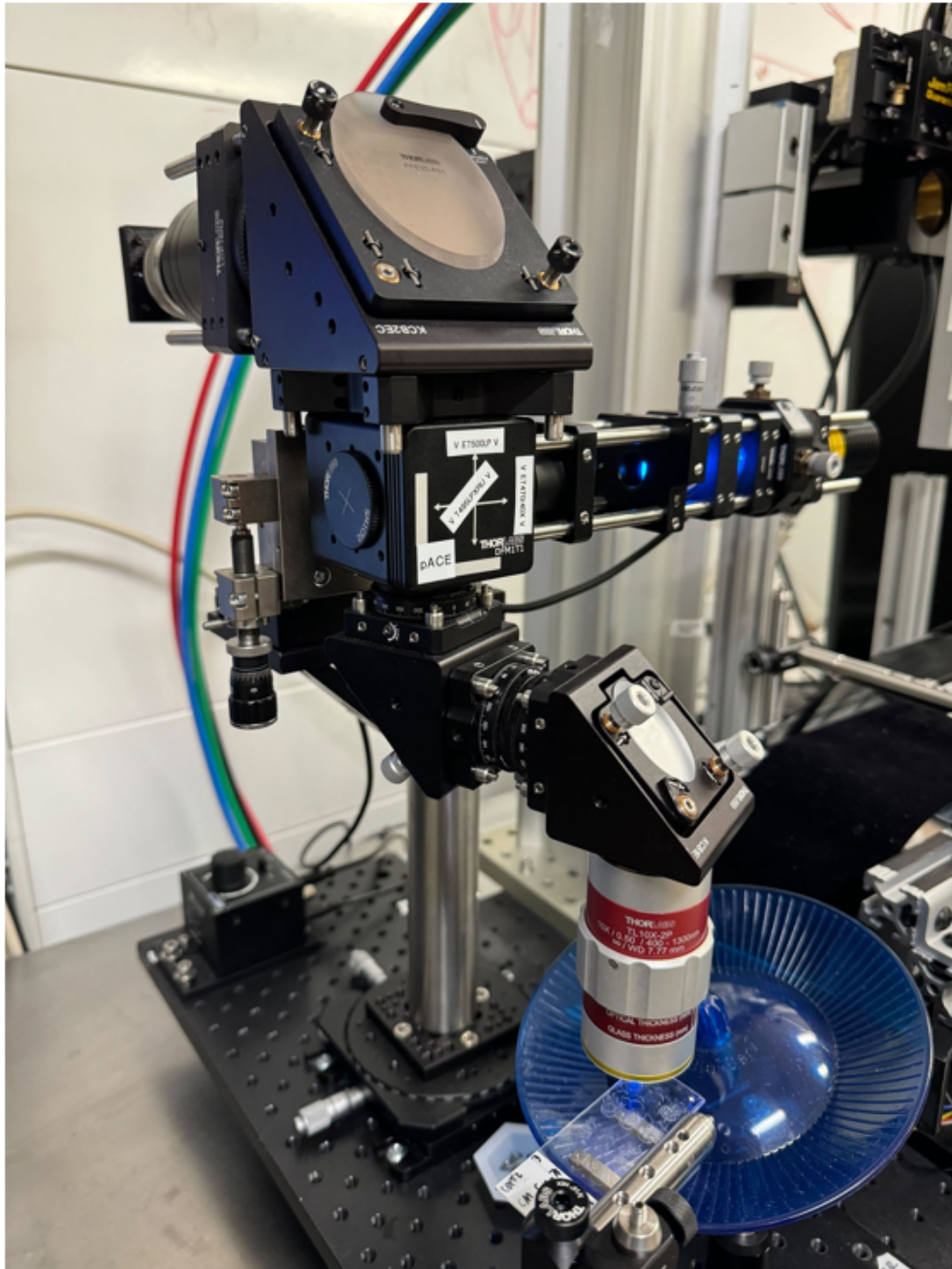


Figure 10.6: **Voltage Imaging Microscope Physical Hardware at UCLA**  
This is the microscope as configured in the Golshani Lab. For logistical reasons, the system is currently using a Sony IMX290 image sensor on an IDS camera board, in place of the Hamamatsu qCMOS camera detailed above. Eventually, the system will be returned to the qCMOS, but the Sony sensor still performs very well in this application, just over a more limited FOV.

## 10.4 Results

### 10.4.1 Resolving Fast-Spiking Interneuron Dynamics Over 10 Minutes

One important aspect of voltage imaging is the capacity to resolve dynamics from cells which fire individual action potentials more quickly than the decay of the calcium transient. One cell type that exhibits this property are inhibitory interneurons which can fire an excess of 100Hz during sharp wave ripples (Tzilivaki et al., 2023). The result of imaging such a neural subtype with calcium reporters would be nearly impossible to interpret, as it would almost uniformly appear bright, given the reporter molecule's inability to respond within a millisecond time frame. Voltage indicators, on the other hand, are able to reliably resolve dynamics from fast spiking interneurons, such as somatostatin + (SST) OLM cells as demonstrated in Figure 10.7. For the recording presented, AAV-CAG-pAce was used with Chrna2-CRE animals to selectively express the pAce voltage indicator in SST+ OLM cells. Small irradiances were needed due to the proximity of the neurons to the imaging window and high expression levels driven by CAG, thus enabling recording over 10 minutes without significant degradation to the signal.

### 10.4.2 Capturing Membrane Potential From Many Neurons At Once

The way in which individual neurons within circuits integrate input from various sources, such as excitatory postsynaptic potentials, that give rise to behavior and learning is largely understudied due to methodological constraints. Firstly, studying subthreshold events like EPSPs is not possible using calcium imaging since they do not result in calcium influx, making the only real viable option (besides voltage imaging) paired electrophysiological recordings either in culture or slice preparations. Such approaches are very low throughput and prevent the ability to assess how the neural circuit properties change as a function of gained experience or learning. As such there is a large gap in understanding as to how the subthreshold inputs, in combination potentially with oscillatory dynamics shape eventual firing properties in excitatory neurons. The voltage imaging microscope system described

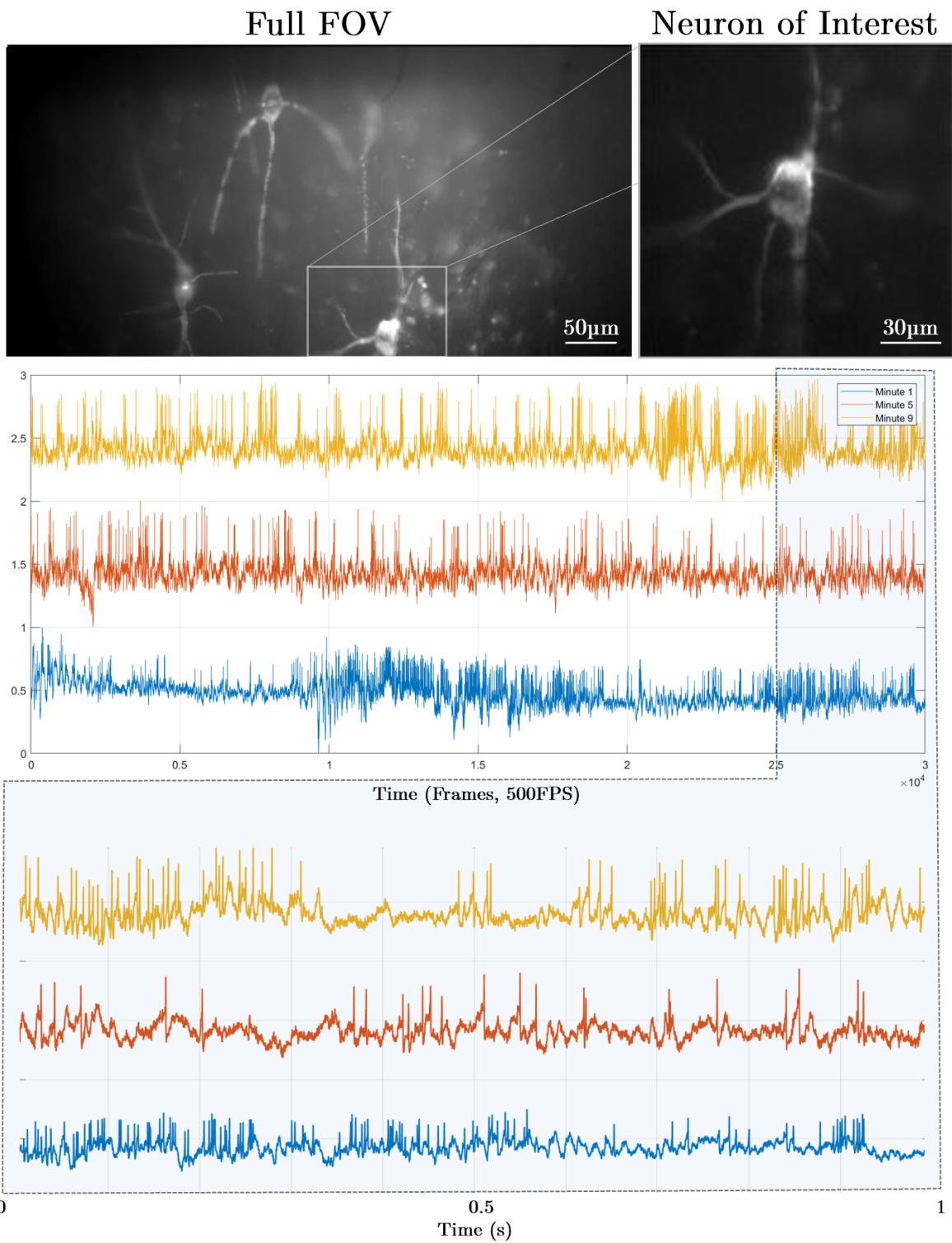


Figure 10.7: Resolving dynamics from three SST+ OLM cells in CA1 over 10 minutes

here is well posed to assess this open question in the field because of its capacity to resolve large fields of view at high speed. We recorded an entire population of excitatory neurons in hippocampal area CA1 using the 10x objective, resulting in a very large FOV (920  $\mu\text{m}$  x 460  $\mu\text{m}$ ) at 500FPS resulting in the identification of more than 30 active neurons simultaneously.

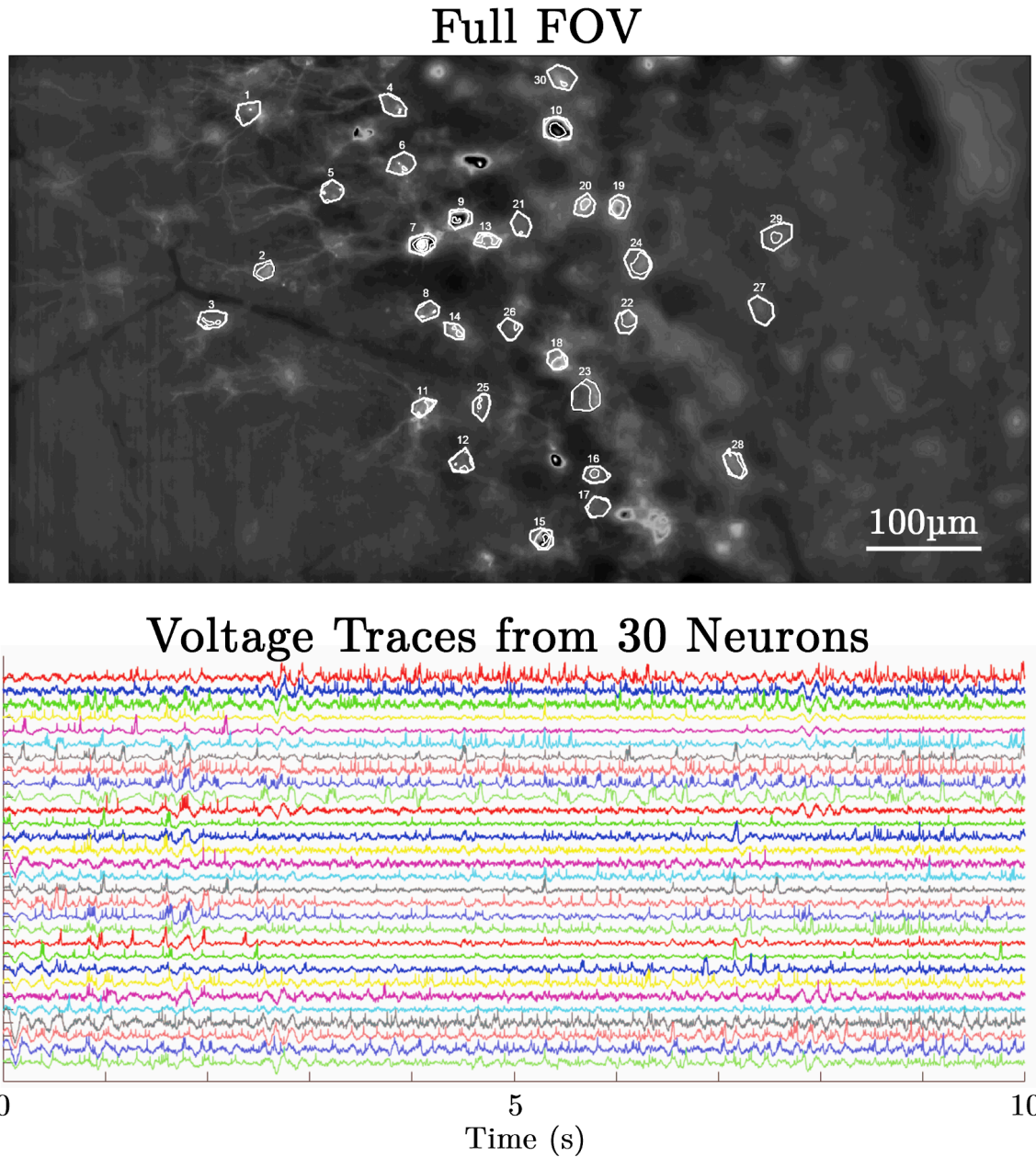


Figure 10.8: Population Voltage Imaging from 30 Active, pAce-Expressing Excitatory Neurons in CA1



## 10.5 Future Directions

Voltage imaging is without a doubt the future of activity monitoring of single cells in the brain over sustained periods of time. The fluorescent indicators for doing so are progressing at a seemingly exponential rate, enabling a rapid and sustained growth in the field over the past several years. As the indicators and optical methodologies improve, there are fewer reasons to settle for the fundamentally incomplete view that calcium imaging provides. I believe that it is not unreasonable to assert that within 10 years, voltage imaging will be the primary imaging method for studying neural circuits *in-vivo*.

### 10.5.1 Extending the Technology

The vast majority of voltage imaging methodologies rely on single photon area excitation as a means to increase the effective temporal bandwidth of the imaging system. While 2P microscope systems provide clear optical benefits in the final recording, as detailed in Section 3.2, challenges associated with scanning a focal volume across 2D space in sufficiently short time spans (approximately 2ms/frame) is significant due to inertial restrictions. As a result, the majority of researchers developing voltage imaging systems (this work included) use static excitation light patterns and solid-state image sensors to sample space directly without any moving parts. Researchers have used patterned excitation through the use of digital micromirror devices (DMDs) to selectively illuminate cells of interest (Adam et al., 2019; Xiao et al., 2021; Meng et al., 2022) but there are still depth limitations and SNR constraints placed on 1P imaging systems that do not apply as strongly to multiphoton approaches. Additionally, photobleaching in 1P systems is a major limiting factor in terms of the total recording length. This problem is dramatically reduced in multiphoton approaches, making them especially appealing to those interested in recording voltage dynamics over longer periods of time (on the 30 minute - 1 hour scale). For these reasons, I think that multiphoton voltage imaging approaches will eventually eclipse those currently in use, but work still needs to be done to improve scanning speeds.

Section 9.3.2 of this dissertation details three areas that I believe to be key not only for miniature 2P microscopes, but voltage imaging microscopes as well: Spatial and Temporal pulse multiplexing, SCAPE, Resonant Scan Multiplexing, and Topographic methodologies. For a detailed explanation of each method, please view Section 9.3.2 for more information. The key insight that all of these methods have in common is their ability to push beyond the inertial limits of traditional resonant scanners using optical means. This increase effectively translates (in most systems) to higher frame rates for a given number of vertical pixels contained within an image. Once that can be expanded by a factor of 10-20 in a reasonably compact and easily configured way, I predict the entire field will shift to using GEVIs in place of the commonly used GECIs due to the substantially increased information content contained in voltage signals.

## **10.5.2 Voltage Imaging Miniature Microscopes**

Another clear future direction is the ability to integrate Parts I and II of this dissertation and build miniature microscopes that are capable of resolving voltage traces over time. While this goal is lofty using 2P means (for the scanning reasons detailed above) there may be avenues using 1P approaches. Some groups have constructed miniature voltage imaging setups, with limited success (Juneau et al., 2020). Due to optical and electronic constraints, recording in freely behaving animals still has not been done to date. However, with the advent of new sensitive image sensors, more efficient miniature optical designs, and new voltage indicators, there is a real case to be made for the validity of recording voltage in freely behaving animals on the horizon.

### **10.5.2.1 Conclusions**

In Part II, a 1P voltage imaging microscope is presented, which is capable of resolving dynamics from fast-spiking interneurons over sustained periods of 10 minutes, as well as from large fields of view (480  $\mu\text{m}$  x 960  $\mu\text{m}$ ) containing 30 active neurons. The microscope is fitted with an excitation module that shapes the light into a corresponding rectangle

to suit the architecture of the qCMOS image sensor and limit background fluorescence generated by exciting off-target cells. A tiltable objective mount is also presented which enables researchers to align the image plane of the microscope to non-orthogonal planes in the brain without angularly displacing the animal. Fluorescence is collected over an efficient demagnification system and relayed to a fast, sensitive qCMOS image sensor that enables readout at rates greater than 500FPS for the regions of interest we are resolving. Altogether this microscope presents as a low-cost, simple to set up voltage imager which can be easily adopted by labs looking to beyond traditional calcium imaging methods of today.

## REFERENCES

- Acharya, L., Aghajani, Z. M., Vuong, C., Moore, J. J., and Mehta, M. R. (2016). Causal influence of visual cues on hippocampal directional selectivity. *Cell*, 164(1):197–207. 23
- Adam, Y., Kim, J. J., Lou, S., Zhao, Y., Xie, M. E., Brinks, D., Wu, H., Mostajo-Radji, M. A., Kheifets, S., Parot, V., et al. (2019). Voltage imaging and optogenetics reveal behaviour-dependent changes in hippocampal dynamics. *Nature*, 569(7756):413–417. 93, 104
- Burgin, E. M., Waxham, M. N., Rickling, S., Westgate, S. A., Mobley, W. C., and Kelly, P. T. (1990). In situ hybridization histochemistry of  $ca^{2+}$ /calmodulin-dependent protein kinase in developing rat brain. *Journal of Neuroscience*, 10(6):1788–1798. 4
- Chaigneau, E., Wright, A. J., Poland, S. P., Girkin, J. M., and Silver, R. A. (2011). Impact of wavefront distortion and scattering on 2-photon microscopy in mammalian brain tissue. *Optics express*, 19(23):22755–22774. 20
- Chen, W., Zhang, Q., Natan, R., Fan, J., and Ji, N. (2022). Bessel-droplet foci enable high-resolution and high-contrast volumetric imaging of synapses and circulation in the brain in vivo. *bioRxiv*, pages 2022–03. 85
- Cheng, A., Gonçalves, J. T., Golshani, P., Arisaka, K., and Portera-Cailliau, C. (2011). Simultaneous two-photon calcium imaging at different depths with spatiotemporal multiplexing. *Nature methods*, 8(2):139–142. 83
- Copernicus, N. (1543). *De revolutionibus orbium coelestium*. Johannes Petreius, Nuremberg. 1
- Delaney, P. and Harris, M. (1995). Fiberoptics in confocal microscopy. In *Handbook of biological confocal microscopy*, pages 515–523. Springer. 25
- Demas, J., Manley, J., Tejera, F., Barber, K., Kim, H., Traub, F. M., Chen, B., and Vaziri, A. (2021). High-speed, cortex-wide volumetric recording of neuroactivity at cellular resolution using light beads microscopy. *Nature Methods*, 18(9):1103–1111. 83
- Denk, W. and Svoboda, K. (1997). Photon upmanship: why multiphoton imaging is more than a gimmick. *Neuron*, 18(3):351–357. 2, 15
- Doischer, D., Hosp, J. A., Yanagawa, Y., Obata, K., Jonas, P., Vida, I., and Bartos, M. (2008). Postnatal differentiation of basket cells from slow to fast signaling devices. *Journal of Neuroscience*, 28(48):12956–12968. 7
- Eriksson, P. S., Perfilieva, E., Björk-Eriksson, T., Alborn, A.-M., Nordborg, C., Peterson, D. A., and Gage, F. H. (1998). Neurogenesis in the adult human hippocampus. *Nature medicine*, 4(11):1313–1317. 69

- Fahrbach, F. O., Simon, P., and Rohrbach, A. (2010). Microscopy with self-reconstructing beams. *Nature photonics*, 4(11):780–785. 85
- Fresnel, A.-J. (1819). Memoir on the diffraction of light. *Annales de Chimie et de Physique*, page 288. 82
- Gao, L., Shao, L., Chen, B.-C., and Betzig, E. (2014). 3d live fluorescence imaging of cellular dynamics using bessel beam plane illumination microscopy. *Nature protocols*, 9(5):1083–1101. 85
- Ghosh, K. K., Burns, L. D., Cocker, E. D., Nimmerjahn, A., Ziv, Y., Gamal, A. E., and Schnitzer, M. J. (2011). Miniaturized integration of a fluorescence microscope. *Nature methods*, 8(10):871–878. 24
- Golgi, C. (1873). Sulla fina anatomia degli organi centrali del sistema nervoso. *Gazzetta Medica Italiana Lombardia*, 33:244–246. 1
- Golub, I. (2006). Fresnel axicon. *Optics letters*, 31(12):1890–1892. 82
- Gonçalves, J. T., Schafer, S. T., and Gage, F. H. (2016). Adult neurogenesis in the hippocampus: from stem cells to behavior. *Cell*, 167(4):897–914. 69
- Guo, C., Blair, G. J., Sehgal, M., Sangiuliano Jimka, F. N., Bellafard, A., Silva, A. J., Golshani, P., Basso, M. A., Blair, H. T., and Aharoni, D. (2023). Miniscope-lfov: A large-field-of-view, single-cell-resolution, miniature microscope for wired and wire-free imaging of neural dynamics in freely behaving animals. *Science Advances*, 9(16):eadg3918. 72, 73
- Hainmueller, T. and Bartos, M. (2018). Parallel emergence of stable and dynamic memory engrams in the hippocampus. *Nature*, 558(7709):292–296. 70
- Hainmueller, T. and Bartos, M. (2020). Dentate gyrus circuits for encoding, retrieval and discrimination of episodic memories. *Nature Reviews Neuroscience*, 21(3):153–168. 69
- Helmchen, F. and Denk, W. (2005). Deep tissue two-photon microscopy. *Nature methods*, 2(12):932–940. 21, 22
- Helmchen, F., Fee, M. S., Tank, D. W., and Denk, W. (2001). A miniature head-mounted two-photon microscope: high-resolution brain imaging in freely moving animals. *Neuron*, 31(6):903–912. 25, 28, 29, 36, 81
- Hodgkin, A. L. and Huxley, A. F. (1952). A quantitative description of membrane current and its application to conduction and excitation in nerve. *The Journal of physiology*, 117(4):500–544. 5, 6, 7

Holtmaat, A., Bonhoeffer, T., Chow, D. K., Chuckowree, J., De Paola, V., Hofer, S. B., Hübener, M., Keck, T., Knott, G., Lee, W.-C. A., et al. (2009). Transcranial two-photon imaging of synaptic structures in the cortex of awake head-restrained mice. *Nature protocols*, 4(8):1215–1228. 5

Hooke, R. (1665). *Micrographia: or Some Physiological Descriptions of Minute Bodies Made by Magnifying Glasses. With Observations and Inquiries Thereupon*. Jo. Martyn and Ja. Allestry, London. 1

Johnston, S. T., Shtrahman, M., Parylak, S., Gonçalves, J. T., and Gage, F. H. (2016). Paradox of pattern separation and adult neurogenesis: A dual role for new neurons balancing memory resolution and robustness. *Neurobiology of learning and memory*, 129:60–68. 69

Juneau, J., Duret, G., Chu, J. P., Rodriguez, A. V., Morozov, S., Aharoni, D., Robinson, J. T., St-Pierre, F., and Kemere, C. (2020). Minifast: A sensitive and fast miniaturized microscope for in vivo neural recording. *BioRxiv*, pages 2020–11. 105

Kazanskiy, N., Khonina, S. N., Karpeev, S. V., and Porfirev, A. P. (2020). Diffractive optical elements for multiplexing structured laser beams. *Quantum Electronics*, 50(7):629. 82

Kazemipour, A., Novak, O., Flickinger, D., Marvin, J. S., Abdelfattah, A. S., King, J., Borden, P. M., Kim, J. J., Al-Abdullatif, S. H., Deal, P. E., et al. (2019). Kiloherz frame-rate two-photon tomography. *Nature methods*, 16(8):778–786. 86

Klioutchnikov, A., Wallace, D. J., Frosz, M. H., Zeltner, R., Sawinski, J., Pawlak, V., Voit, K.-M., Russell, P. S. J., and Kerr, J. N. (2020). Three-photon head-mounted microscope for imaging deep cortical layers in freely moving rats. *Nature methods*, 17(5):509–513. 28, 76

Klioutchnikov, A., Wallace, D. J., Sawinski, J., Voit, K.-M., Groemping, Y., and Kerr, J. N. (2023). A three-photon head-mounted microscope for imaging all layers of visual cortex in freely moving mice. *Nature methods*, 20(4):610–616. 29, 31, 36, 75, 76

KM-Lab (2020). Minipc. <https://github.com/KM-Lab/MiniPC>. 72

Lees, R. M., Bianco, I. H., Campbell, R. A., Orlova, N., Peterka, D. S., Pichler, B., Smith, S. L., Yatsenko, D., Yu, C.-H., and Packer, A. M. (2024). Standardised measurements for monitoring and comparing multiphoton microscope systems. *bioRxiv*, pages 2024–01. 18, 58

Lissajous, J. A. (1857). Mémoire sur l'Étude optique des mouvements vibratoires. *Annales de chimie et de physique*, 51:147–232. 25

Mathis, A., Mamidanna, P., Cury, K. M., Abe, T., Murthy, V. N., Mathis, M. W., and Bethge, M. (2018). Deeplabcut: markerless pose estimation of user-defined body parts with deep learning. *Nature neuroscience*, 21(9):1281–1289. 65, 70

- Meng, X., Huisman, L., Huijben, T., Szabo, G., Van Tol, R., De Heer, I., Ganapathy, S., and Brinks, D. (2022). A compact microscope for voltage imaging. *Journal of Optics*, 24(5):054004. 104
- Miyawaki, A., Griesbeck, O., Heim, R., and Tsien, R. Y. (1999). Dynamic and quantitative  $ca^{2+}$  measurements using improved cameleons. *Proceedings of the National Academy of Sciences of the United States of America*, 96(5):2135–2140. 5
- Modi, M. N., Daie, K., Turner, G. C., and Podgorski, K. (2019). Two-photon imaging with silicon photomultipliers. *Optics express*, 27(24):35830–35841. 20, 36, 42
- Moreno-Jiménez, E. P., Terreros-Roncal, J., Flor-García, M., Rábano, A., and Llorens-Martín, M. (2021). Evidences for adult hippocampal neurogenesis in humans. *Journal of Neuroscience*, 41(12):2541–2553. 69
- Ormö, M., Cubitt, A. B., Kallio, K., Gross, L. A., Tsien, R. Y., and Remington, S. J. (1996). Crystal structure of the aequorea victoria green fluorescent protein. *Science*, 273(5280):1392–1395. 2
- Ozbay, B. N., Futia, G. L., Ma, M., Bright, V. M., Gopinath, J. T., Hughes, E. G., Restrepo, D., and Gibson, E. A. (2018). Three dimensional two-photon brain imaging in freely moving mice using a miniature fiber coupled microscope with active axial-scanning. *Scientific reports*, 8(1):8108. 28, 86
- Pachitariu, M., Stringer, C., Schröder, S., Dipoppa, M., Rossi, L. F., Carandini, M., and Harris, K. D. (2016). Suite2p: beyond 10,000 neurons with standard two-photon microscopy. *BioRxiv*, page 061507. 65, 70
- Piyawattanametha, W., Cocker, E. D., Burns, L. D., Barretto, R. P., Jung, J. C., Ra, H., Solgaard, O., and Schnitzer, M. J. (2009). In vivo brain imaging using a portable 2.9 g two-photon microscope based on a microelectromechanical systems scanning mirror. *Optics letters*, 34(15):2309–2311. 26
- Podgorski, K., Negrean, A., Xie, M., Charles, A., Flickinger, D., Rohde, J., Kinsey, L., Aggarwal, A., Jaindl, G., King, J., Gibiser, R., and Team, T. G. P. (2023). Recording neurons’ synaptic input patterns with scanned line projection microscopy. In *Society for Neuroscience (SfN) Annual Meeting*, Washington, DC, USA. Poster presentation. 86
- Ramón y Cajal, S. (1899). *Textura del Sistema Nervioso del Hombre y de los Vertebrados*. Imprenta y Librería de Nicolás Moya, Madrid. 1
- Ravassard, P., Kees, A., Willers, B., Ho, D., Aharoni, D., Cushman, J., Aghajan, Z. M., and Mehta, M. R. (2013). Multisensory control of hippocampal spatiotemporal selectivity. *Science*, 340(6138):1342–1346. 70
- Ren, Y.-X., He, H., Tang, H., and Wong, K. K. (2021). Non-diffracting light wave: Fundamentals and biomedical applications. *Frontiers in Physics*, 9:698343. 85

- Rodríguez, C., Liang, Y., Lu, R., and Ji, N. (2018). Three-photon fluorescence microscopy with an axially elongated bessel focus. *Optics letters*, 43(8):1914–1917. 85
- Sauer, B. and Henderson, N. (1988). Site-specific dna recombination in mammalian cells by the cre recombinase of bacteriophage p1. *Proceedings of the National Academy of Sciences of the United States of America*, 85(14):5166–5170. 4
- Sawinski, J., Wallace, D. J., Greenberg, D. S., Grossmann, S., Denk, W., and Kerr, J. N. (2009). Visually evoked activity in cortical cells imaged in freely moving animals. *Proceedings of the National Academy of Sciences*, 106(46):19557–19562. 26, 28
- Silva, A. J., Paylor, R., Wehner, J. M., and Tonegawa, S. (1992). Impaired spatial learning in  $\alpha$ -calcium-calmodulin kinase ii mutant mice. *Science*, 257(5067):206–211. 7
- Skocek, O., Nöbauer, T., Weilguny, L., Martínez Traub, F., Xia, C. N., Molodtsov, M. I., Grama, A., Yamagata, M., Aharoni, D., Cox, D. D., et al. (2018). High-speed volumetric imaging of neuronal activity in freely moving rodents. *Nature methods*, 15(6):429–432. 84
- Srinivasan, T. and Yildirim, M. (2023). Advances in ultrafast fiber lasers for multiphoton microscopy in neuroscience. In *Photonics*, volume 10, page 1307. MDPI. 17
- Stefanini, F., Kushnir, L., Jimenez, J. C., Jennings, J. H., Woods, N. I., Stuber, G. D., Kheirbek, M. A., Hen, R., and Fusi, S. (2020). A distributed neural code in the dentate gyrus and in ca1. *Neuron*, 107(4):703–716. 70
- Stokes, G. G. (1852). On the change of refrangibility of light. *Philosophical Transactions of the Royal Society of London*, 142:463–562. 2
- Tian, L., Hires, S. A., Mao, T., Huber, D., Chiappe, M. E., Chalasani, S. H., Petreanu, L., Akerboom, J., McKinney, S. A., Schreiter, E. R., et al. (2009). Imaging neural activity in worms, flies and mice with improved gcamp calcium indicators. *Nature methods*, 6(12):875–881. 7
- Tuncdemir, S. N., Lacefield, C. O., and Hen, R. (2019). Contributions of adult neurogenesis to dentate gyrus network activity and computations. *Behavioural Brain Research*, 374:112112. 69
- Tzilivaki, A., Tukker, J. J., Maier, N., Poirazi, P., Sammons, R. P., and Schmitz, D. (2023). Hippocampal gabaergic interneurons and memory. *Neuron*. 101
- Voleti, V., Patel, K. B., Li, W., Perez Campos, C., Bharadwaj, S., Yu, H., Ford, C., Casper, M. J., Yan, R. W., Liang, W., et al. (2019). Real-time volumetric microscopy of in vivo dynamics and large-scale samples with scape 2.0. *Nature methods*, 16(10):1054–1062. 84
- Wagner, M. J., Kim, T. H., Savall, J., Schnitzer, M. J., and Luo, L. (2017). Cerebellar purkinje cells encode expected reward size. *eLife*, 6:e28623. 7



- Wan, X. and Tao, X. (2021). Design of a cell phone lens-based miniature microscope with configurable magnification ratio. *Applied Sciences*, 11(8):3392. [82](#)
- Xiao, S., Lowet, E., Gritton, H. J., Fabris, P., Wang, Y., Sherman, J., Mount, R. A., Tseng, H.-a., Man, H.-Y., Straub, C., et al. (2021). Large-scale voltage imaging in behaving mice using targeted illumination. *IScience*, 24(11). [104](#)
- Xiao, S. and Mertz, J. (2022). Point-scanning two-photon microscopy at multi-kilohertz frame rate. In *Microscopy Histopathology and Analytics*, pages MM4A–5. Optica Publishing Group. [86](#)
- Yang, H. H. and St-Pierre, F. (2016). Genetically encoded voltage indicators: opportunities and challenges. *Journal of Neuroscience*, 36(39):9977–9989. [8](#)
- Youvan, D. C. and Michel-Beyerle, M. E. (1996). Structure and fluorescence mechanism of gfp. *Nature Biotechnology*, 14(10):1219–1220. [3](#)
- Yuste, R. and Bonhoeffer, T. (2001). Morphological changes in dendritic spines associated with long-term synaptic plasticity. *Annual Review of Neuroscience*, 24:1071–1089. [5](#)
- Zong, W., Obenaus, H. A., Skytøen, E. R., Eneqvist, H., de Jong, N. L., Vale, R., Jorge, M. R., Moser, M.-B., and Moser, E. I. (2022). Large-scale two-photon calcium imaging in freely moving mice. *Cell*, 185(7):1240–1256. [29](#), [30](#), [66](#), [74](#)
- Zong, W., Wu, R., Chen, S., Wu, J., Wang, H., Zhao, Z., Chen, G., Tu, R., Wu, D., Hu, Y., et al. (2021). Miniature two-photon microscopy for enlarged field-of-view, multi-plane and long-term brain imaging. *Nature methods*, 18(1):46–49. [27](#), [29](#), [30](#)
- Zong, W., Wu, R., Li, M., Hu, Y., Li, Y., Li, J., Rong, H., Wu, H., Xu, Y., Lu, Y., et al. (2017). Fast high-resolution miniature two-photon microscopy for brain imaging in freely behaving mice. *Nature methods*, 14(7):713–719. [27](#), [30](#), [32](#)